

**A European aerosol phenomenology-6: Scattering properties of atmospheric aerosol particles from 28 ACTRIS sites**

Marco Pandolfi<sup>1</sup>, Lucas Alados-Arboledas<sup>2</sup>, Andrés Alastuey<sup>1</sup>, Marcos Andrade<sup>3</sup>, Christo Angelov<sup>4</sup>, Begoña Artiñano<sup>5</sup>, John Backman<sup>6,7</sup>, Urs Baltensperger<sup>8</sup>, Paolo Bonasoni<sup>9</sup>, Nicolas Bukowiecki<sup>8</sup>, Martine Collaud Coen<sup>10</sup>, Sébastien Conil<sup>11</sup>, Esther Coz<sup>5</sup>, Vincent Crenn<sup>12,13</sup>, Vadimas Dudoitis<sup>14</sup>, Marina Ealo<sup>1</sup>, Kostas Eleftheriadis<sup>15</sup>, Olivier Favez<sup>16</sup>, Prodromos Fefatzis<sup>15</sup>, Markus Fiebig<sup>17</sup>, Harald Flentje<sup>18</sup>, Patrick Ginot<sup>19</sup>, Martin Gysel<sup>8</sup>, Bas Henzing<sup>20</sup>, Andras Hoffer<sup>21</sup>, Adela Holubova Smejkalova<sup>22,23</sup>, Ivo Kalapov<sup>4</sup>, Nikos Kalivitis<sup>24,25</sup>, Giorgos Kouvarakis<sup>24</sup>, Adam Kristensson<sup>26</sup>, Markku Kulmala<sup>6</sup>, Heikki Lihavainen<sup>7</sup>, Chris Lunder<sup>17</sup>, Krista Luoma<sup>6</sup>, Hassan Lyamani<sup>2</sup>, Angela Marinoni<sup>9</sup>, Nikos Mihalopoulos<sup>24,25</sup>, Marcel Moerman<sup>20</sup>, José Nicolas<sup>27</sup>, Colin O'Dowd<sup>28</sup>, Tuukka Petäjä<sup>6</sup>, Jean-Eudes Petit<sup>12,16</sup>, Jean Marc Pichon<sup>27</sup>, Nina Prokopciuk<sup>14</sup>, Jean-Philippe Putaud<sup>29</sup>, Sergio Rodríguez<sup>30</sup>, Jean Sciare<sup>12,a</sup>, Karine Sellegri<sup>27</sup>, Erik Swietlicki<sup>26</sup>, Gloria Titos<sup>2</sup>, Thomas Tuch<sup>31</sup>, Peter Tunved<sup>32</sup>, Vidmantas Ulevicius<sup>14</sup>, Aditya Vaishya<sup>28,33</sup>, Milan Vana<sup>22,23</sup>, Aki Virkkula<sup>6</sup>, Stergios Vratolis<sup>15</sup>, Ernest Weingartner<sup>8,b</sup>, Alfred Wiedensohler<sup>31</sup>, and Paolo Laj<sup>6,9,19</sup>

<sup>1</sup> Institute of Environmental Assessment and Water Research, c/ Jordi-Girona 18-26, 08034, Barcelona, Spain

<sup>2</sup> Andalusian Institute for Earth System Research, IISTA-CEAMA, University of Granada, Granada 18006, Spain

<sup>3</sup> Atmospheric Physics Laboratory, ALP, UMSA, Campus Cota Cota calle 27, Edificio FCPN piso 3, La Paz, Bolivia

<sup>4</sup> Institute for Nuclear Research and Nuclear Energy by the Bulgarian Academy of Sciences, 72 Tsarigradsko Chaussee Blvd, 1784-Sofia, Bulgaria

<sup>5</sup> Centro de Investigaciones Energéticas, Medioambientales y Tecnológicas, CIEMAT, Unidad Asociada en Contaminación Atmosférica, CIEMAT-CSIC, Avda. Complutense, 40, 28040 Madrid

<sup>6</sup> University of Helsinki, UHEL, Division of Atmospheric Sciences, PO BOX 64, FI-00014, Helsinki, Finland

<sup>7</sup> Finnish Meteorological Institute, FMI, Erik Palménin aukio 1, FI-00560, Helsinki, Finland

<sup>8</sup> Paul Scherrer Institut, PSI, Laboratory of Atmospheric Chemistry (LAC), OFLB, 5232, Villigen PSI, Switzerland

<sup>9</sup> Institute of Atmospheric Sciences and Climate, ISAC, Via P. Gobetti 101, I-40129, Bologna, Italy

<sup>10</sup> Federal Office of Meteorology and Climatology, MeteoSwiss, Chemin de l'aérodrome, 1530 Payerne, Switzerland

<sup>11</sup> ANDRA – DRD – Observation Surveillance, Observatoire Pérenne de l'Environnement, Bure, France

<sup>12</sup> LSCE-Orme point courrier 129 CEA-Orme des Merisiers, 91191 Gif-sur-Yvette, France

<sup>13</sup> ADDAIR, BP 70207 - 189, rue Audemars, 78530, Buc, France

<sup>14</sup> SRI Center for Physical Sciences and Technology, CPST, Sauletekio ave. 3, LT-10257, Vilnius, Lithuania

<sup>15</sup> Institute of Nuclear & Radiological Science & Technology, Energy & Safety, N.C.S.R. "Demokritos", Athens, 15341, Greece

<sup>16</sup> Institut National de l'Environnement Industriel et des Risques, Verneuil en Halatte, 60550, France

<sup>17</sup> Norwegian Institute for Air Research, Atmosphere and Climate Department, NILU, Instituttveien 18, 2007, Kjeller, Norway

<sup>18</sup> Deutscher Wetterdienst, Met. Obs. Hohenpeissenberg, DE-82383 Hohenpeissenberg, Germany

<sup>19</sup> Univ. Grenoble-Alpes, CNRS, IRD, INPG, IGE F-38000 Grenoble, France

<sup>20</sup> TNO B&O, Princetonlaan 6, 3584TA, The Hague, The Netherlands

<sup>21</sup> MTA-PE Air Chemistry Research Group, Veszprém, P.O. Box 158, H-8201, Hungary

<sup>22</sup> Global Change Research Institute AS CR, Belidla 4a, 603 00, Brno, Czech Republic

<sup>23</sup> Czech Hydrometeorological Institute, Na Sabatce 17, 143 06, Praha, Czech Republic.

<sup>24</sup> Environmental Chemical Processes Laboratory, Dept. of Chemistry, Univ. of Crete, Heraklion, 71003, Greece

<sup>25</sup> Institute for Environmental Research & Sustainable Development, National Observatory of Athens (NOA), I. Metaxa & Vas. Pavlou, 15236 Palea Penteli, Greece

<sup>26</sup> Lund University, Department of Physics, P. O. Box 118, SE-22100, Lund, Sweden

<sup>27</sup> CNRS-LaMP Université Blaise Pascal 4, Avenue Blaise Pascal 63178 Aubiere Cedex, France

- 1 <sup>28</sup> *School of Physics and Centre for Climate & Air Pollution Studies, Ryan Institute, National University of*  
2 *Ireland Galway, University Road, Galway, Ireland*
- 3 <sup>29</sup> *EC Joint Research Centre, EC-JRC-IES, Institute for Environment and Sustainability, Via Enrico Fermi*  
4 *2749, 21027, Ispra, Italy*
- 5 <sup>30</sup> *Agencia Estatal de Meteorología, AEMET, Izaña Atmospheric Research Center, La Marina 20, E-38071,*  
6 *Santa Cruz de Tenerife, Spain*
- 7 <sup>31</sup> *Leibniz Institute for Tropospheric Research, (TROPOS), Permoserstraße 15, 04318, Leipzig, Germany*
- 8 <sup>32</sup> *Department of Environmental Science and Analytical Chemistry (ACES) and the Bolin Centre for Climate*  
9 *Research, Stockholm University, SE-106 91 Stockholm, Sweden*
- 10 <sup>33</sup> *Space Physics Laboratory, Vikram Sarabhai Space Centre, ISRO, Thiruvananthapuram – 695022, India.*
- 11
- 12 <sup>a</sup> *now at: EEWRC, The Cyprus Institute, Nicosia, Cyprus*
- 13 <sup>b</sup> *now at: Institute for Aerosol and Sensor Technology, University of Applied Sciences (FHNW), Windisch,*  
14 *Switzerland*
- 15  
16  
17  
18  
19  
20  
21  
22  
23  
24  
25  
26  
27  
28  
29  
30  
31  
32  
33  
34  
35  
36  
37  
38  
39  
40  
41  
42  
43  
44  
45  
46  
47  
48  
49  
50  
51  
52  
53  
54  
55  
56  
57  
58  
59  
60

## Abstract

This paper presents the light scattering properties of atmospheric aerosol particles measured over the past decade at 28 ACTRIS observatories which are located mainly in Europe. The data include particle light scattering ( $\sigma_{sp}$ ) and hemispheric backscattering ( $\sigma_{bsp}$ ) coefficients, scattering Ångström exponent (SAE), backscatter fraction (BF) and asymmetry parameter ( $g$ ). An increasing gradient of  $\sigma_{sp}$  is observed when moving from remote environments (Arctic/mountain) to regional and to urban environments. At regional level in Europe,  $\sigma_{sp}$  also increases when moving from Nordic and Baltic countries and Western Europe to Central/Eastern Europe whereas no clear spatial gradient is observed for other station environments. The SAE does not show a clear gradient as a function of the placement of the station. However, a West to East increasing gradient is observed for both regional and mountain placements suggesting a lower fraction of fine-mode particle in Western/Southwestern Europe compared to Central and Eastern Europe where the fine-mode particles dominate the scattering. The  $g$  does not show any clear gradient by station placement or geographical location reflecting the complex relationship of this parameter with the aerosol particles physical properties. Both the station placement and the geographical location are important factors affecting the intra-annual variability. At mountain sites, higher  $\sigma_{sp}$  and SAE values are measured in the summer due to the enhanced boundary layer influence and/or new particles formation episodes. Conversely, the lower horizontal and vertical dispersion during winter leads to higher  $\sigma_{sp}$  values at all low altitude sites in Central and Eastern Europe compared to summer. These sites also show SAE maxima in the summer (with corresponding  $g$  minima). At all sites, both SAE and  $g$  show a strong variation with aerosol particle loading. The lowest values of  $g$  are always observed together with low  $\sigma_{sp}$  values, indicating a larger contribution from particles in the smaller accumulation mode. During periods of high  $\sigma_{sp}$  values, the variation of  $g$  is less pronounced whereas the SAE increases or decreases, suggesting changes mostly in the coarse aerosol particle mode rather than in the fine mode. Statistically significant decreasing trends of  $\sigma_{sp}$  are observed at 5 out of the 13 stations included in the trend analyses. The total reductions of  $\sigma_{sp}$  are consistent with those reported for  $PM_{2.5}$  and  $PM_{10}$  mass concentrations over similar periods across Europe.

## 1. Introduction

Atmospheric aerosol particles are recognized as an important atmospheric constituent which have demonstrated effects on climate and health. The radiative forcing of aerosol particles, estimated as  $-0.9$  [ $-1.9$  to  $-0.1$ ]  $W/m^2$  (IPCC, 2014), has two competing components: a cooling effect from most particle types and a partially offsetting warming contribution from black carbon (BC) particle light absorption of solar radiation. The aerosol cooling is the dominant effect; thus aerosol particles counteract a substantial portion of the warming effect from well-mixed greenhouse gases (GHGs). This process is driven by the scattering properties of most aerosol particle types (e.g. secondary

1 sulphate and nitrate particles, mineral and organic matter), which reduce the amount of solar  
2 radiation reaching the Earth's surface, instead reflecting it back into space thus modifying the  
3 Earth's radiative balance.

4 However, the high temporal and spatial variability of atmospheric aerosol particles, due to the  
5 wide variety of aerosol sources and sinks, together with their short and variable lifetimes (hours to  
6 weeks in the planetary boundary layer) and spatial non-uniformity, constitute the largest  
7 uncertainties in the estimation of the total radiative forcing. Reducing these uncertainties is  
8 mandatory in view of the global warming the planet has experienced over the past 50 years. In  
9 fact, there is evidence suggesting that the observed (and projected) decrease in emissions of  
10 anthropogenic aerosol particles in response to air quality policies will eventually exert a positive  
11 aerosol effective radiative forcing at the top of the atmosphere (Rotstayn et al., 2013). Thus,  
12 current emission controls could both enhance climate warming while improving air quality (e.g.  
13 Stohl et al., 2015).

14 The measurements of aerosol particle optical properties, such as light scattering and  
15 absorption, together with measurements of their physical and chemical properties, are fundamental  
16 in order to better understand the current trade-off between the impacts of aerosols on  
17 environmental health and the Earth's climate. In recent decades, several international projects  
18 have provided important information on atmospheric particle properties worldwide. Near-surface in  
19 situ observations of aerosol particle properties are being made worldwide under the GAW/WMO  
20 (Global Atmosphere Watch; [http://www.wmo.int/pages/prog/arep/gaw/gaw\\_home\\_en.html](http://www.wmo.int/pages/prog/arep/gaw/gaw_home_en.html))  
21 program and are complemented with policy-oriented programs such as IMPROVE (Interagency  
22 Monitoring of Protected Visual Environments; <http://vista.cira.colostate.edu/Improve/>) in the United  
23 States and EMEP (European Monitoring and Evaluation Programme; <http://www.emep.int/>) in  
24 Europe. Additional information specifically targeting advanced aerosol particle properties have  
25 been obtained in Europe using information from the European research infrastructure ACTRIS  
26 (Aerosols, Clouds, and Trace gases Research InfraStructure; <http://www.actris.eu>) and from short-  
27 term RTD (Research and Technological Development) projects such as EUCAARI (European  
28 Integrated Project on Aerosol Cloud Climate and Air Quality Interactions;  
29 <http://www.cas.manchester.ac.uk/resprojects/eucaari/>).

30 The implementation of the GAW program in Europe is performed under ACTRIS in regard to  
31 the advanced observation of aerosol particle properties. ACTRIS provides harmonized  
32 measurements of different (physical, chemical and optical) aerosol properties in a systematic way  
33 at major observation sites across Europe. More than 60 measuring sites worldwide are currently  
34 providing ground-based in situ aerosol particle light scattering measurements (EBAS database;  
35 [www. http://ebas.nilu.no/](http://ebas.nilu.no/)) and this number has increased substantially in the last decade.  
36 However, EBAS also includes data from the IMPROVE network nephelometers, which latter are

1 operated at ambient conditions with no size cut, as a result of which these IMPROVE data are not  
2 directly comparable to the ACTRIS dataset discussed in this investigation.

3 The objective of this work is to integrate the total aerosol light scattering coefficient ( $\sigma_{sp}$ ) and  
4 hemispheric backscattering coefficient ( $\sigma_{bsp}$ ) measurements performed over several years at the  
5 ground based in situ ACTRIS stations. A total of 28 stations (26 European + 2 non-European) are  
6 included in order to document the variability in near-surface aerosol particle light scattering across  
7 the ACTRIS network. Moreover, at some of the ACTRIS stations more than 10 years of  $\sigma_{sp}$  data  
8 are available, allowing us to perform trend analyses. The study of the trend of  $\sigma_{sp}$  is important  
9 given that a decreasing or increasing trend of  $\sigma_{sp}$  over time would be indicative of the effectiveness  
10 of the air quality control measures. In fact, many studies have shown that the concentrations of  
11 particulate matter (PM), and other air pollutants such as sulphur dioxide (SO<sub>2</sub>) and carbon  
12 monoxide (CO), have clearly decreased during the last 20 years in many European countries  
13 (Barnpadimos et al., 2012; Cusack et al., 2012; EEA, 2013; Querol et al., 2014; Guerreiro et al.,  
14 2014; Pandolfi et al., 2016, Tørseth et al., 2012, among others).

15 Previous studies presenting multi-site ground-based in situ aerosol particle optical  
16 measurements were, for example, performed by Delene and Ogren (2002), Sherman et al. (2015),  
17 Collaud Coen et al. (2013) and Andrews et al. (2011). Delene and Ogren (2002) and Sherman et  
18 al. (2015) reported on the variability of aerosol particle optical properties at four North American  
19 surface monitoring sites. Collaud Coen et al. (2013) presented long term (>8-9 years) aerosol  
20 particle light scattering and absorption measurements performed at 24 regional/remote  
21 observatories located mostly in the United States (although 5 are located in Europe). Andrews et  
22 al. (2011) reported aerosol particle optical measurements performed at 12 mountain top  
23 observatories (4 of which are located in Europe, 5 in the United States and Canada and 3 in Asia).

24 Our work is focused mainly on European observatories and is aimed at presenting a  
25 representative phenomenology of aerosol particle light scattering coefficients measurements at  
26 ACTRIS stations. Thanks to the establishment of European monitoring networks and/or research  
27 projects, five papers relating to aerosol phenomenology have been published in Europe: Van  
28 Dingenen et al. (2004) and Putaud et al. (2004), respectively, on the physical and chemical  
29 characteristics of particulate matter (PM) at the kerbside, urban, rural and background sites in  
30 Europe; Putaud et al. (2010) on the physical and chemical characteristics of PM measured at 60  
31 sites across Europe; Cavalli et al. (2016) on the harmonized concentrations of carbonaceous  
32 aerosols at ten regional background sites in Europe; and Zanatta et al. (2016) presenting a  
33 climatology of BC optical properties at nine European regional background sites. The importance  
34 of these studies and of the present work rests on the premise that a reliable assessment of the  
35 physical, chemical and optical properties of aerosol particles at a European scale is of crucial  
36 importance for an accurate estimation of the radiative forcing of atmospheric aerosols. This work is  
37 the first European phenomenology study dedicated to the light scattering properties of aerosol

1 particles measured in situ at near-surface ground-based observatories. Moreover, the trend  
2 analyses presented can be used to evaluate how the European mitigation strategies adopted to  
3 improve air quality have impacted aerosol particle optical properties.

## 4 5 **2. Experimental**

### 6 **2.1 Atmospheric Observatories**

7 Figure 1 shows the location of the observatories which are grouped according to their geographical  
8 locations, a grouping employed in other European phenomenology studies (e.g. Putaud et al.,  
9 2010). Observatory information (country, code, coordinates, altitude, geographical location, among  
10 others) and measurement periods are summarized in Table 1. The observatories are also divided  
11 into five different categories depending on their placement within each geographical sector. Arctic:  
12 includes stations located in the Arctic/sub-Arctic region; mountain: includes those observatories  
13 located at more than 985 m above sea level (the lowest altitude among the mountain observatories  
14 included here); coastal: includes observatories located close to the coast (<1-4 km); regional/rural:  
15 includes those observatories that are representative of large regional areas; urban/sub-urban:  
16 includes observatories located in a background of an urban or suburban area. Two non-European  
17 stations are also included; one Antarctic site and one mountain site in Bolivia. Given that this work  
18 mainly focuses on European ACTRIS observatories, the results from these two non-European  
19 stations are reported in the Supporting Information.

20 The altitude of the mountain stations considered here range between 985 m at HPB and  
21 5240 m at CHC (cf. Table 1). Some of the mountain stations included in this investigation have  
22 already been included in the work of Andrews et al. (2011), namely IZO, JFJ, CMN, and BEO.  
23 Moreover, the FKL, HPB, JFJ, MHD and PAL stations have been included in the study by Collaud  
24 Coen et al. (2013). Both studies presented in situ aerosol particle optical measurements taken at  
25 these stations. The main results of these previous investigations are summarized in the results  
26 section.

## 27 28 **2.2 Scattering measurements**

### 29 **2.2.1 Instruments**

30 The measurements of  $\sigma_{sp}$  and  $\sigma_{bsp}$  included in this study were obtained from TSI and Ecotech  
31 integrating nephelometers (Table 1). These optical instruments measure the amount of light  
32 scattered by particles in the visible spectrum and provide  $\sigma_{sp}$  and  $\sigma_{bsp}$  coefficients of the sampled  
33 aerosols. The most common nephelometers in the ACTRIS program are the TSI3563 and the  
34 Ecotech AURORA3000 nephelometers, both of which provide both  $\sigma_{sp}$  and  $\sigma_{bsp}$ . Model TSI3563  
35 measures  $\sigma_{sp}$  and  $\sigma_{bsp}$  at 450, 550 and 700 nm whereas the Ecotech AURORA3000 measures at

1 450, 525 and 635 nm. Other models used are the M9003 from Ecotech (SIR and CMN) and the RR  
2 (Radiance Research) nephelometer model M903 (FKL) measuring  $\sigma_{sp}$  at 520 nm and 532 nm,  
3 respectively. Due to the non-homogeneity of the angular distribution of light intensity of model  
4 M9003 (cf. Müller et al., 2009), the light source was changed at SIR in 2013 with the  
5 AURORA3000 light source and at CMN in 2009 with an opal glass light source. After the change of  
6 the light sources, both nephelometers were examined at the World Calibration Center for Aerosol  
7 Physical properties in Leipzig and both performed very well (personal communication from CMN  
8 and SIR data providers). The detailed description of the main characteristics and the working  
9 principle of the integrating nephelometers can be found e.g. in Müller et al. (2011) for the Ecotech  
10 AURORA3000 and in Anderson and Ogren (1998) for the model TSI 3563.

11 Recommended quality assurance procedures during on-site operation, as described in GAW  
12 (WMO-GAW Report, 2016), help to ensure the quality and comparability of the data. The  
13 nephelometers included in this investigation are regularly calibrated using span gas and are zero  
14 adjusted using particle-free air. Additionally, most of the integrating nephelometers employed in  
15 ACTRIS have undergone a schedule of performance checks at the World Calibration Center for  
16 Aerosol Physics of ACTRIS/GAW.

## 17

### 18 **2.2.2 Data treatment**

19 Data used in this investigation include hourly averaged Level 2 aerosol particle scattering data  
20 downloaded from the ACTRIS/EBAS Data Centre web portals ([www.actris.nilu.no](http://www.actris.nilu.no);  
21 [www.ebas.nilu.no](http://www.ebas.nilu.no); last downloads August 2017). The  $\sigma_{sp}$  and  $\sigma_{bsp}$  data reported to EBAS and used  
22 in this work are referenced to standard T (273.15 °C) and P (1013 hPa) conditions. Data  
23 consistency is critical when comparing many years' worth of data from different stations. In this  
24 work, the Level 2 scattering data were further reviewed in order to ensure a high quality of the data  
25 presented. There are however station-to-station differences (e.g. sizecut, RH control, wavelength,  
26 data processing, etc.) which are addressed in the sections below.

#### 27

##### 28 **2.2.2.1 Truncation correction**

29 Data from the integrating nephelometers used here are corrected for non-ideal illumination of the  
30 light source (deviation from a Lambertian distribution of light) and for truncation of the sensing  
31 volumes in the near-forward (around 0-10°) and near-backward (around 170-180°) directions  
32 (Müller et al., 2009 and Anderson and Ogren, 1998). Correction schemes have been provided by  
33 Müller et al. (2009; 2011) for the RR M903 and Ecotech models M9003 and AURORA3000, and by  
34 Anderson and Ogren (1998) for the TSI3563. These schemes consist of a simple linear correction  
35 based on the scattering Ångström exponent (SAE) determined from the raw nephelometer data to  
36 take account of the size-distribution-dependent truncation error. It has been demonstrated that

1 these simple correction schemes are accurate for a wide range of atmospheric aerosols and that  
2 the uncertainties in the corrections are not expected to be larger than 2% for an aerosol particle  
3 population with a single scattering albedos (SSA) greater than 0.8 (Bond et al., 2009).

4 The majority of the  $\sigma_{sp}$  data in the EBAS database are corrected for non-ideal illumination  
5 and for truncation by the data providers. Exceptions are the scattering data submitted for KOS,  
6 MHD, PLA, CMN, FKL and SIR. Scattering data from KOS, MHD and PLA were corrected in this  
7 work using the correction scheme provided by Anderson and Ogren (1998) (cf. Table S1 of the  
8 Supporting Material). The  $\sigma_{sp}$  data collected at CMN, FKL and SIR are not corrected because the  
9 nephelometers deployed at these three stations provide scattering only at one wavelength, thus  
10 preventing the estimation of the SAE. Given that the nephelometer correction factors vary as a  
11 function of SAE, the assumption of a constant correction factor to correct the  $1-\lambda$  scattering data  
12 could introduce undesired noise. Moreover, at SIR and CMN, the  $\sigma_{sp}$  is measured with the single  
13 wavelength Ecotech nephelometer model M9003 (until 2013 at CMN). The correction curve from  
14 Müller et al. (2009; Figure 4) provides a correction factor of around 0.97 to 1.0 for the M9003 for a  
15 SAE of around 1.5 to 2. Using the TSI3563 scattering measurements performed at CMN during  
16 2014-2015, we estimated a mean SAE of around 2 for CMN (cf. Table S5). Thus, given the rather  
17 small effect of the correction factor estimated for the Ecotech M9003, scattering data from CMN  
18 and SIR were not corrected in this work. At FKL the nephelometer models RR M903 (until 2011)  
19 and Ecotech 1000 (from 2012) were used (cf. Table 1). To the best of our knowledge, no correction  
20 scheme has been provided for the Ecotech 1000. Moreover, at FKL, the inlet was changed many  
21 times (cf. Table 1) and the correction factors provided in the literature are a strong function of the  
22 size cut-off used. For these reasons, scattering data collected at FKL are not corrected in this  
23 investigation.

#### 24 25 **2.2.2.2 Relative humidity**

26 The integrating nephelometer measurements within ACTRIS and WMO-GAW should be performed  
27 at a low relative humidity (RH<40%) in order to avoid enhanced scattering due to water uptake of  
28 aerosol particles and in order to make the measurements comparable. For the Ecotech integrating  
29 nephelometers, the RH threshold can be set by using a processor-controlled automatic heater  
30 inside the instrument. At some mountain sites, where whole air is sampled (cf. Table 1), the natural  
31 temperature difference between the outside and inside air dries cloud droplets to the aerosol phase  
32 when a cloud is present at the station. RH is also controlled by de-humidifying in the inlet pipe, as  
33 reported in GAW report 226, to ensure a sampling RH of less than 40%. This recommendation is  
34 intended to ensure that the data are comparable across the network, as measurements would  
35 otherwise would be a strong function of the highly variable sample RH. Currently, at the majority of  
36 ACTRIS observatories, the aerosol particle light scattering measurements are performed at a RH



1 below 40%. However, given that at some stations the 40% RH threshold is sometimes exceeded,  
2 we selected in this work a RH threshold of 50% in order to improve the data coverage.

3 Estimating the aerosol particle light scattering enhancement due to an increase of RH from  
4 40% to 50% is difficult using the data available here because the  $\sigma_{sp}$  measurements at a RH>40%  
5 are not evenly distributed over the measurement periods, with the majority of the stations  
6 registering a RH higher than 40% during the summer. Moreover, the chemical composition of  
7 atmospheric aerosol particles is an important factor determining the magnitude of the scattering  
8 enhancement due to water uptake, which can then change from one site to another (e.g.  
9 Fierz-Schmidhauser et al., 2010a,b; Zieger et al., 2014, 2017). However, the scattering  
10 enhancement due to a change in RH between 40% and 50% should be small and will not exceed  
11 few percent even for more hygroscopic particles (e.g. Fierz-Schmidhauser et al., 2010a,b). Table  
12 S2 in the Supporting Material reports the percentage of hourly  $\sigma_{sp}$  values collected in the range  
13 40%<RH<50% whereas the frequency distributions of the measured RH are shown in Figure S1.

### 15 **2.2.2.3 Available wavelengths**

16 In this work we present and discuss the  $\sigma_{sp}$ , backscatter fraction (BF) and asymmetry parameter  
17 ( $g$ ) measurements obtained using the green wavelength of the integrating nephelometers. The  
18 available wavelengths ranged from 520 nm (2 stations; CMN and VHL) to 550 nm (18 stations).  
19 Other wavelengths used are 525 nm (6 stations) and 532 nm (used at FKL until 2010; cf. Table 2).  
20 An exception is SIR, where only  $\sigma_{sp}$  values at 450 nm are available. The measurements of  $\sigma_{sp}$   
21 reported here are not adjusted to 550 nm, which is generally the most common wavelength (e.g.  
22 Andrews et al., 2011) because of the different data availability of  $\sigma_{sp}$  and SAE at the measuring  
23 stations. As discussed in the following sections, the SAE is calculated for  $\sigma_{sp}$  data higher than 0.8  
24  $Mm^{-1}$ , thus leading to different data coverage for  $\sigma_{sp}$  and SAE and preventing the adjustment of all  
25 measured  $\sigma_{sp}$  to 550 nm. Moreover, the SAE is not available at FKL and SIR (or at CMN until  
26 2014) thus preventing any wavelength adjustment at these stations. Using the mean SAE  
27 calculated at those stations, where  $\sigma_{sp}$  is measured at wavelengths in addition to 550 nm (cf.  
28 Tables S4 and S5 in Supporting material), we estimate differences in the  $\sigma_{sp}$  values of less than  
29 6% after adjusting to 550 nm. At FKL and SIR, where the SAE is not available, and assuming a  
30 reasonable SAE range between 1.5 and 1.0, the difference due to the adjustment to 550 nm is 4.9-  
31 3.0% at FKL and 26-18% at SIR. The higher difference at SIR is due to the fact that measurements  
32 at this station are performed at 450 nm. Finally, at CMN, the effect of the adjustment of  $\sigma_{sp}$  to 550  
33 nm (from 520 nm) using a mean SAE of 2 (calculated using the 3- $\lambda$  nephelometer data from 2014;  
34 cf. Table S5) is below 10%.

#### 2.2.2.4 Inlet size cut changes

It should be noted that any comparison of the  $\sigma_{sp}$  and SAE values among the different stations and the presented trend analyses could be slightly biased by the different particle size cuts upstream of the integrating nephelometers used in this work (cf. Table 1). Currently, all ACTRIS integrating nephelometers measure whole air or  $PM_{10}$ , with the exception of SIR, where the  $PM_1$  inlet is used. Whole air is currently measured at mountain observatories (BEO, CMN, JFJ, PUY, CHC), one coastal observatory (MHD) and one urban observatory (UGR) (cf. Table 1).

At some stations, the inlet was changed from whole air to  $PM_{10}$  at some point, namely at OPE, FKL and TRL. Given the lower scattering efficiency of aerosol particles larger than  $10\ \mu m$ , no important differences in the aerosol particle optical parameters should be expected between aerosol particles sampled with a whole air and a  $PM_{10}$  cut-off. At the other stations the inlet was changed during the measurement period from a cut-off lower than  $10\ \mu m$  ( $1\ \mu m$  at KPS;  $2.5\ \mu m$  or  $5\ \mu m$  at PAL, MSA and MAD) to  $PM_{10}$ . For PAL (where a median SAE of around 1.8 was measured; cf. Paragraph 3.2 and Table S5), Lihavainen et al. (2015a) assumed that the inlet changes (from  $PM_5$  to  $PM_{2.5}$  in 2005 and from  $PM_{2.5}$  to  $PM_{10}$ , cf. Table 1) had only minor effects on scattering because the number concentration of coarse particles is very low at PAL. Similarly, the KPS observatory registers among the highest SAE values observed in the network (median value of around 2; cf. Paragraph 3.2 and Table S5) suggesting an aerosol particle size distribution dominated by fine particles. Moreover, at KPS, the inlet was changed in April 2008, less than 1.5 years after the measurements commenced, and thus likely has also a minor effect in the trend analyses and climatology performed at this site over the period 2006 to 2014. Two stations (MSA and MAD) changed the inlet from a  $PM_{2.5}$  diameter cut-off to  $PM_{10}$ . For these two Southern European stations the inlet change may have had an effect on the SAE, especially during Saharan dust outbreaks, which are however sporadic events. Finally, the FKL observatory was removed from the trend analysis because the inlet was changed from whole air to  $PM_{10}$  in 2009, from  $PM_{10}$  to  $PM_1$  in 2011 and again from  $PM_1$  to  $PM_{10}$  in 2013 (cf. Table 1). These events likely had a major effect on the measured particle optical properties.

A sensitivity study (not shown) was performed to assess the effect of the inlet changes on the SAE values measured at the aforementioned stations. We looked at the climatology of SAE for different inlet sizes and for different time periods (with and without inlet size changes) and we did not observe any obvious change in the climatology as a function of size cut due to interannual variability. Thus, despite the differences in the particle diameter cut-off, the comparison between the different stations seems feasible.

### 2.2.3 Calculation of aerosol particle intensive optical properties

Starting from the spectral  $\sigma_{sp}$  measurements performed at the ACTRIS observatories, three intensive aerosol particle optical parameters can be estimated, namely; the scattering Ångström exponent (SAE), the backscattering fraction (BF) and the asymmetry parameter ( $g$ ). These intensive properties do not depend on the PM mass concentration and are directly related to aerosol particle properties such as size, shape, size distribution and chemical composition. The SAE can be considered as a proxy for the aerosol particle size range with a higher (lower) SAE associated with predominance of fine (coarse) aerosol particles (e.g. Seinfeld and Pandis, 1998; Esteve et al., 2012; Valenzuela et al., 2015 among others). The BF and  $g$  parameters are calculated quantities that influence the variability of the radiative forcing efficiency and that represent the angular light scattering of aerosol particles. For computational efficiency, the angular light scattering is often represented by a single value (BF,  $\sigma_{sp}/\sigma_{bsp}$  or  $g$ ) (Andrews et al., 2006).

The SAE characterizes the wavelength dependency of  $\sigma_{sp}$  and it can be calculated as follows:

$$SAE = - \frac{\log\left(\frac{\sigma_{sp}^{\lambda_1}}{\sigma_{sp}^{\lambda_2}}\right)}{\log\left(\frac{\lambda_1}{\lambda_2}\right)} \quad . \quad (Eq. 1)$$

Here, the SAE is derived from a multispectral log linear fit based on the three nephelometer wavelengths. The SAE depends on the particle size distribution and takes values greater than 2 when the light scattering is dominated by fine particles (radii  $\leq 0.5 \mu\text{m}$  as e.g. in Schuster et al. (2006)), while it is lower than one when the light scattering is dominated by coarse particles (Seinfeld and Pandis, 1998; Schuster et al., 2006).

The asymmetry parameter ( $g$ ) (Andrews et al., 2006; Delene and Ogren, 2002) describes the probability that the radiation is scattered in a given direction and it is defined as the cosine-weighted average of the phase function. Thus,  $g$  yields information regarding the amount of radiation that a particle scatters in the forward direction compared to the backward direction. Theoretically, the values of  $g$  can range from  $-1$  for only back scattering to  $+1$  for complete forward scattering, with a value of  $0.7$  commonly used in radiative transfer models. The  $g$  parameter can be estimated from the backscatter fraction (BF), which is the ratio of  $\sigma_{bsp}$  and  $\sigma_{sp}$  (Andrews et al., 2006):

$$g = -7.14(BF)^3 + 7.46(BF)^2 - 3.96(BF) + 0.9893 \quad . \quad (Eq. 2)$$

### 2.2.4 Data coverage

Table S3 in the Supporting Material reports the percentage [%] of data coverage at the 28 ACTRIS stations included in this study. Removed data include data flagged as non-valid by the data

1 providers (instrument failure, calibration periods, unspecified contamination or local influence, etc.)  
2 or obtained at a RH of greater than 50%. The data coverage for the extensive measured aerosol  
3 particle optical properties ( $\sigma_{sp}$  and  $\sigma_{bsp}$ ) is generally high, ranging from around 60% to 95%.  
4 Exceptions are the  $\sigma_{sp}$  measurements at CMN in the blue (450 nm) and red (700 nm) wavelengths  
5 which have much less data coverage compared to the green wavelength because the three  
6 wavelength nephelometer was implemented at CMN in 2014. Consequently, also the SAE and  $g$   
7 have low data coverage at CMN. Moreover, lower data coverage (< 40%) was registered at PLA  
8 and VHL.

9 The data coverage for the intensive aerosol particle optical properties (SAE and  $g$ ) is  
10 generally lower compared to the data coverage of  $\sigma_{sp}$  and  $\sigma_{bsp}$ . This is because the intensive  
11 optical properties are calculated from hourly  $\sigma_{sp}$  and  $\sigma_{bsp}$  data higher than  $0.8 \text{ Mm}^{-1}$  to avoid noise  
12 in the calculations. As a consequence, the data coverage of the intensive properties is lower at  
13 those stations measuring low  $\sigma_{sp}$  and  $\sigma_{bsp}$  values (e.g. mountain and remote sites). For example, at  
14 JFJ, the SAE and  $g$  data coverages are around 54% and 22%, respectively. At TRL, these values  
15 are even lower, at 21% and 1%, respectively. However, as reported in Table S3, at the majority of  
16 the stations the data coverage of SAE and  $g$  is higher than 60%.

### 18 3. Results/Discussion

#### 19 3.1 Variability of $\sigma_{sp}$

20 Figure 2 shows the box-and-whiskers plots of  $\sigma_{sp}$  measured at the stations included in this  
21 investigation. In Figure 2, the observatories are grouped based on their placement and ordered  
22 according to their geographical location. Table S4 and Figure S2 in the Supplementary Material  
23 report, respectively, the statistics of  $\sigma_{sp}$  (mean, standard deviation, minimum and maximum values  
24 and 5th, 25th, 50th, 75th, and 95th percentiles) and frequency and cumulative frequency  
25 distributions.  
26

27 In each geographical sector, an increasing gradient of  $\sigma_{sp}$  is generally observed when  
28 moving from mountain to regional and to urban sites. Thus, the  $\sigma_{sp}$  values measured at mountain  
29 sites are lower than the measurements made at other locations (coastal to urban) even if  
30 exceptions are observed in some sectors.

31 A large range of  $\sigma_{sp}$  coefficients is observed across the network, ranging from median values  
32 lower than  $10 \text{ Mm}^{-1}$  to values higher than  $40 \text{ Mm}^{-1}$ . Overall, the lowest  $\sigma_{sp}$  is on average measured  
33 at remote stations because of either: a) their altitude, for example JFJ is located in Central Europe  
34 at more than 3500 m a.s.l. and CHC in Bolivia is at around 5300 m a.s.l. (cf. Figure S3), or b)  
35 because of their large distance from pollution sources, for example the Arctic ZEP and PAL  
36 stations, TRL station (cf. Figure S3) and some regional sites in the Nordic and Baltic sector such

1 as BIR and SMR. Higher  $\sigma_{sp}$  values (medians  $> 40 \text{ Mm}^{-1}$ ) are on average registered at more  
2 polluted sites, such as some urban sites in Southern Europe (UGR and DEM), some regional sites  
3 in Eastern and Central Europe (KPS and IPR, respectively) and one coastal site in the Nordic and  
4 Baltic sector (PLA).

5 The observed variation is consistent with the differences in particulate matter (PM) mass  
6 concentrations, PM chemical composition, particle number concentration and absorption  
7 coefficients observed across Europe, as described for example by Putaud et al. (2010), Asmi et al.  
8 (2011) and Zanatta et al. (2016).

9 Figures 3a and 3b show the relationship between the mean particle number concentration  
10 measured at different stations during 2008 to 2009 (and reported in Asmi et al. (2011)) and the  
11 mean  $\sigma_{sp}$  measured over the same period (where available). As reported in Figure 3, good  
12 correlations are observed between N50 (Figure 3a: mean/median particle number between 50 nm  
13 and 500 nm) and N100 (Figure 3b: mean/median particle number between 100 nm and 500 nm)  
14 and mean  $\sigma_{sp}$ . Figure 3c shows the relationship (for some stations) between absorption coefficients  
15 reported in Zanatta et al. (2016) and the total scattering. The good correlations reported in Figure  
16 3c (especially high for the winter and autumn periods) suggest an increase of both scattering and  
17 absorption coefficients with increasing aerosol loading. Figure 3c also reports the mean single  
18 scattering albedo (SSA). On average lower SSA is observed at IPR, whereas higher SSA is  
19 observed at the Nordic and Baltic VHL and BIR observatories.

20 Finally, at all stations included in this work, the skewness of the  $\sigma_{sp}$  distributions (cf. Table  
21 S4) is higher than one and ranges between 1.4 at PLA and 10.6 at TRL (skewness calculated from  
22 hourly averaged data). The skewness can be used to evaluate the asymmetry of a distribution.  
23 Positive skewness is usually observed for parameters which are defined to be positive and it  
24 indicates that the tail on the right side of the distribution is longer or fatter than that on the left side.  
25 Thus, for a right-skewed distribution, the mass of the distribution is concentrated on the left, and  
26 there is a higher probability of measuring a high value compared to a left-skewed distribution. For  
27 example Querol et al. (2009) used the skewness to assess the importance of Saharan dust  
28 outbreaks on  $\text{PM}_{10}$  levels measured at different sites across the Mediterranean basin. They found  
29 a positive correlation between the calculated skewness and the net dust contribution to the  
30 measured  $\text{PM}_{10}$  concentration (i.e. the strength of dust pollution episodes; cf. Fig. 6 in Querol et al.,  
31 2009). Figure S2 in the Supporting Material shows the frequency and cumulative frequency  
32 distributions for  $\sigma_{sp}$  for each station, evidencing the presence of these right-skewed tails.

### 34 3.1.1 $\sigma_{sp}$ at Arctic/Antarctic observatories

35 The Arctic (ZEP and PAL; cf. Fig 2) and Antarctic (TRL; cf. Figure S3) monitoring stations are  
36 located in undisturbed environments with minimal influence from the local settlement because they

1 are located above the inversion layer. The mean  $\sigma_{sp}$  values measured at ZEP and TRL are by far  
2 the lowest across the network, whereas higher  $\sigma_{sp}$  values are measured at PAL. PAL is located in  
3 a remote continental area characterized by the absence of large local and regional pollution  
4 sources (e.g. Aaltonen et al., 2006). However, Lihavainen et al. (2015a) reported that high values  
5 of the absorption coefficient and low values of the single scattering albedo at PAL are related to  
6 continental air masses from lower latitudes. Despite this, the mean  $\sigma_{sp}$  at PAL is among the lowest  
7 in the ACTRIS network and is comparable to the mean  $\sigma_{sp}$  observed at the JFJ and CHC  
8 mountaintop observatories (cf. Table S4).

### 9 10 **3.1.2 $\sigma_{sp}$ at mountain observatories**

11 Differences can be observed among stations with similar environments but different geographical  
12 locations. For mountain observatories, a clear gradient is not observed when moving from West to  
13 Southeast Europe, because the altitude of the station is an important parameter contributing to the  
14  $\sigma_{sp}$  measured at these observatories. Among the mountain stations a higher mean  $\sigma_{sp}$  is on  
15 average measured at HPB and IZO (cf. Table S4). The HPB station is likely to be more influenced  
16 by the PBL than other mountain stations due to its lower altitude (Nyeki et al., 2012; Collaud Coen  
17 et al., 2017), whereas IZO is largely influenced by Saharan dust outbreaks transporting dust  
18 toward the station (e.g. Rodriguez et al., 2011) thus increasing  $\sigma_{sp}$ . In fact, at IZO, the median  
19 value of  $\sigma_{sp}$  is among the lowest measured at these mountain sites (around  $7 \text{ Mm}^{-1}$ ; cf. Table S4)  
20 indicating that the sporadic but extremely intense pollution episodes due to Saharan mineral dust  
21 outbreaks strongly affect the mean  $\sigma_{sp}$  at this station.

22 Despite their placement at higher altitudes, both CMN and BEO (more than 2 km a.s.l.) register  
23 similar  $\sigma_{sp}$  values compared to PUY and MSA (around 1.5 km a.s.l.) likely because the effect of  
24 important regional pollution sources (i.e. the Po Valley for CMN) affecting, under favourable  
25 meteorological conditions, these Central and Eastern European observatories (i.e. Marengo et al.,  
26 2004). Conversely, the region around the MSA observatory is sparsely populated and the station is  
27 isolated from large urban and industrial agglomerations (i.e. Pandolfi et al., 2014; Ripoll et al.,  
28 2014; Ealo et al., 2016). PUY observatory is surrounded by a protected area with fields and forests  
29 and previous works have shown that the influence of the Clermont-Ferrand city on the PUY  
30 measurements remains too small to be detected (i.e. Asmi et al. 2011).

31 The lowest median  $\sigma_{sp}$  values at mountain sites are on average measured at JFJ, probably due to  
32 the higher altitude of this station compared to other mountain stations included in this work and/or  
33 its distance from important pollution sources. Moreover, Collaud Coen et al. (2017) reported a low  
34 PBL influence at this site due to the location of the station in a dominant position within the whole  
35 mountainous massif. CHC (cf. Figure S3) registers higher median  $\sigma_{sp}$  values compared to JFJ  
36 despite its location at around 5300 m a.s.l. likely due to the influence of the emissions from the city

1 of La Paz (3600 m a.s.l.), located around 30 km from the CHC site, and the local topography,  
2 which facilitates the uplift of air masses toward the CHC observatory (Collaud Coen et al., 2017).

### 3 4 **3.1.3 $\sigma_{sp}$ at coastal observatories**

5 The PLA coastal station registered  $\sigma_{sp}$  values which are higher compared to both other Nordic and  
6 Baltic stations and other coastal sites (e.g. MHD and FKL) and which are amongst the highest in  
7 Europe. Kecorius et al. (2016) have shown that ship emissions in the Baltic Sea contribute strongly  
8 to pollution levels at PLA and that up to 50% of particles arriving at PLA are generated by  
9 processes and emissions, including shipping, taking place in areas upwind of the station.  
10 Moreover, Asmi et al. (2011) presented a number of similarities in particle number concentrations  
11 measured at PLA to those measured at some Central European sites, such as IPR, which are due  
12 to the influence of multiple source areas (cf. Figure 3). It should be noted however, that the period  
13 with available  $\sigma_{sp}$  measurements is very short at PLA (cf. Table 1 and Figure 7) and the data  
14 coverage is also low (cf. Table S3). Consequently, more measurements at this site are needed in  
15 order to confirm the  $\sigma_{sp}$  values reported there. The other two coastal stations (MHD and FKL)  
16 register median  $\sigma_{sp}$  values in the upper range of  $\sigma_{sp}$  measured across the network, mostly due to  
17 the contribution of marine aerosols in winter and mineral dust in summer at MHD and FKL,  
18 respectively (cf. Section 3.5).

### 19 20 **3.1.4 $\sigma_{sp}$ at regional/rural observatories**

21 Regional sites exhibit a large variability in  $\sigma_{sp}$  coefficients across Europe, with the lowest values  
22 measured at BIR and SMR (Nordic and Baltic) and the highest at IPR (central Europe) and KPS  
23 (Eastern Europe). Thus, a gradient is observed in  $\sigma_{sp}$  when moving from West to East Europe. At  
24 both IPR and KPS, the frequent winter time episodes, linked to stable air due to strong thermal  
25 inversions, affect the level of pollution at these sites (e.g. Putaud et al., 2014; Molnár et al., 2016).  
26 It is known that at the IPR station, even though it lies several tens of kilometres away from large  
27 pollution sources, is located in an area (the Po Valley) which is one of the most polluted regions in  
28 Europe (e.g. van Donkelaar et al., 2010). The VHL observatory registers an on average higher  $\sigma_{sp}$   
29 compared to PAL and compared to the BIR and SMR regional sites likely because VHL is located  
30 closer to the European continent and it is consequently more affected by polluted continental air  
31 masses. Moreover, the emissions from the densely populated areas of Helsingborg and Malmö  
32 and the city of Copenhagen, located 25 km to the west, 50 km to the south and 45 km to the south-  
33 east, respectively, could also explain the relatively high  $\sigma_{sp}$  measured at VHL (Kecorius et al.,  
34 2016). The  $\sigma_{sp}$  values at a regional level in Western Europe (OPE and CBW) are on average  
35 higher compared to those measured in the Nordic and Baltic regions and lower compared to those

1 measured at a regional level in Southern Europe (MSY). The relatively higher  $\sigma_{sp}$  values measured  
2 at MSY are due to both the contaminated air transported by the sea breeze from the close  
3 metropolitan area of Barcelona to the mountains and the frequent Saharan dust outbreaks (i.e.  
4 Pandolfi et al., 2011; 2014a).

### 6 **3.1.5 $\sigma_{sp}$ at urban/sub-urban observatories**

7 Among the urban background sites, lower  $\sigma_{sp}$  values are measured at MAD and SIR compared to  
8 DEM and UGR. The low  $\sigma_{sp}$  at MAD during the period presented here (only 2014 data are available  
9 for MAD) could be related to the reduced formation of secondary nitrate aerosols due to the limited  
10 availability of ammonia in this urban environment (Revuelta et al., 2014). However, it should be  
11 noted that winter episodes with high secondary nitrate concentrations are not uncommon in Madrid  
12 and we are presenting here only one year of measurements for this station. On the other hand,  
13 secondary inorganic aerosol concentrations recorded at the SIR sub-urban observatory can be  
14 considered as representative of a large geographical zone, given the rather flat orography of the  
15 Parisian basin. At UGR, the accumulation, mainly in winter, of fine particles from traffic, domestic  
16 heating and the burning of biomass explains the relatively higher  $\sigma_{sp}$  (e.g. Lyamani et al., 2012;  
17 Titos et al., 2017). Traffic emissions, the high level of formation of secondary sulphate and organic  
18 aerosols in the summer and the transport of dust from Africa are the main contributory factors to  
19 the high  $\sigma_{sp}$  at DEM where high  $PM_{2.5}$  and  $PM_{10}$  values are usually measured as compared to other  
20 important Mediterranean cities (e.g.: Diapouli et al., 2017; Eleftheriadis et al., 2014; Karanasiou et  
21 al. 2014; Querol et al., 2009).

## 23 **3.2 Variability of SAE**

24 Figure 4 shows the box-and-whiskers plots of the SAE calculated at the different stations. Table S5  
25 and Figure S4 in the Supplementary Material report the statistics of the SAE and frequency and  
26 cumulative frequency distributions, respectively.

### 29 **3.2.1 Variability of SAE by geographical sector**

30 The SAE shows a large variability across the geographical sectors considered in this study (Figure  
31 4). On average, independently from of the station setting, the highest SAE is observed at the  
32 Central and Eastern European observatories (cf. Table S5) with station-averaged values of  $1.88 \pm$   
33  $0.49$  and  $1.88 \pm 0.53$ , respectively. The high SAE values in Central and Eastern Europe indicate  
34 clearly the predominance of fine particles. In fact, high  $PM_{2.5}/PM_{10}$  ratios, indicative of the presence  
35 of small particles, are typical for rural lowland sites in Central Europe (e.g. Spindler et al., 2010;  
36 EMEP, 2008). Figure S4 shows that the frequency plots of SAE data have very similar unimodal  
delta-like distributions and the variability of the SAE within the 5th to the 95th percentile range is



1 much lower than that of the other European regions, suggesting a greater homogeneity in some  
2 microphysical properties of atmospheric particles such as size. Exceptions are the CMN, JFJ and  
3 BEO mountain sites, where left-tailed SAE distributions are observed, likely due to the reduced  
4 effect of fine particles from the PBL in winter and an increase in the relative importance of coarse  
5 mineral dust, sea salt particles as well as aged aerosols compared to lower altitude stations in the  
6 same geographical sector.

7 On average, the SAE is lower for all other geographical sectors. Station-averaged mean SAE  
8 of around  $1.60 \pm 0.61$ ,  $1.25 \pm 0.86$  and  $1.36 \pm 0.67$  are observed in the Nordic and Baltic, Western  
9 and Southwestern sectors, respectively. Exceptions are however observed. For example, at CBW  
10 (Western Europe) the median SAE reaches values of around 2.1. Indeed, both polluted air masses  
11 from the industrialized zones of the Benelux countries and clean air masses from the sea  
12 contribute to the presence of aerosol particles at this site (Crumeyrole, et al., 2010). Moreover,  
13 CBW is surrounded by several large cities at distances of approximately 20 to 40 km from the  
14 station, which may have contributed to the high SAE values measured in this geographical  
15 location. Asmi et al. (2011) have also shown that background particle number concentrations at  
16 CBW are much higher than, for example, at BIR.

17 Median SAE values close to one or lower, indicative of the fact that the  $\sigma_{sp}$  is dominated by  
18 large particles, are observed at remote sites in Western Europe (MHD), Southwestern Europe  
19 (IZO) and the Nordic and Baltic (ZEP) and Antarctic (TRL) regions. A low SAE at MHD has already  
20 been reported by Vaishya et al. (2011, 2012) and justified by the frequent presence, mainly in  
21 winter, of coarse-mode sea-salt particles, since mineral dust particles can be ruled out. In fact, air  
22 masses originating from dust sources are infrequent at these sites. Similarly, the low SAE  
23 observed at ZEP and TRL can be associated with the presence of coarse sea-salt particles (e.g.  
24 Zieger et al., 2010 for ZEP). Conversely, the SAE obtained at IZO is mainly due to the frequent  
25 presence of mineral dust particles from African deserts (e.g. Rodríguez et al., 2011). Very similar  
26 bi-modal frequency distributions are observed at MHD and IZO, showing a pronounced left peak  
27 indicative of the high probability of encountering coarse particles at these sites. BIR and PLA also  
28 show an enhanced left peak in the SAE frequency distributions likely due to the presence of coarse  
29 marine aerosols at these sites.

### 31 **3.2.2 Variability of SAE by station type**

32 Unlike  $\sigma_{sp}$ , the SAE does not show any clear gradient when moving from mountainous to  
33 regional/urban sites in each geographical sector. For example, at mountain sites the median SAE  
34 ranges between around 0.7 at IZO (Southwest Europe) and values higher than two at JFJ and  
35 CMN (Central Europe). As reported by Zieger et al. (2012) a SAE value of around 2 prevails for  
36 most of the time at JFJ and can be regarded as the typical background under non-dusty conditions.  
37 Thus, the SAE values at JFJ and CMN can be considered as representative of Central Europe's  
38 free troposphere, especially in winter when the PBL emissions at these sites are reduced. This  
39 high variability of SAE at mountain sites was also reported by Andrews et al. (2011) with values

1 from 11 mountaintop stations worldwide ranging from less than one to more than two. Moreover,  
2 Bourcier et al. (2012) have shown that coarse particles are transported more efficiently at high  
3 altitude by the higher wind speed, thus probably also contributing to the observed variability of SAE  
4 at mountain sites.

5 Also at coastal sites (PLA and MHD), the SAE shows large variability, with higher SAE  
6 measured at PLA compared to MHD, confirming a higher effect of anthropogenic emissions at PLA  
7 compared to MHD.

8 An increasing gradient of SAE is observed when moving from regional/rural observatories in  
9 the Northwest of Europe to regional/rural observatories in the east of Europe. Among these  
10 stations, the lowest SAE is observed at VHL (Nordic and Baltic) and MSY (Southwestern Europe),  
11 whereas, as already observed, central and eastern regional areas are characterized by high SAE  
12 values. This gradient is also driven by the importance of sea salt or dust particle contributions  
13 affecting more the Northwestern and Southwestern European countries compared to countries in  
14 Central and Eastern Europe.

15 Among the urban sites, MAD registers the lowest median SAE (1.47) compared to UGR  
16 (1.69) and DEM (1.60). The lower SAE at MAD could be explained, as already noted, by the  
17 reduced formation of secondary inorganic aerosols during the available measurement period.  
18 Moreover, re-suspended dust from vehicles could also explain the lower SAE observed at the MAD  
19 observatory.

### 21 **3.3 Variability of $g$**

22 The asymmetry parameter is widely used in radiative transfer models because it provides  
23 information regarding how much radiation is scattered back compared to the amount of radiation  
24 scattered in the forward direction. Figure 5 shows the box-and-whiskers plots of  $g$  calculated at the  
25 different stations. Table S6 and Figure S5 in the Supporting Material report the statistics of  $g$  and  
26 the frequency and cumulative frequency distributions, respectively. Given that  $g$  is calculated from  
27 BF using Equation 2 (Section 2.2.3), we report in Figure S6 of the Supporting material the box-and-  
28 whiskers plots of BF, whereas Table S7 reports the statistics of BF. Figure 5 and Figure S6 are  
29 symmetrical, with a lower BF corresponding to a higher  $g$ .

#### 31 **3.3.1 Variability of $g$ by geographical sector**

32 Unlike the SAE, the  $g$  parameter does not show any clear gradient when moving from the west to  
33 the east of Europe. Slightly higher  $g$  values are observed in Western Europe (station-averaged  
34 mean  $g$  of  $0.61 \pm 0.08$ ) compared to Central and Eastern Europe (mean  $g = 0.59 \pm 0.07$  and  $0.57 \pm$   
35  $0.06$ , respectively). These differences in the  $g$  values, even if small, are consistent with the  
36 opposite gradient observed for SAE, this latter being smaller in Western Europe. However, the  
37 station-averaged  $g$  in Central and Eastern Europe is similar to the mean  $g$  observed in the Nordic  
38 and Baltic regions (mean  $g = 0.58 \pm 0.08$ ) and in Southwestern Europe (mean  $g = 0.57 \pm 0.06$ ).

1 Thus, contrary to the SAE, a clear relationship between aerosol size and  $g$  is not observed. The  
2 possible reasons for this are reported below.

### 3.3.2 Variability of $g$ by station type

4 At some mountain sites higher median  $g$  values are observed relative to the  $g$  values obtained at  
5 regional or urban locations. This is the case for example for IZO compared to MSY, UGR and MAD  
6 in the Southwestern European sector and for HPB and JFJ compared to IPR, MPZ and KOS in  
7 Central Europe. However, exceptions are observed. For example at CMN, where the median  $g$   
8 value (only 2 years of data are available) is the lowest in the Central European sector and among  
9 the lowest observed in this study. On average,  $g$  values range between 0.49 and 0.64 at mountain  
10 sites, with a mean value of  $0.58 \pm 0.05$ . This value is consistent with the mean value of  $0.61 \pm 0.05$   
11 reported by Andrews et al. (2011) at the mountain sites included in their work.

12 Figure S7 in the Supporting Material reports the mean SAE (ordered from low to high values  
13 for each station setting) and  $g$  at each station used in this work together with the SAE- $g$  scatter  
14 plot. Figure S7 shows that no clear relationship between  $g$  and SAE is observed. For example, the  
15 TRL and MHD observatories register among the highest  $g$  values observed in the network which is  
16 consistent with the very low SAE measured at these stations because of the frequent presence of  
17 coarse-mode sea-salt particles (cf. Figure 4). However, high  $g$  values, similar to TRL and MHD, are  
18 also observed at stations such as PLA, BIR, JFJ and DEM, which are dominated on average by  
19 fine aerosol particles (with SAE values similar to or higher than 1.5). Similarly, similar  $g$  values are  
20 observed at IZA and PUY or HPB despite the differences in SAE values at these observatories.

21 Differences in the shape of the particle number size distribution, particle shape and chemical  
22 composition (e.g. refractive index, RI) are likely factors contributing to the poor relationship  
23 observed between  $g$  and SAE. The Mie theory of polydisperse spherical particles predicts that the  
24 BF is lower and  $g$  correspondingly higher for coarse-mode aerosol particles (for which the SAE will  
25 be low) compared to fine-mode particles. However, some studies deploying integrating  
26 nephelometers have found that the BF can be higher for coarse-mode aerosol particles (such as  
27 mineral dust) than for fine-mode aerosol particles (Carrico et al., 2003; Doherty et al., 2005).  
28 Doherty et al. (2005) suggested that an under-correction for the  $\sigma_{sp}$  truncation of the forward-  
29 scattered radiation (which is relatively larger for coarse particles) could bias the calculated BF  
30 toward high values. Moreover, the shape of the particle number size distribution is another factor  
31 affecting the BF and SAE. Thus, differences in the relative fractions of the fine and coarse modes  
32 could also drive the BF-SAE relationship. In fact, the SAE is most sensitive to the presence of  
33 coarse-mode aerosol particles compared to the BF, which is most sensitive to small accumulation-  
34 mode particles (Delene and Ogren, 2002; Collaud Coen et al., 2007). Thus, depending on the  
35 shape of the particle number size distribution, the BF and SAE values might or might not correlate.

36 The refractive index (RI), which is strongly related to the chemical composition of the  
37 particles, is another important variable that can affect  $g$  (e.g. Marshall et al., 1995). In the work of  
38 Hansen and Travis (1974; Figure 12) the authors showed that, for a given particle diameter, the  $g$   
39

1 parameter non-linearly decreased with increasing real RI. Thus, coarse-mode particles with a given  
2 RI could have an asymmetry parameter similar to or lower than that of fine particles with lower RI.  
3 Recently, Obiso et al. (2017) confirmed the findings of Hansen and Travis (1974), showing also  
4 that for fine particles a perturbation in the RI of 20% has a larger effect on  $g$  than a similar relative  
5 perturbation of particle shape. Obiso et al. (2017) also showed that a variation of the RI for coarse  
6 particles can have a small effect on the mass scattering efficiency of a particle and its spectral  
7 dependence, and consequently also on SAE.

### 8 9 **3.4 Seasonal variability**

10 Figures 6, 7 and 8 present the annual cycles of  $\sigma_{sp}$ , SAE and  $g$ , respectively, at each site. The  
11 annual cycles for the non-European CHC and TRL stations are reported in Figure S8 in the  
12 Supporting Material. Overall, strong seasonal cycles of  $\sigma_{sp}$  and intensive aerosol particle optical  
13 parameters are observed at the majority of the stations, although exceptions are observed. The  
14 analysis of the annual cycles is presented below separately for different station settings.

#### 15 16 **3.4.1 Seasonal variability at Arctic observatories**

17 ZEP and PAL observatories present quite different annual cycles of  $\sigma_{sp}$ . At ZEP, the highest  $\sigma_{sp}$  is  
18 observed in late winter and in spring whereas the lowest  $\sigma_{sp}$  is observed in the summer. The  $\sigma_{sp}$   
19 values increase in late winter and spring due to the Arctic Haze phenomenon, i.e. layers with  
20 enhanced concentrations of aerosols and precursor gases in the Arctic troposphere caused by  
21 anthropogenic sources and long-range transport (i.e. Engvall et al., 2008; Ström et al., 2003).  
22 Ström et al. (2003) have shown that, during winter and spring, the aerosol particle accumulation-  
23 mode dominates. Conversely, in summer, this mode is significantly smaller and Aitken-mode-sized  
24 aerosols dominate the size distribution. The change in the aerosol size distribution between  
25 winter/spring and summer is likely the cause of the observed variations of  $\sigma_{sp}$  and  $g$  at ZEP, the  
26 latter being slightly larger in late winter and spring compared to the summer. At PAL observatory,  
27 an on average higher  $\sigma_{sp}$  is observed in spring/summer compared to autumn/winter. As reported by  
28 Lihavainen et al. (2015a), low values of  $\sigma_{sp}$  in autumn and early winter can be related to frequent  
29 precipitation events, whereas the high values of  $\sigma_{sp}$  in summer are probably related to biogenic  
30 organic aerosols from natural sources. At PAL, the monthly variation of SAE and  $g$  is rather  
31 pronounced: SAE ( $g$ ) increases (decreases) in summer compared to winter, indicating the  
32 predominance of relatively smaller particles during the warmest months. Lihavainen et al. (2015a)  
33 observed that the seasonal variations in intensive aerosol optical properties at PAL are related to  
34 both the transport of different air masses at this remote site depending on the season, and the  
35 enhanced formation of BSOA (biogenic secondary organic aerosols) in the summer. Lihavainen et  
36 al. (2015a) also reported a lower single scattering albedo in winter compared to summer at PAL  
37 due to a significant contribution from light absorbing carbon, mostly from residential wood

1 combustion. Thus, they have shown that aerosol particles observed in the summer at PAL have  
2 the potential to cool the atmosphere more efficiently than those observed during winter.

### 3 4 **3.4.2 Seasonal variability at mountain observatories**

5 At the mountain stations (PUY, HPB, JFJ, CMN, BEO, MSA and IZO), the  $\sigma_{sp}$  peaks in  
6 spring/summer whereas lower  $\sigma_{sp}$  values are measured in autumn/winter. Similar findings were, for  
7 example, already reported by Nyeki et al. (1998) for JFJ and summarized by Andrews et al. (2011)  
8 for many mountain top stations worldwide and by Pandolfi et al. (2014) for MSA station. Different  
9 factors contribute to the  $\sigma_{sp}$  increase in spring/summer at the mountaintop observatories, such as  
10 the increase of the boundary layer height and the stronger upslope winds during the warmest  
11 months. Moreover, specific events, such as Saharan mineral dust outbreaks, may contribute to the  
12 increased  $\sigma_{sp}$  observed at mountain stations in spring/summer, especially in Southern Europe (e.g.  
13 Pey et al., 2013; Pandolfi et al., 2014; Rodríguez et al., 2011). At IZO,  $\sigma_{sp}$  peaks strongly in July-  
14 August because of the very high influence of African mineral dust at this station during these  
15 months (e.g. Alastuey et al., 2005; Diaz et al., 2006; Rodríguez et al., 2015). At the mountaintop  
16 CHC observatory (cf. Figure S8),  $\sigma_{sp}$  progressively increases during the dry season, from May to  
17 October, reaching lower values during the rainy season (from December to April). Moreover, during  
18 the dry season, the new particle formation events, taking place at CHC with one of the highest  
19 frequencies reported in the literature so far (Rose et al. 2015), can introduce very small particles  
20 that grow to nucleation and the Aitken mode.

21 At the mountain stations, both SAE and  $\sigma_{sp}$  are on average higher in summer compared to  
22 the winter period, thus suggesting a higher anthropogenic influence at these sites during the  
23 warmest months. The summer SAE increase is more evident at some mountain stations, e.g. HPB,  
24 CMN and BEO, compared to other mountain stations such as JFJ and MSA. The less pronounced  
25 SAE seasonal variation at JFJ was related by Bukowiecki et al. (2016) to the rather constant  
26 composition of the JFJ aerosol. At MSA in Southwestern Europe, the observed less pronounced  
27 seasonal cycle of SAE could be due to the contribution of Saharan dust in spring/summer, which  
28 contrasts with the PBL transport of fine particles observed at other mountain sites during the warm  
29 season. At IZO, the SAE reaches its lowest values during July-August in conjunction with the peak  
30 frequency of dust events (Rodríguez et al., 2015).

31 Overall, the  $g$  parameter shows an opposite seasonal cycle compared to the SAE at almost  
32 all mountain stations, with the exception of JFJ and BEO, where  $g$  slightly increases with SAE in  
33 the summer. At almost all mountain stations, the seasonal variations of SAE and  $g$  are less  
34 pronounced compared to the seasonal variation of  $\sigma_{sp}$ , indicating a larger seasonal variation in the  
35 extensive aerosol optical properties than in the intensive properties. At CHC, the SAE decreases  
36 as the  $\sigma_{sp}$  increases when moving from the wet to the dry season, indicating an increasing effect of  
37 coarse particles on the  $\sigma_{sp}$  during the dry season. At PUY,  $\sigma_{sp}$  peaks from March to September and

1 this increase is accompanied by a small increase in SAE. Venzac et al. (2009) and Boulon et al.  
2 (2011) have shown that PUY is more often influenced by the free troposphere or residual layers in  
3 winter and spring compared to the summer season.

#### 4 5 **3.4.3 Seasonal variability at coastal observatories**

6 A very different seasonal variation of  $\sigma_{sp}$  is observed at the two coastal observatories, MHD and  
7 FKL (at PLA, the lack of spring/summer measurements prevents the analysis of the annual cycles).  
8 The  $\sigma_{sp}$  at MHD (Western Europe) peaks in winter, whereas a higher  $\sigma_{sp}$  is observed in summer at  
9 FKL (Southeastern Europe). At FKL, where no intensive optical aerosol properties are available,  
10 the higher  $\sigma_{sp}$  in summer can be associated with mineral dust storm events, such as reported by  
11 Vrekoussis et al. (2005). However, mineral dust storms in the Mediterranean are not the only  
12 reason for the observed increased  $\sigma_{sp}$  in the summer at FKL. In fact, as for example reported by  
13 Kalivitis et al. (2011), ammonium sulphate and particulate organic matter, whose concentrations  
14 increase in summer in the Mediterranean Basin, can also be assumed to be important contributors  
15 to  $\sigma_{sp}$  during the warm season. At MHD, the higher  $\sigma_{sp}$  in winter is related to the higher contribution  
16 of wind-speed-generated sea-salt particles in the marine boundary layer during winter time  
17 (Vaishya et al., 2011). At MHD, the SAE ( $g$ ) is higher (lower) in summer compared to winter.  
18 O'Connor et al. (2008) and Vaishya et al. (2011, 2012) showed that the background marine aerosol  
19 level measured at MHD contains a strong and significant seasonal cycle with sea salt dominating  
20 in winter and biogenic organic aerosols dominating at the submicron scale in summer. This is  
21 consistent with the observed seasonal cycles of SAE and  $g$  reported here for MHD.

#### 22 23 **3.4.4 Seasonal variability at regional/rural observatories**

24 Regional observatories in Central and Eastern Europe show marked seasonal cycles of both  
25 extensive and intensive aerosol particle optical properties. In these regions, less horizontal and  
26 vertical pollutant dispersion in winter, due to a higher frequency of stagnant conditions and  
27 temperature inversions, play an important role in the accumulation of aerosols. As a consequence,  
28 the  $\sigma_{sp}$  is much higher in winter compared to summer. SAE and  $g$  also show marked seasonal  
29 cycles in these regions, with the SAE ( $g$ ) being higher (lower) in summer compared to winter. Ma et  
30 al. (2014) have shown that, at MPZ, an increased SAE in summer is mainly explained by the  
31 variation of the particle number size distribution. Thus, high concentrations in spring and summer  
32 of small particles during new particle formation and subsequent growth periods cause the observed  
33 increase of SAE (and correspondingly a decrease of  $g$ ) during the warmest months.

34 At regional sites in the Nordic and Baltic region, the monthly variation of  $\sigma_{sp}$  is on average  
35 less pronounced compared to the Central or Eastern European stations, especially at BIR and  
36 SMR. This is likely due to the placement of these stations in remote areas with a different  
37 meteorology (e.g. less pronounced PBL variations) where on average much lower  $\sigma_{sp}$  values are  
38 measured compared to other European sites. Moreover, this could also indicate the importance of

1 anthropogenic sources such as domestic heating in Central and Eastern Europe in winter.  
2 However, both SAE and  $g$  show marked seasonal cycles at these Nordic and Baltic observatories,  
3 similar to those reported for Central and Eastern European observatories with higher (lower) SAE  
4 ( $g$ ) in summer compared to winter.

5 Differences are observed in the annual cycle of  $\sigma_{sp}$  at a regional level in Southwestern  
6 Europe (represented by the MSY observatory) where higher  $\sigma_{sp}$  values are registered in summer.  
7 At the MSY regional site (located at around 720 m a.s.l.), the higher efficiency of the sea breeze in  
8 transporting pollutants from the urbanized/industrialized coastline toward regional elevated inland  
9 areas during the warmer season mainly explains the summer increase in aerosol particle mass  
10 concentration and scattering coefficient observed at this site (e.g. Pandolfi et al., 2011). Moreover,  
11 the enhanced formation of secondary sulphate and organic matter in the summer, together with  
12 frequent Saharan mineral dust outbreaks, strongly contribute to the observed seasonal cycle for  
13  $\sigma_{sp}$  and the intensive properties at the MSY site. The  $\sigma_{sp}$  peak observed at MSY in March is due to  
14 the winter pollution episodes typical of the western Mediterranean Basin (WMB) (e.g. Pandolfi et  
15 al., 2014a and references therein). During these episodes, the accumulation of pollutants close to  
16 the emission sources is favoured by anticyclonic conditions coupled with strong atmospheric  
17 inversions. During such conditions, pollutants accumulate in the PBL and can subsequently reach  
18 the MSY station when the PBL height increases.

#### 19 20 **3.4.5 Seasonal variability at urban/sub-urban observatories**

21 Among the urban sites, marked variations of  $\sigma_{sp}$  and the intensive properties are observed at UGR  
22 and DEM. At the urban UGR site, the mean aerosol type is very different in winter compared to  
23 summer. As evidenced by the seasonal cycles of SAE and  $g$ , aerosol particles are generally finer  
24 during the winter at UGR compared to the summer season, as already observed for example by  
25 Lyamani et al. (2010; 2012) and Titos et al. (2012). This is likely due to the accumulation of fine  
26 particles, mainly from traffic, domestic heating and biomass burning, favoured by stagnant  
27 conditions and atmospheric inversions during winter. In summer, the higher frequency of Saharan  
28 mineral dust outbreaks at this site increases the mean size of the particles during the warmest  
29 months. At the DEM urban observatories, the high  $\sigma_{sp}$  values measured in spring are linked to  
30 Saharan dust outbreaks, as also supported by the seasonal cycles of SAE and  $g$  which show the  
31 lowest and highest, respectively, values in spring.

#### 32 33 **3.5 SAE and $g$ vs. $\sigma_{sp}$ relationships**

34 Figure 9 shows the relationships between  $\sigma_{sp}$  and SAE and between  $\sigma_{sp}$  and  $g$  at each station.  
35 Mean SAE and  $g$  are calculated for each  $\sigma_{sp}$  bin and the bin size at each station is calculated  
36 following the Freedman–Diaconis rule:

$$37 \text{ Bin size} = 2 \frac{\text{IQR}(x)}{\sqrt[3]{n}}, \quad \text{(Eq. 3)}$$

1  
2 where  $IQR(x)$  is the interquartile range of the data and  $n$  is the number of observations in the  
3 sample  $x$ . These graphs help in understanding which aerosol type on average dominates the  
4 particle light scattering, depending on the degree of scattering measured. It should be noted that,  
5 in Figure 9, the number of samples available at each station is not evenly distributed among the  
6 considered bins. Figure S9 in the Supplementary Material shows, for some stations, the SAE- $\sigma_{sp}$   
7 pairs coloured by the number of samples in each bin to highlight how the samples are distributed  
8 amongst the bins.

### 10 **3.5.1 $g$ - $\sigma_{sp}$ relationships**

11 The asymmetry parameter  $g$  shows the lowest values for very low  $\sigma_{sp}$ , suggesting the  
12 predominance of small fine-mode particles. Andrews et al. (2011) reported similar  $g$ - $\sigma_{sp}$   
13 relationships at different mountain sites and suggested that the removal of large particles by cloud  
14 scavenging or by deposition during transport could explain the observed low  $g$  values in a clean  
15 atmosphere. They also suggested that the formation of new particles followed by  
16 condensation/coagulation could generate small but optically active particles. Here, we show that  
17 this behaviour of BF or  $g$  as a function of  $\sigma_{sp}$  was observed at all sites, not only at mountain sites.

18 The parameter  $g$  then increases with increasing  $\sigma_{sp}$ , indicating a shift of the particle number size  
19 distribution toward the larger end of the accumulation mode. Delene and Ogren (2002), Andrews et  
20 al. (2011), Pandolfi et al. (2014) and Sherman et al. (2015) showed that the BF tends to decrease  
21 with increasing aerosol loading, consistent with the observed increase of  $g$ . For comparison with  
22 previous works, Figure S10 in the Supplementary Material shows the BF- $\sigma_{sp}$  relationships for all  
23 observatories, evidencing the aforementioned BF decrease with increasing  $\sigma_{sp}$ .

24 The shift of the particle number size distribution toward the large end of the fine mode with  
25 increasing  $\sigma_{sp}$  is probably the main reason causing the observed increase of  $g$  (and the decrease  
26 of BF, cf. Figure S10). A possible explanation for this shift is a progressive aging of atmospheric  
27 aerosol particles. Then, at the majority of stations, the variation of  $g$  is less pronounced during  
28 periods of high particle mass concentration, suggesting changes mostly in the coarse aerosol  
29 particle mode rather than in the fine mode.

### 31 **3.5.2 SAE- $\sigma_{sp}$ relationships**

32 As reported in Figure 9, at some stations the SAE progressively increases with  $\sigma_{sp}$  in the  $\sigma_{sp}$  range  
33 where the  $g$  parameter also increases. The increase of both  $g$  and SAE with  $\sigma_{sp}$ , observed for  
34 example at the Nordic and Baltic regions, and Central and Eastern European observatories, could  
35 be related to the different effects that different particle sizes have on the SAE and  $g$ . A progressive  
36 increase of SAE with  $\sigma_{sp}$  would suggest an increasing relative importance of fine aerosol particles.  
37 The origin of these fine particles is probably different depending on the location of the measuring  
38 site. For the remote PAL site, for example, Lihavainen et al. (2015b) observed an increase of both



1  $\sigma_{sp}$  and SAE with increasing temperature due to the increasing rate of formation of BSOA with  
2 increasing ambient temperature, thus likely driving the  $\sigma_{sp}$ -SAE relationships reported in Figure 9  
3 for PAL. The BSOA from gas-to-particle formation over regions substantially lacking in  
4 anthropogenic aerosol sources, such as the European boreal region (Tunved et al., 2006),  
5 probably contribute strongly to the  $\sigma_{sp}$ -SAE relationships observed at other Nordic and Baltic sites,  
6 such as SMR. At polluted sites, such as those located in Central and Eastern Europe, the  
7 anthropogenic aerosol emissions and active secondary aerosol production in the region (e.g. Ma et  
8 al., 2014) are probably driving the  $\sigma_{sp}$ -SAE relationships reported in Figure 9.

9  
10 For higher  $\sigma_{sp}$ , the  $\sigma_{sp}$ -SAE relationships change and a progressive shift toward relatively  
11 larger particles is on average observed with increasing  $\sigma_{sp}$ . However, at the majority of  
12 Northwestern, Central and Eastern European stations, the SAE maintains values around, or higher  
13 than, 1.5 at high particle loads, indicating that the high  $\sigma_{sp}$  is dominated by fine particles. An  
14 exception is MHD, where the SAE increases with increasing  $\sigma_{sp}$ , maintaining values on average  
15 lower than 1.4 at high particle loads (cf. Figure 9). As already observed, the low SAE at MHD is  
16 mainly due to the predominance of sea-salt coarse particles at this site (Vaishya et al., 2011).  
17 Conversely, at some sites in Southern Europe (e.g. MSA, MSY, IZO, DEM) the SAE reaches  
18 values of around one or lower for high particle loads, indicating that, at these stations, the high  $\sigma_{sp}$   
19 is dominated by mineral dust coarse particles mainly from African deserts. Exceptions are two  
20 urban sites in Southwestern Europe (UGR and MAD) where fine particles, probably generated for  
21 the most part by traffic (and also from biomass burning at UGR) on average dominate the highest  
22 measured  $\sigma_{sp}$  values.

23  
24 Similar  $\sigma_{sp}$ -SAE relationships to those reported in Figure 9 were observed by Andrews et al.  
25 (2011) at mountain sites and by Delene and Ogren (2002) at marine sites. Among the lowest SAE  
26 are observed at IZO, the station closest to the African continent. Interestingly, at IZO, the SAE  
27 shows the highest gradient for  $\sigma_{sp}$  coefficients in the range of 0 to 50  $Mm^{-1}$  whereas the gradient is  
28 much lower for  $\sigma_{sp}$  values higher than 50  $Mm^{-1}$ , with the SAE being almost constant for  $\sigma_{sp}$  higher  
29 than 100  $Mm^{-1}$ . The IZO station is often in the free troposphere and high loadings at this station are  
30 only registered during Saharan dust events, thus it is virtually only the mineral dust that is  
31 measured at IZO. Normally, the long-range transport mineral dust particles do not represent a  
32 significant fraction of the particle population above 10  $\mu m$  because of their short lifetimes, which  
33 likely explains the constant SAE observed at the IZO site under high aerosol loading.

### 34 **3.6 Trends**

35  
36 Trends of  $\sigma_{sp}$ , SAE and BF are studied for those stations having more than 8 years' worth of data  
37 (13 observatories). Among the ACTRIS stations, PAL, SMR, MHD, HPB, IPR, JFJ and UGR have  
38 more than 10 years of data, whereas at PUY, MPZ, CMN, BEO, KPS and IZO, 8 or 9 years of data

1 are available. These stations are included in order to improve the spatial coverage, as is the case  
2 in Collaud Coen et al. (2013). The Theil Sen statistical estimator (Theil, 1950; Sen, 1968) is used  
3 here to determine the regression parameters of the data trends, including slope, uncertainty in the  
4 slope and p-value. The Theil Sen method provides similar results to the Mann-Kendall test and it is  
5 implemented for example in the Openair Package available for R software (Carslaw, 2012;  
6 Carslaw and Ropkins, 2012). The applied method yields accurate confidence intervals, even with  
7 non-normal data, and it is less sensitive to outliers and missing values (Hollander and Wolfe,  
8 1999). Monthly means are used for trend analysis and the data are corrected for seasonal effects.

9 The data coverage for  $\sigma_{sp}$  is higher than 70% at all stations included in the trend analyses  
10 with the exception of IZO, where the  $\sigma_{sp}$  data coverage is 55%. For SAE, the data coverage is  
11 higher than 65% at all sites with the exception of PAL (54%), PUY (59%) and IZO (52%). For BF,  
12 the data coverage is higher than 65% with the exception of PAL (26%), PUY (43%), BEO (47%)  
13 and IZO (27%). At the remote (PAL) or mountain stations (PUY, BEO and IZO), the percentage for  
14 the intensive aerosol particle optical properties is lower because there is a higher probability of  
15 measuring  $\sigma_{sp}$  lower than the threshold ( $0.8 \text{ Mm}^{-1}$ ) selected for the calculation of SAE and BF.

16 Table 2 reports the trends observed for  $\sigma_{sp}$ , SAE and BF at the thirteen observatories  
17 included in this analysis. Magnitude and statistical significance of the trends for these parameters  
18 are reported in Table S8 in the Supporting Material. In Table 2, comparisons with the previous  
19 trend analysis results presented by Collaud Coen et al. (2013) for aerosol particle optical properties  
20 and by Asmi et al. (2013) for particle number concentrations are also reported.

### 22 3.6.1 Trends of $\sigma_{sp}$

23 Overall, a statistically significant decreasing trend for  $\sigma_{sp}$  is observed at around 50% of the stations  
24 considered here (Table 2). Significantly, decreasing trends for  $\sigma_{sp}$  are observed at the two Nordic  
25 and Baltic observatories (PAL for the period 2000 to 2010 and SMR); at two observatories (HPB  
26 and IPR) out of the five observatories in Central Europe; and at the two observatories in  
27 Southwestern Europe (IZO and UGR). The trends are not statistically significant in Western (MHD  
28 and PUY) and Eastern (BEO and KPS) Europe. The highest magnitude for the  $\sigma_{sp}$  trend [ $\text{Mm}^{-1}/\text{yr}$ ]  
29 (cf. Table S8 in the Supplementary Material) is observed at the polluted IPR observatory.  
30 Conversely, the lowest magnitude is observed at the remote PAL observatory.

31 For the periods considered in this work, the total reductions (TR) for  $\sigma_{sp}$  range between  
32 approximately 30% (SMR) and 60% (IZO). The high TR observed at IZO might be affected by the  
33 intensity and frequency of Saharan dust outbreaks at this site. However, estimating the effects of  
34 these events at IZO is beyond the scope of this study. Overall, the observed decreasing trends of

1  $\sigma_{sp}$  are consistent with a uniform decrease in the aerosol optical depth observed in Europe  
2 (AERONET data in Li et al., 2014).

3 The observed statistically significant and decreasing trends of  $\sigma_{sp}$  are consistent with the  
4 demonstrated reduction of PM concentration in the atmosphere in Europe in recent decades  
5 thanks to the implementation of European/national/regional/local mitigation strategies. These  
6 decreasing trends are also consistent with the trends in the aerosol chemistry derived from  
7 observations in urban environments in Europe (e.g. EEA, 2013; Barmpadimos et al., 2011; Titos et  
8 al., 2014; Pandolfi et al., 2016), regional and remote environments in the western Mediterranean  
9 (Cusack et al., 2012; Pandolfi et al., 2016) and in general with trends derived for the aerosol  
10 chemistry across Europe (Tørseth et al., 2012). Recently, Collaud Coen et al. (2013) showed that  
11 trends in  $\sigma_{sp}$  are observed at most of the US continental sites and that these trends are generally  
12 consistent with the strong SO<sub>2</sub> and PM reductions observed in the United States (Asmi et al., 2013;  
13 EPA, 2011). Conversely, in Europe, the strong decreasing trend observed for SO<sub>2</sub> (e.g. Tørseth et  
14 al., 2012; Henschel et al., 2013) and, with a lower spatial homogeneity and statistical significance,  
15 for PM<sub>2.5</sub> (e.g. EEA, 2016) is not observed for aerosol optical properties. As reported in Collaud  
16 Coen et al. (2013) the reasons that at some of the European sites no significant trends are  
17 observed, might be related to the spatial inhomogeneities and under-representation of continental  
18 Europe PBL sites (e.g. Laj et al., 2009) and/or the timing of the SO<sub>2</sub> and PM trends for the United  
19 States and Europe. In Europe, the emission reductions were greater for the period 1980 to 2000  
20 compared to the period 2000 to 2010 (e.g. Colette et al., 2016; Tørseth et al., 2012; Manktelow et  
21 al., 2007), thus the measurements of optical particle properties in Europe may not go back far  
22 enough to reflect the time period with the largest emission reductions. Tørseth et al. (2012)  
23 reported average reductions for ambient sulphate and nitrate mass concentrations in Europe of  
24 -12% and -1%, respectively, during 2000 to 2009 compared to -24% and -7%, respectively,  
25 during 1990 to 2000. These authors also reported statistically significant decreases of the PM<sub>10</sub>  
26 and PM<sub>2.5</sub> mass concentrations at around 50% of European sites, with total reductions of -18%  
27 and -27%, for PM<sub>10</sub> (24 sites) and PM<sub>2.5</sub> (13 sites), respectively, during 2000 to 2009. A direct  
28 comparison between the stations included in this work and those included in the study of Tørseth  
29 et al. (2012) is not possible because of the different timings of the reported  $\sigma_{sp}$  and PM mass  
30 concentration measurements. At those stations, where a significant decreasing trend for  $\sigma_{sp}$  is  
31 observed and considering a period of 10 years (even if not coincident for all stations), the total  
32 reduction for  $\sigma_{sp}$  in Europe is around -35% (cf. Table S8), consistent with the trend reported by  
33 Tørseth et al. (2012) for PM in Europe.

34 Quite good agreement, although again likely biased by the different timings, is also observed  
35 when comparing the PM mass concentration and  $\sigma_{sp}$  trends by geographical sector. A significant  
36 total reduction of around -40 to -30% was reported for PM<sub>10</sub> and PM<sub>2.5</sub> in the Nordic and Baltic  
37 sector by Tørseth et al. (2012; cf. Figure 7 in Tørseth et al. (2012)), in close agreement with the

1 statistically significant total decrease of  $\sigma_{sp}$  of around -34% reported for PAL during 2000 to 2010  
2 (cf. Table S8). In the western sector (MHD), the decreasing trend for  $PM_{2.5}$  during 2000 to 2009  
3 was insignificant (-10 to 0%) as reported here for  $\sigma_{sp}$  during the period 2001 to 2010. In the central  
4 sector, statistically significant decreases for the  $PM_{2.5}$  and  $PM_{10}$  mass concentrations ranging  
5 between -20% and -40% were observed during a 10 year period (2000 to 2009) and the total  
6 reduction for  $\sigma_{sp}$  ranged between -38% (HPB) and around -48% (IPR). In the Southwest  
7 European sector the total reduction for  $\sigma_{sp}$  is around -32% (at UGR) and -60% (at IZO), whereas  
8 Tørseth et al. (2012) reported decreases of around -20 to -40% for the  $PM_{10}$  mass concentration  
9 in the same geographical sector.

10 To further confirm the observed close agreement between the PM trends reported in the  
11 literature and the trends of  $\sigma_{sp}$  detailed in this work, Table S9 in the Supporting Material reports the  
12 comparison between  $\sigma_{sp}$  and  $PM_{10}$  and/or  $PM_{2.5}$  mass concentration trends calculated at those  
13 stations where simultaneous  $\sigma_{sp}$  and PM mass concentration measurements are available. As  
14 reported in Table S9, both the observed total reductions and the statistical significance levels of the  
15 trends are very similar for  $\sigma_{sp}$  and  $PM_{10}$ .

### 17 **3.6.2 Trends of SAE and BF**

18 The trends for SAE are estimated for three different quantities, namely the SAE is calculated using  
19 the three wavelengths (b-g-r), using the blue and the green wavelengths (b-g) and using the green  
20 and red wavelengths (g-r). For the periods considered in this work (in bold in Table 2), the SAE  
21 calculated using the three wavelengths (b-g-r) shows statistically significant trends at five sites. At  
22 PAL (Nordic and Baltic), PUY (Western Europe) and BEO (Eastern Europe) decreasing trends are  
23 observed, whereas increasing trends are observed at HPB (Central Europe) and UGR  
24 (Southwestern Europe). Uniform negative trends of the columnar Ångström exponent from  
25 AERONET data were reported by Li et al. (2014) across Europe and these trends were ascribed to  
26 reduced fine-mode anthropogenic emissions. The positive SAE trend observed at HPB and UGR  
27 would suggest a shift of the accumulation-mode particles toward smaller sizes and/or a change in  
28 the coarse aerosol mode. For example, the SAE increase at UGR might be explained by a  
29 progressive relative importance of fine particle emissions driven by a progressive reduction of  
30 coarse particles, for example from construction/demolition works due to the economic crisis which  
31 affected Spain from 2008 (e.g. Lyamani et al., 2011; Querol et al., 2014; Pandolfi et al., 2016). In  
32 fact, Titos et al. (2014) reported a statistically significant decreasing trend for the  $PM_{10}$  fraction  
33 during the period 2006 to 2010 whereas no trend was observed for the  $PM_1$  fraction. Moreover, at  
34 UGR, a statistically significant increasing trend is also observed for the SAE calculated using the  
35 green and red wavelengths (g-r), which are likely more sensitive to the coarser particle mode,  
36 whereas the trend was non-statistically significant for the SAE at b-g wavelengths.

1 The possible change in the coarse aerosol mode at UGR is likely also the cause of the  
2 observed statistically significant increasing trend of BF (cf. Table 2), given that a positive trend of  
3 BF would be consistent with a shift of the accumulation-mode particles toward smaller sizes.  
4 Similarly, statistically significant increasing trends for both SAE and BF are also observed at SMR  
5 (SAE b-g) and HPB. Statistically significant increasing trends of BF are also observed at the other  
6 Nordic and Baltic stations (PAL) and at PUY (Western Europe), where the SAE shows statistically  
7 significant decreasing trends, and at IPR (Central Europe) where the trend of SAE is insignificant.  
8 Thus, overall, the trends of BF are positive at all stations where BF measurements are available.  
9 The opposite sign of the trends for SAE and BF at PAL and PUY could be due to the different  
10 effects that the different particle sizes have on SAE and  $g$  or a progressive change in the mean  
11 diameter of the fine-mode aerosols. Further research involving, for example, size distribution data  
12 and a Mie calculation could help in understanding the differences observed in some cases  
13 between SAE and BF (or  $g$ ).

14 Recently, Korras-Carraca et al. (2015) have shown that the column integrated  $g$  from Modis-  
15 Terra showed widely statistically significant positive trends (2002-2010) with stronger increases  
16 observed in the eastern and southern Black Sea, as well as over the Baltic and Barents seas.  
17 Moreover, both Modis-Terra and Modis-Aqua produce positive trends of  $g$  in the eastern  
18 Mediterranean Sea and the eastern coast of the Iberian Peninsula. Positive trends for  $g$   
19 correspond to negative trends for BF. The difference observed in our work could be due to the  
20 different variability often observed between near-surface measurements and column integrated  
21 measurements which can confound the relationship between surface and column optical properties  
22 (e.g. Bergin et al., 2000; Lyamani et al., 2010), although it has been shown that a mid-altitude  
23 station might be globally representative of the whole atmospheric column (Chauvigne et al., 2016).

### 24 25 **3.6.3 Comparison with previous trend analyses**

26 Table 2 shows the comparison, over the same time periods, between the trend analyses performed  
27 in this work and the analyses presented by Collaud Coen et al. (2013) for aerosol particle optical  
28 properties and by Asmi et al. (2013) for particle number concentrations ( $N_{LDL-500}$ ,  $N_{20-500}$  and  $N_{100-500}$ ).  
29 An agreement with the results from Collaud Coen et al. (2013) is observed for JFJ, where  
30 consistent insignificant trends are detected for the three periods reported in Collaud Coen et al.  
31 (2013). For MHD, we observed a non-significant increasing trend for  $\sigma_{sp}$  during 2001 to 2010,  
32 whereas Collaud Coen et al. (2013) reported a statistically significant increasing trend for the same  
33 period. At PAL, a non-statistically significant trend for  $\sigma_{sp}$  is observed both in the current work and  
34 in Collaud-Coen et al. (2013) for the period 2001 to 2010, whereas we observe a statistically  
35 significant decreasing trend for the period 2000 to 2010. Moreover, at PAL, we observe a  
36 statistically significant decreasing trend for SAE during the two common periods which were  
37 insignificant in Collaud Coen et al. (2013). It should be noted that Collaud Coen et al. (2013)

1 reported an insignificant SAE trend at PAL using the Mann-Kendall test whereas they reported  
2 statistically significant decreasing trends using the GLS/ARB (generalized least square trends with  
3 either autoregressive or block bootstrap confidence intervals) and LMS (least-mean square)  
4 methods, consistent with our work. These differences are thus likely due to the relative short period  
5 used in these trend analyses and the different sensitivity of the methods used to missing values or  
6 the presence of outliers, especially at PAL, where  $\sigma_{sp}$  is very low (cf. Figure 2). For example, in this  
7 work, the SAE calculated for PAL during the year 2007 was removed from the trend analysis due  
8 to the presence of too many extremely high SAE values, likely explaining the difference observed  
9 in SAE compared to the work of Collaud Coen et al. (2013). Moreover, here we use de-  
10 seasonalized monthly means for trend analyses whereas Collaud-Coen et al. (2013) used de-  
11 seasonalized medians with a different time granularity (3 days), likely affecting the comparison,  
12 especially over relatively short periods.

13 A comparison of trends analysis results between  $\sigma_{sp}$  and the particle number concentration is not  
14 straightforward as the  $\sigma_{sp}$  measurements are more sensitive to the particle number concentration in  
15 the upper end of the fine mode than to smaller particles. For example, Asmi et al. (2013) reported  
16 that, globally, no strong similarities were observed between  $\sigma_{sp}$  and particle number concentration  
17 (N) trends and that the N trends are controlled by particles in the larger range of the Aitken mode  
18 and the smaller range of the accumulation mode, i.e. ca. 50–150 nm diameter. In this work, as  
19 reported in Table 2, the statistically significant decreasing trend reported for N during the period  
20 2001 to 2010 is not observed for  $\sigma_{sp}$ . However, differences are also observed at PAL between N20  
21 and N100, mainly due to the fact that the DMPS measurements at PAL had long gaps during  
22 periods with unusually low concentrations, thus effectively removing low concentrations from the  
23 trend analysis (Asmi et al., 2013).

24

#### 25 **3.6.4 Daytime and night time trend analyses at mountain sites**

26 Finally, the analysis of the trends during daytime (08:00 to 16:00 GMT) and night time (21:00 to  
27 05:00 GMT) by season at the mountain stations are also analysed (Table 3). This analysis could  
28 provide information about changes in  $\sigma_{sp}$  during periods when the mountain stations are likely  
29 affected by the PBL (e.g. daytime and/or summer) or by the residual layer (e.g. night time in  
30 summer) or when the mountain stations are representative of the free troposphere (e.g. night time  
31 in winter). Consistent with what is reported in Table 2 for  $\sigma_{sp}$ , the trends are insignificant at JFJ,  
32 PUY, CMN and BEO irrespective of the time of the day or season. The decreasing trends observed  
33 at HPB, also reported in Table 2, are statistically significant only during autumn, irrespective of the  
34 time of day. Conversely, the trend observed for  $\sigma_{sp}$  at IZO reported in Table 2, is not observed on  
35 splitting the analysis by time of day and/or season.

36

## 1 **Conclusions**

2  
3 This investigation presented the near-surface in situ  $\sigma_{sp}$  (aerosol particle light scattering), SAE  
4 (scattering Ångström exponent), BF (backscatter fraction) and  $g$  (asymmetry parameter)  
5 measurements obtained over the past decade at 28 atmospheric observatories which are part of  
6 the ACTRIS Research Infrastructure, with most belonging to the GAW network. Results show a  
7 large variability of both extensive and intensive aerosol particle optical properties across the  
8 network, which is consistent with the previously reported variability observed for other aerosol  
9 particle properties such as particle mass concentration, particle number concentration and  
10 chemical composition. Main findings can be summarized as follows:

- 11  
12 - An increasing gradient of  $\sigma_{sp}$  is observed when moving from remote environments  
13 (Arctic/mountain) to regional and to urban environments. At regional level in Europe,  $\sigma_{sp}$  also  
14 increases when moving from Nordic and Baltic countries and Western Europe to  
15 Central/Eastern Europe whereas no clear spatial gradient is observed for other station  
16 environments. For example, the lack of a clear spatial gradient of  $\sigma_{sp}$  measured at mountain  
17 observatories is likely due to the different altitudes of the observatories in the different  
18 geographical sectors considered in this study. Among the European mountain observatories a  
19 relationship was observed between station altitude and the median  $\sigma_{sp}$ , this latter being the  
20 highest at the station located at the lower altitude and vice versa.
- 21 - Overall, the highest  $\sigma_{sp}$  values are measured at low altitude observatories in Central and  
22 Eastern Europe and at some urban observatory in Southern Europe whereas the lowest  $\sigma_{sp}$   
23 values are observed at mountain stations and at Arctic and Antarctic observatories. Low  $\sigma_{sp}$   
24 levels, comparable to those measured at mountain sites, are also observed at the majority of  
25 the regional Nordic and Baltic observatories. The  $\sigma_{sp}$  values in Western Europe are on average  
26 higher compared to those measured in the Nordic and Baltic regions and lower compared to  
27 those measured at a regional level in Southern Europe. Some exceptions to these general  
28 features are however observed.
- 29 - The SAE does not show any clear gradient as a function of the placement of the station.  
30 However, a West to East increasing gradient is observed for both regional and mountain  
31 placements suggesting a lower fraction of fine-mode particle in Western/Southwestern Europe  
32 compared to Central and Eastern Europe where the fine-mode particles dominate the  
33 scattering.
- 34 - In fact, in Central and Eastern Europe, independently of the station placement, the SAE is  
35 among the highest observed across the network, indicating a large predominance of fine  
36 particles. In these regions, the SAE is even higher in summer compared to winter, suggesting  
37 the shift toward the small end of the aerosol particle size distribution likely linked to new particle  
38 formation events during the warmest months. On average SAE is lower in the Nordic and Baltic  
39 and western geographical sectors (likely due to the contribution from coarse-mode sea salt

1 particles), and southern sectors (likely because of the presence of mineral dust particles from  
2 African deserts), compared to Central and Eastern Europe.

3 - The  $g$  does not show any clear gradient by station placement or geographical location  
4 reflecting the complex relationship of this parameter with the aerosol particles properties such  
5 as size distribution, particle shape or refractive index.

6 - Slightly higher  $g$  values are observed in Western Europe compared to Central and Eastern  
7 Europe. These differences in the  $g$  values, even if small, are consistent with the opposite  
8 gradient observed for SAE, this latter being smaller in Western Europe. However, the station-  
9 averaged  $g$  in Central and Eastern Europe is similar to the mean  $g$  observed in the Nordic and  
10 Baltic regions and in Southwestern Europe. Thus, contrary to the SAE, a clear relationship  
11 between aerosol size and  $g$  is not observed.

12 - Seasonal cycles for  $\sigma_{sp}$ , SAE and  $g$  are observed in all geographical sectors and explained by  
13 different factors. The seasonal cycles are especially marked at a regional level in Central and  
14 Eastern Europe where winter time episodes linked with stable air and thermal inversions favour  
15 the accumulation of pollutants. In these European regions the SAE ( $g$ ) is higher (lower) in  
16 summer compared to winter due to variations in particle number size distribution due to the  
17 enhanced formation of small and optically active particles during new particles formation and  
18 subsequent growth. Clear annual cycles are also observed at mountain sites where  $\sigma_{sp}$  is  
19 higher in summer because of the enhanced influence of the boundary layer. In some cases, the  
20 SAE ( $g$ ) is also high (low) in summer at mountain sites indicating a higher PBL anthropogenic  
21 influence during the warmer months and/or new particles formation episodes. In the Nordic and  
22 Baltic regions, the seasonal variation of  $\sigma_{sp}$  is less pronounced compared to Central and  
23 Eastern Europe, likely due to the different meteorology and less pronounced PBL variations.  
24 Despite the relatively small  $\sigma_{sp}$  seasonal cycles in the Nordic and Baltic regions, SAE ( $g$ )  
25 increases (decreases) in these regions in summer compared to the winter period likely due to a  
26 season-dependent transport of air masses at these remote sites and the enhanced formation of  
27 secondary organic aerosols previously observed at these sites during the warmest months. At  
28 coastal sites in Northwestern Europe, the presence of sea-salt particles in winter also  
29 contributes to the observed pronounced seasonal cycles of SAE and  $g$ . In Southern Europe the  
30 seasonal cycles are strongly driven by the enhanced formation of secondary sulphate and  
31 organic matter in the summer, together with frequent Saharan mineral dust outbreaks.

32 - The analyses of the systematic variabilities of SAE and  $g$  as a function aerosol loading ( $\sigma_{sp}$ )  
33 reveal some common patterns. At all stations,  $g$  shows the lowest values at very low  $\sigma_{sp}$  likely  
34 because of the formation of new particles in a clean atmosphere followed by  
35 condensation/coagulation with, as a consequence, the generation of small but optically active  
36 particles. The  $g$  value then sharply increases with increasing  $\sigma_{sp}$ , indicating the shift of the  
37 particle number size distribution toward the larger end of the accumulation mode. Then, during  
38 periods of high  $\sigma_{sp}$  values, the variation of  $g$  is less pronounced at the majority of the stations,



1 contrary to the SAE, which increases or decreases, suggesting changes mostly in the coarse  
2 aerosol particle mode rather than in the fine mode. At the majority of Northwestern, Central and  
3 Eastern European stations, the SAE maintains high values at high  $\sigma_{sp}$  values, indicating that  
4 the high  $\sigma_{sp}$  is dominated by fine particles. Conversely, at some sites in Southern Europe the  
5 SAE reaches values of around one or lower for high particle loads, indicating that, at these  
6 stations, the high  $\sigma_{sp}$  is dominated by mineral dust coarse particles mainly from African  
7 deserts. Exceptions are two urban sites in Southwestern Europe where fine particles, probably  
8 generated for the most part by traffic (and also from biomass burning) on average dominate the  
9 highest measured  $\sigma_{sp}$  values.

- 10 - The analyses of the trends reported in this investigation provide evidence that both extensive  
11 and intensive aerosol optical properties have significantly changed at some of the locations  
12 included here over the last 10 and 15 years. The  $\sigma_{sp}$  decreasing trends reported here are  
13 statistically significant at 5 out of 13 stations included in the analyses. These 5 stations are  
14 located in the Nordic and Baltic regions, and the central and southwestern sectors. Conversely,  
15  $\sigma_{sp}$  trends which are decreasing are not statistically significant in Western and Eastern Europe.  
16 Statistically significant decreasing trends of SAE are observed at 3 out of 10 observatories  
17 included in the analysis: one site in the Nordic and Baltic sector and two mountain sites in the  
18 western and eastern sectors. These negative trends could be ascribed to reduced fine-mode  
19 anthropogenic emissions, as already observed in the literature for columnar SAE in Europe.  
20 Conversely, at two stations (one mountain site in Central Europe and one urban site in  
21 Southwestern Europe), the SAE shows a statistically significant increasing trend, suggesting a  
22 shift in the accumulation-mode particles toward smaller sizes and/or a change in the coarse  
23 aerosol mode. At the remaining 5 observatories, the reported SAE trends are not statistically  
24 significant. The backscatter fraction shows a statistically significant increasing trend at 5 out of  
25 the 9 sites where BF measurements are available. At three stations (the mountain site in  
26 Central Europe, the urban site in Southwestern Europe and one of the two sites in the Nordic  
27 and Baltic sector), both BF and SAE increase, suggesting consistent evidence of a shift in the  
28 accumulation-mode particles toward a smaller size. Conversely, at the other site in the Nordic  
29 and Baltic sector and at one mountain site in the western sector the BF increases whereas the  
30 SAE decreases.
- 31 - A general agreement is observed between the trend analyses performed in this work and the  
32 analyses presented in a previous work confirming the general decreasing trends observed for  
33  $\sigma_{sp}$  in Europe. However, some differences are also observed and likely due to the relative short  
34 periods used in these trend analyses and the different sensitivity of the methods used to  
35 missing values or presence of outliers. (Mann-Kendall or Theil-Sen vs. GLS/ARB or MLS;  
36 means vs. medians; different time granularity)

1 In conclusion, this investigation provides a clear and useful picture of the spatial and temporal  
2 variability of the surface in situ aerosol particle optical properties in Europe. The results presented  
3 here give a comprehensive view of the particle optical properties and provide a reliable analysis of  
4 aerosol optical parameters for model constraints. In addition, the analyses presented here suggest  
5 findings that may need additional investigation. For example, the fact that at some of the stations  
6 the trend of  $\sigma_{sp}$  changes in terms of both statistical significance and sign depending on the period  
7 used, suggests that trend analyses are necessary in the future when longer-duration records will  
8 be available. Moreover, the fact that at some sites BF and SAE show different signs in their trends  
9 suggests that further analysis is needed to better understand how other aerosol parameters, such  
10 as particle size distribution and mean diameter, affect the relationships between BF and SAE.

## 11 **Acknowledgments**

12 This project has received funding from the European Union's Horizon 2020 research and  
13 innovation programme under grant agreement No 654109, ACTRIS (project No. 262254), ACTRIS-  
14 PPP (project No 739530). We also thank the International Foundation High Altitude Research  
15 Stations Jungfraujoch and Gornergrat (HFSJG), which made it possible to carry out the  
16 experiments at the High Altitude Research Station at the Jungfraujoch and the support of  
17 MeteoSwiss within the Swiss program of the Global Atmosphere Watch (GAW) of the WMO. MAD  
18 station is co-financed by the PROACLIM (CGL2014-52877-R) project. SMR station acknowledges  
19 BACCHUS (project No. 603445), CRAICC (project No. 26060) and Academy of Finland (project  
20 No. 3073314). UGR station is co-financed by the Spanish Ministry of Economy and  
21 Competitiveness through project CGL2016-81092-R. Measurements at Montseny and Montsec  
22 stations were supported by the MINECO (Spanish Ministry of Economy and Competitiveness) and  
23 FEDER funds under the PRISMA project (CGL2012-39623-C02/00), by the MAGRAMA (Spanish  
24 Ministry of Agriculture, Food and Environment) and by the Generalitat de Catalunya (AGAUR 2014  
25 SGR33 and the DGQA). Measurements at Izaña were supported by the AEROATLAN project  
26 (CGL2015-17 66229-P), co-funded by the Ministry of Economy and Competitiveness of Spain and  
27 the European Regional Development Fund. Station Košetice is supported by the Ministry of  
28 Education, Youth and Sports of the Czech Republic within the project for support of national  
29 research infrastructure ACTRIS – participation of the Czech Republic (ACTRIS-CZ – LM2015037).  
30 Measurements at Puy de Dôme were partly supported by CNRS-INSU, University Clermont-  
31 Auvergne, OPGC and the french CLAP program. PAL station acknowledges KONE Foundation,  
32 Academy of Finland (project No. 269095 and No. 296302). CHC station received support from  
33 Institut de Recherche pour le Développement (IRD) under both Jeune Equipe program attributed to  
34 LFA and support to ACTRIS-FR program. CHC received grants from Labex OSUG@2020  
35 (Investissements d'avenir – ANR10 LABX56). Marco Pandolfi is funded by a Ramón y Cajal  
36 Fellowship (RYC-2013-14036) awarded by the Spanish Ministry of Economy and Competitiveness.  
37 The authors would like to express their gratitude to D. C. Carslaw and K. Ropkins for providing the  
38

1 OpenAir software used in this paper (Carslaw and Ropkins, 2012; Carslaw, 2012). We also thank  
2 the co-editor Andreas Petzold and two anonymous reviewers for their constructive comments.  
3  
4  
5  
6  
7  
8  
9  
10  
11  
12  
13  
14  
15  
16  
17  
18  
19  
20  
21  
22  
23  
24  
25  
26  
27  
28  
29  
30  
31  
32  
33  
34  
35  
36  
37  
38  
39

## Bibliography

- Aaltonen, V., Lihavainen, H., Kerminen, V.-M., Komppula, M., Hatakka, J., Eneroth, K., Kulmala, M., and Viisanen, Y.: Measurements of optical properties of atmospheric aerosols in Northern Finland, *Atmos. Chem. Phys.*, 6, 1155–1164, doi:10.5194/acp-6-1155-2006, 2006.
- Alastuey, A., Querol, X., Castillo, S., Escudero, M., Avila, A., Cuevas, E., Torres, C., Romero, P.-M., Exposito, F., García, O., Diaz, J. P., Van Dingenen, R., and Putaud, J. P.: Characterisation of TSP and PM<sub>2.5</sub> at Izaña and Sta. Cruz de Tenerife (Canary Islands, Spain) during a Saharan dust episode (July 2002), *Atmos. Environ.*, 39, 4715–4728, doi:10.1016/j.atmosenv.2005.04.018, 2005.
- Anderson, T. L. and Ogren, J. A.: Determining Aerosol Radiative Properties Using the TSI 3563 Integrating Nephelometer, *Aerosol Sci. Tech.*, 29, 57–69, 1998.
- Andrews, E., Sheridan, P. J., Fiebig, M., McComiskey, A., Ogren, J. A., Arnott, P., Covert, D., Elleman, R., Gasparini, R., Collins, D., Jonsson, H., Schmid, B., and Wang, J.: Comparison of methods for deriving aerosol asymmetry parameter, *J. Geophys. Res. Atmos.*, 111, D05S04, doi:10.1029/2004JD005734, 2006.
- Andrews, E., Ogren, J. A., Bonasoni, P., Marinoni, A., Cuevas, E., Rodríguez, S., Sun, J. Y., Jaffe, D. A., Fischer, E. V., Baltensperger, U., Weingartner, E., Collaud Coen, M., Sharma, S., Macdonald, A. M., Leaitch, W. R., Lin, N.-H., Laj, P., Arsov, T., Kalapov, I., Jefferson, A., and Sheridan, P.: Climatology of aerosol radiative properties in the free troposphere, *Atmos. Res.*, 102, 365–393, doi:10.1016/j.atmosres.2011.08.017, 2011.
- Asmi, A., Wiedensohler, A., Laj, P., Fjaeraa, A.-M., Sellegri, K., Birmili, W., Weingartner, E., Baltensperger, U., Zdimal, V., Zikova, N., Putaud, J.-P., Marinoni, A., Tunved, P., Hansson, H.-C., Fiebig, M., Kivekäs, N., Lihavainen, H., Asmi, E., Ulevicius, V., Aalto, P. P., Swietlicki, E., Kristensson, A., Mihalopoulos, N., Kalivitis, N., Kalapov, I., Kiss, G., de Leeuw, G., Henzing, B., Harrison, R. M., Beddows, D., O'Dowd, C., Jennings, S. G., Flentje, H., Weinhold, K., Meinhardt, F., Ries, L., and Kulmala, M.: Number size distributions and seasonality of submicron particles in Europe 2008–2009, *Atmos. Chem. Phys.*, 11, 5505–5538, doi:10.5194/acp-11-5505-2011, 2011.
- Asmi, A., Collaud Coen, M., Ogren, J. A., Andrews, E., Sheridan, P., Jefferson, A., Weingartner, E., Baltensperger, U., Bukowiecki, N., Lihavainen, H., Kivekäs, N., Asmi, E., Aalto, P. P., Kulmala, M., Wiedensohler, A., Birmili, W., Hamed, A., O'Dowd, C., Jennings, S. G., Weller, R., Flentje, H., Mari Fjaeraa, A., Fiebig, M., Lund Myhre, C., Hallar, A. G., Swietlicki, E., Kristensson, A., and Laj, P.: Aerosol decadal trends – Part 2: In-situ aerosol particle number concentrations at GAW and ACTRIS stations, *Atmos. Chem. Phys.*, 13, 895–916, doi:10.5194/acp-13-895-2013, 2013.
- Barnpadimos, I., Hueglin, C., Keller, J., Henne, S., and Prevot, A. S. H.: Influence of meteorology on PM<sub>10</sub> trends and variability in Switzerland from 1991 to 2008, *Atmos. Chem. Phys.*, 11, 1813–1835, doi:10.5194/acp-11-1813-2011, 2011.
- Barnpadimos, I., Keller, J., Oderbolz, D., Hueglin, C., and Prévôt, A. S. H.: One decade of parallel fine (PM<sub>2.5</sub>) and coarse (PM<sub>10</sub>–PM<sub>2.5</sub>) particulate matter measurements in Europe: trends and variability, *Atmos. Chem. Phys.*, 12, 3189–3203, doi:10.5194/acp-12-3189-2012, 2012.
- Bergin, M. H., Schwartz, S. E., Halthore, R. N., Ogren, J. A., and Hlavka, D. L.: Comparison of aerosol optical depth inferred from surface measurements with that determined by Sun photometry for cloud-free conditions at a continental US site, *J. Geophys. Res.*, 105, 6807–6816, 2000.
- Bond, T. C., Covert, D. S., and Muller, T.: Truncation and Angular-Scattering Corrections for Absorbing Aerosol in the TSI 3563 Nephelometer, *Aerosol Sci. Tech.*, 43, 866–871, 2009.
- Boulon, J., Sellegri, K., Hervo, M., and Laj, P.: Observations of nucleation of new particles in a volcanic plume, *P. Natl. Acad. Sci. USA*, 108, 12223–12226, doi:10.1073/pnas.1104923108, 2011.
- Bourcier L., K. Sellegri, P. Chausse, J. M. Pichon and P. Laj "Seasonal variation of water-soluble inorganic component in size-segregated aerosol at the puy de Dôme station (1465 m a.s.l.), France", *Journal of Atmospheric Chemistry*, DOI: 10.1007/s10874-012-9229-2, 2012.
- Bukowiecki, N., Weingartner, E., Gysel, M., Collaud Coen, M., Zieger, P., Herrmann, E., Steinbacher, M., Heinz, Gägeler, W., Baltensperger, U.: A review of more than 20 years of aerosol observation at the high

1 altitude research station Jungfraujoch, Switzerland (3580 m asl), *Aerosol and Air Quality Research*, 16: 764–  
2 788, doi: 10.4209/aaqr.2015.05.0305, 2016.

3

4 Carrico, C.M., Kus, P., Rood, M.J., Quinn, P.K., Bates, T.S.: Mixtures of pollution, dust, sea salt, and  
5 volcanic aerosol during ACE-Asia: radiative properties as a function of relative humidity, *J. Geophys. Res.*,  
6 108, doi:10.1029/2003JD003405, 2003.

7

8 Carslaw, D. C.: The openair manual – open-source tools for analysing air pollution data, Manual for version  
9 0.7-0, King's College, London, 2012.

10

11 Carslaw, D. C. and Ropkins, K.: openair – an R package for air quality data analysis, *Environ. Modell. Softw.*,  
12 27–28, 52–61, 2012.

13

14 Cavalli, F., Alastuey, A., Areskoug, H., Ceburnis, D., Cech, J., Genberg, J., Harrison, R.M., Jaffrezo, J.L.,  
15 Kiss, G., Laj, P., Mihalopoulos, N., Perez, N., Quincey, P., Schwarz, J., Sellegri, K., Spindler, G., Swietlicki,  
16 E., Theodosi, C., Yttri, K.E., Aas, W., Putaud, J.P.: European aerosol phenomenology -4: Harmonized  
17 concentrations of carbonaceous aerosol at 10 regional background sites across Europe, *Atmos.*  
18 *Environ.*, 144, 133-145, 2016.

19

20 Chauvigné A., K. Sellegri, M. Hervo, N. Montoux, P. Freville, and Goloub, P.: Comparison of the aerosol  
21 optical properties and size distribution retrieved by Sun photometer with in-situ measurements at mid-latitude,  
22 *Atmos. Meas. Tech.*, 9, 4569-4585, doi:10.5194/amt-9-4569-2016, 2016.

23

24 Colette, A., Aas, W., Banin, L., Braban, C., Ferm, M., González Ortiz, A., Ilyin, I., Mar, K., Pandolfi, M.,  
25 Putaud, J.-P., Shatalov, V., Solberg, S., Spindler, G., Tarasova, O., Vana, M., Adani, M., Almodovar, P.,  
26 Berton, E., Bessagnet, B., Bohlin-Nizzetto, P., Boruvkova, J., Breivik, K., Briganti, G., Cappelletti, A.,  
27 Cuvelier, K., Derwent, R., D'Isidoro, M., Fagerli, H., Funk, C., Garcia Vivanco, M., González Ortiz, A.,  
28 Haeuber, R., Hueglin, C., Jenkins, S., Kerr, J., de Leeuw, F., Lynch, J., Manders, A., Mircea, M., Pay, M.,  
29 Pritula, D., Putaud, J.-P., Querol, X., Raffort, V., Reiss, I., Roustan, Y., Sauvage, S., Scavo, K., Simpson, D.,  
30 Smith, R., Tang, Y., Theobald, M., Tørseth, K., Tsyro, S., van Pul, A., Vidic, S., Wallasch, M., and Wind, P.:  
31 Air Pollution trends in the EMEP region between 1990 and 2012., Tech. Rep. Joint Report of the EMEP Task  
32 Force on Measurements and Modelling (TFMM), Chemical Co-ordinating Centre (CCC), Meteorological  
33 Synthesizing Centre- East (MSC-E), Meteorological Synthesizing Centre-West (MSC-W) EMEP/CCC Report  
34 1/2016, Norwegian Institute for Air Research, Kjeller, Norway, URL [http://www.  
35 unece.org/fileadmin/DAM/env/documents/2016/AIR/Publications/  
36 Air\\_pollution\\_trends\\_in\\_the\\_EMEP\\_region.pdf](http://www.unece.org/fileadmin/DAM/env/documents/2016/AIR/Publications/Air_pollution_trends_in_the_EMEP_region.pdf), 2016., 2016.

37

38 Collaud Coen, M., Weingartner, E., Nyeki, S., Cozic, J., Henning, S., Verheggen, B., Gehrig, R., and  
39 Baltensperger, U.: Long-term trend analysis of aerosol variables at the highalpine site Jungfraujoch, *J.*  
40 *Geophys. Res.*, 112, D13213, doi:10.1029/2006JD007995, 2007.

41

42 Collaud Coen, M., Weingartner, E., Apituley, A., Ceburnis, D., Fierz-Schmidhauser, R., Flentje, H., Henzing,  
43 J. S., Jennings, S. G., Moerman, M., Petzold, A., Schmid, O., and Baltensperger, U.: Minimizing light  
44 absorption measurement artifacts of the Aethalometer: evaluation of five correction algorithms, *Atmos. Meas.*  
45 *Tech.*, 3, 457–474, doi:10.5194/amt-3-457-2010, 2010.

46

47 Collaud Coen, M., Andrews, E., Asmi, A., Baltensperger, U., Bukowiecki, N., Day, D., Fiebig, M., Fjaeraa, A.  
48 M., Flentje, H., Hyvärinen, A., Jefferson, A., Jennings, S. G., Kouvarakis, G., Lihavainen, H., Lund Myhre, C.,  
49 Malm, W. C., Mihalopoulos, N., Molenaar, J. V., O'Dowd, C., Ogren, J. A., Schichtel, B. A., Sheridan, P.,  
50 Virkkula, A., Weingartner, E., Weller, R., and Laj, P.: Aerosol decadal trends – Part 1: In-situ optical  
51 measurements at GAW and IMPROVE stations, *Atmos. Chem. Phys.*, 13, 869-894, doi:10.5194/acp-13-869-  
52 2013, 2013.

53

54 Collaud Coen, M., Andrews, E., Aliaga, D., Andrade, M., Angelov, H., Bukowiecki, N., Ealo, M., Fialho, P.,  
55 Flentje, H., Gannet Hallar, A., Hooda, R., Kalapov, I., Krejci, R., Lin, N-H., Marinoni, A., Ming, J., Nguyen, N.  
56 A., Pandolfi, M., Pont, V., Ries, L., Rodríguez, S., Schauer, G., Sellegri, K., Sharma, S., Sun, J., Tunved, P.,  
57 Velasquez, P., and Ruffieux, D.: The topography contribution to the influence of the atmospheric boundary  
58 layer at high altitude stations, submitted to *Atm. Chem. Phys. Discuss.*, July 2017.

59

60 Crumeyrolle, S., Manninen, H. E., Sellegri, K., Roberts, G., Gomes, L., Kulmala, M., Weigel, R., Laj, P., and  
61 Schwarzenboeck, A.: New particle formation events measured on board the ATR-42 aircraft during the  
62 EUCAARI campaign, *Atmos. Chem. Phys.*, 10, 6721–6735, doi:10.5194/acp-10-6721-2010, 2010.

63

- 1 Cusack, M., Alastuey, A., Pérez, N., Pey, J., and Querol, X.: Trends of particulate matter (PM<sub>2.5</sub>) and  
2 chemical composition at a regional background site in the Western Mediterranean over the last nine years  
3 (2002–2010), *Atmos. Chem. Phys.*, 12, 8341–8357, doi:10.5194/acp-12-8341-2012, 2012.
- 4  
5 Delene, D. J. and Ogren, J. A.: Variability of aerosol optical properties at four North American surface  
6 monitoring sites, *J. Atmos. Sci.*, 59, 1135–1149, 2002.
- 7  
8 Eleftheriadis, K., Ochsenkuhn, K.M., Lymperopoulou, T., Karanasiou, A., Razos, P., Ochsenkuhn-  
9 Petropoulou, M.: Influence of local and regional sources on the observed spatial and temporal variability of  
10 size resolved atmospheric aerosol mass concentrations and water-soluble species in the Athens  
11 metropolitan area, *Atm. Environ.*, 97, 252-261, <http://dx.doi.org/10.1016/j.atmosenv.2014.08.013>, 2014.
- 12  
13 Diaz, A.M., Diaz, J.P., Exposito, F.J., Hernandez-Leal, P.A., Savoie, D., Querol, X.: Air masses and aerosols  
14 chemical components in the free troposphere at the subtropical northeast Atlantic region, *J. Atmos. Chem.*,  
15 53, 63–90, 2006.
- 16  
17 Diapouli, E., Manousakas, M. I., Vratolis, S., Vasilatou, V., Pateraki, S., Bairachtari, K. A., Querol, X., Amato,  
18 F., Alastuey, A., Karanasiou, A. A., Lucarelli, F., Nava, S., Calzolari, G., Gianelle, V. L., Colombi, C., Alves,  
19 C., Custódio, D., Pio, C., Spyrou, C., Kallos, G. B., Eleftheriadis, K.: AIRUSE-LIFE +: estimation of natural  
20 source contributions to urban ambient air PM<sub>10</sub> and PM<sub>2.5</sub> concentrations in southern Europe – implications  
21 to compliance with limit values. *Atmos. Chem. Phys.*, 17, 3673–3685, 2017..
- 22  
23 Doherty, S.J., Quinn, P.K., Jefferson, A., Carrico, C.M., Anderson, T.L., Hegg, D.: A comparison and  
24 summary of aerosol optical properties as observed in situ from aircraft, ship, and land during ACE-Asia, *J.*  
25 *Geophys. Res.*, 110, D04201. doi:10.1029/2004JD004964, 2005.
- 26  
27 Ealo, M., Alastuey, A., Ripoll, A., Pérez, N., Minguillón, M. C., Querol, X., and Pandolfi, M.: Detection of  
28 Saharan dust and biomass burning events using near-real-time intensive aerosol optical properties in the  
29 north-western Mediterranean, *Atmos. Chem. Phys.*, 16, 12567-12586, [https://doi.org/10.5194/acp-16-12567-](https://doi.org/10.5194/acp-16-12567-2016)  
30 2016, 2016.
- 31  
32 EEA: European Environmental Agency Air quality in Europe – 2013 report, EEA report 9/2013, Copenhagen,  
33 1725–9177, available at: <http://www.eea.europa.eu/publications/air-quality-in-europe-2013>, 2013.
- 34  
35 EEA: European Environmental Agency Air quality in Europe – 2016 report, EEA Report No 28/2016,  
36 Copenhagen, available at:  
37 [file:///D:/Usuari/Descargas/Air%20quality%20in%20Europe%202016%20report%20THAL16027ENN%20\(1\).](file:///D:/Usuari/Descargas/Air%20quality%20in%20Europe%202016%20report%20THAL16027ENN%20(1).pdf)  
38 pdf, 2016.
- 39  
40 EMEP, Transboundary particulate matter in Europe Status report 2008 NILU Reference: O-98134. Edited by  
41 Yttri, K.-E., Aas, W., Tørseth, K., Stebel, K., Nyiri, Á., Tsyro, S., Merckova, K., Wankmüller, R., Winiwarter,  
42 W., Bauer, H., Caseiro, A., Puxbaum, H., Holzer-Popp, T., Schroedter-Homscheidt, M.  
43 (<http://tarantula.nilu.no/projects/ccc/reports/emep4-2008.pdf>), 2008.
- 44  
45 Engvall, A.-C., Krejci, R., Ström, J., Treffeisen, R., Scheele, R., Hermansen, O., and Paatero, J.: Changes in  
46 aerosol properties during spring-summer period in the Arctic troposphere, *Atmos. Chem. Phys.*, 8, 445-462,  
47 <https://doi.org/10.5194/acp-8-445-2008>, 2008.
- 48  
49 EPA: Emissions of primary particulate matter and secondary particulate matter precursors, Assessment  
50 published December 2011, available at: <http://www.epa.gov/ttn/chief/trends/>, CSI 003, 2011.
- 51  
52 Esteve, A.R., Estellés, V., Utrillas, M.P., Martínez-Lozano, J.A.: In-situ integrating nephelometer  
53 measurements of the scattering properties of atmospheric aerosols at an urban coastal site in western  
54 Mediterranean, *Atm. Env.*, 47, 43-50, 2012.
- 55  
56 Fierz-Schmidhauser, R., Zieger, P., Vaishya, A., Monahan, C., Bialek, J., O'Dowd, C. D., Jennings, S. G.,  
57 Baltensperger, U., Weingartner, E.: Light scattering enhancement factors in the marine boundary layer  
58 (Mace Head, Ireland), *J. Geophys. Res.*, 115, D20204, doi:10.1029/2009JD013755, 2010a.
- 59  
60 Fierz-Schmidhauser, R., Zieger, P., Gysel, M., Kammermann, L., DeCarlo, P. F., Baltensperger, U., and  
61 Weingartner, E.: Measured and predicted aerosol light scattering enhancement factors at the high alpine site  
62 Jungfraujoch, *Atmos. Chem. Phys.*, 10, 2319–2333, doi:10.5194/acp-10-2319-2010, 2010b.
- 63

- 1 Guerreiro, C., Leeuw, F. de, Foltescu, V., Horálek, J., and European Environment Agency: Air quality in  
2 Europe 2014 report, Luxembourg: Publications Office, available at: [http://bookshop.europa.  
3 eu/uri?target=EUB:NOTICE:THAL14005:EN:HTML](http://bookshop.europa.eu/uri?target=EUB:NOTICE:THAL14005:EN:HTML) (last access: 2 June 2016), 2014.  
4
- 5 Hansen, J.E. and Travis, L.D.: Light scattering in the planetary atmosphere, *Space Science Reviews*, 16  
6 527-610, 1974.  
7
- 8 Henschel, S., Querol, X., Atkinson, R., Pandolfi, M., Zeca, A., Le Tertre, A., Analitis, A., Katsouyanni, K.,  
9 Chanel, O., Pascal, M., Bouland, C., Haluza, D., Medina, S., and Goodman, P. G.: Ambient air SO<sub>2</sub> patterns  
10 in 6 European cities, *Atmos. Environ.*, 79, 236–247, 2013.  
11
- 12 Hollander, M., and Wolfe, D. A.: *Nonparametric statistical methods*, 2nd ed. Wiley, New York, New York,  
13 787, 1999.  
14
- 15 IPCC: *Climate Change 2014: Synthesis Report. Contribution of Working Groups I, II and III to the Fifth  
16 Assessment Report of the Intergovernmental Panel on Climate Change* [Core Writing Team, R.K. Pachauri  
17 and L.A. Meyer (eds.)]. IPCC, Geneva, Switzerland, 151 pp, 2014.  
18
- 19 Kalivitis, N., Bougiatioti, A., Kouvarakis, G., Mihalopoulos, N.: Long term measurements of atmospheric  
20 aerosol optical properties in the Eastern Mediterranean, *Atmosp. Res.*, 102, 351–357, 2011.  
21
- 22 Karanasiou, A., Querol, X., Alastuey, A., Perez, N., Pey, J., Perrino, C., Berti, G., Gandini, M., Poluzzi, V.,  
23 Ferrari, S., de la Rosa, J.: Particulate matter and gaseous pollutants in the Mediterranean Basin: Results  
24 from the MED-PARTICLES project, *Sci. of Tot. Environ.*, 488–489, 297–315, 2014.  
25
- 26 Kecorius, S., Kivekäs, N., Kristensson, A., Tuch, T., Covert, D.S., Birmili, W., Lihavainen, H., Hyvärinen,  
27 A.P., Martinsson, J., Sporre, M.K., Swietlicki, E., Wiedensohler, A. Ulevicius, V.: Significant increase of  
28 aerosol number concentrations in air masses crossing a densely trafficked sea area, *Oceanologia*, 58, 1—  
29 12, 2016.  
30
- 31 Korras-Carraca, M. B., Hatzianastassiou, N., Matsoukas, C., Gkikas, A., and Papadimas, C. D.: The regime  
32 of aerosol asymmetry parameter over Europe, the Mediterranean and the Middle East based on MODIS  
33 satellite data: evaluation against surface AERONET measurements, *Atmos. Chem. Phys.*, 15, 13113-13132,  
34 doi:10.5194/acp-15-13113-2015, 2015.  
35
- 36 Laj, P., Klausen, J., Bilde, M., Plaß-Duelmer, C., Pappalardo, G., Clerbaux, C, Baltensperger, U., Hjorth, J.,  
37 Simpson, D., Reimann, S., Coheur, P.-F., Richter, A., De Mazie, M., Rudich, Y., McFiggans, G., Torseth, K.,  
38 Wiedensohler, A., Morin, S., Schulz, M., Allan, J. D., Attie, J.-L., Barnes, I., Birmili, W., Cammas, J. P.,  
39 Dommen, J., Dorn, H.-P., Fowler, D., Fuzzi, S., Glasius, M., Granier, C., Hermann, M., Isaksen, I. S. A.,  
40 Kinne, S., Koren, I., Madonna, F., Maione, M., Massling, A., Moehler, O., Mona, L., Monks, P. S., Müller, D.,  
41 Müller, T., Orphal, J., Peuch, V.-H., Stratmann, F., Tanre, D., Tyn dall, F., Abo Riziqmm, A., Van  
42 Roozendaal, M., Villani P., Wehner, B., Wex, H., and Zardini, A. A.: Measuring atmospheric composition  
43 change, *Atmos. Environ*, 43, 5351–5414, doi:10.1016/j.atmosenv.2009.08.020, 2009.  
44
- 45 Li, J., Carlson, B. E., Dubovik, O., and Laciš, A. A.: Recent trends in aerosol optical properties derived from  
46 AERONET measurements, *Atmos. Chem. Phys.*, 14, 12271–12289, doi:10.5194/acp-14-12271-2014, 2014.  
47
- 48 Lihavainen, H., Hyvärinen, A., Asmi, E., Hatakka, J. and Viisanen, Y.: Long-term variability of aerosol optical  
49 properties in northern Finland, *Boreal Environment Research*, 20, 526–541, 2015a.  
50
- 51 Lihavainen, H., Asmi, E., Aaltonen, V., Makkonen, U. and Kerminen, V-M.: Direct radiative feedback due to  
52 biogenic secondary organic aerosol estimated from boreal forest site observations, *Environ. Res. Lett.*, 10,  
53 doi:10.1088/1748-9326/10/10/104005, 2015b.  
54
- 55 Lyamani, H., Olmo, F. J., and Alados-Arboledas, L.: Physical and optical properties of aerosols over an  
56 urban location in Spain: seasonal and diurnal variability, *Atmos. Chem. Phys.*, 10, 239-254, doi:10.5194/acp-  
57 10-239-2010, 2010.  
58
- 59 Lyamani, H., Olmo, F.J., Foyo, I., Alados-Arboledas, L.: Black carbon aerosols over an urban area in south-  
60 eastern Spain: Changes detected after the 2008 economic crisis, *Atmos. Environ.*, 45, 6423–6432, 2011.  
61
- 62 Lyamani, H., Fernández-Gálvez, J., Pérez-Ramírez, D., Valenzuela, A., Antón, M., Alados, I., Titos, G.,  
63 Olmo, F.J., Alados-Arboledas, L.: Aerosol properties over two urban sites in South Spain during an extended  
64 stagnation episode in winter season, *Atmos. Environ.*, 62, 424-432, 2012.

- 1 Ma, N., Birmili, W., Müller, T., Tuch, T., Cheng, Y. F., Xu, W. Y., Zhao, C. S., and Wiedensohler, A.:  
2 Tropospheric aerosol scattering and absorption over central Europe: a closure study for the dry particle state,  
3 *Atmos. Chem. Phys.*, 14, 6241-6259, doi:10.5194/acp-14-6241-2014, 2014.
- 4  
5 Manktelow, P. T., Mann, G. W., Carslaw, K. S., Spracklen, D. V., and Chipperfield, M. P.: Regional and  
6 global trends in sulphate aerosol since the 1980's, *Geophys. Res. Lett.*, 34, L14803,  
7 doi:10.1029/2006GL028668, 2007.
- 8  
9 Marengo, F., Bonasoni, P., Calzolari, F., Ceriani, M., Chiari, M., Cristofanelli, P., D'Alessandro, A., Fermo, P.,  
10 Lucarelli, F., Mazzei, F., Nava, S., Piazzalunga, A., Prati, P., Valli, G., and Vecchi, R.: Characterization of  
11 atmospheric aerosols at Monte Cimone, Italy, during summer 2004: Source apportionment and transport  
12 mechanisms, *J. Geoph. Res.*, 111, doi:10.1029/2006JD007145, 2006.
- 13  
14 Marshall, S.F., Covert, D.S., and Charlson, R.J.: Relationship between asymmetry parameter and  
15 hemispheric backscatter ratio: implications for climate forcing by aerosols, *App. Opt.*, 34, 27, 6306 – 6311,  
16 1995.
- 17  
18 Molnár, A., Bécsi, Z., Imre, K., Gácsér, V., Zita Ferenczi, Z.: Characterization of background aerosol  
19 properties during a wintertime smog episode, *Aerosol and Air Quality Research*, 16, 1793–1804, 2016.
- 20  
21 Müller, T., Nowak, A., Weidensohler, A., Sheridan, P., Laborde, M., Covert, D.S., Marinoni, A., Imre, K.,  
22 Henzing, B., Roger, J.-C., Martins dos Santos, S., Wilhelm, R., Wang, Y.-Q., de Leeuw, G.: Angular  
23 illumination and truncation of three different integrating nephelometers: implications for empirical size-based  
24 corrections, *Aerosol Sci. Technol.*, 43, 581–586, 2009.
- 25  
26 Müller, T., Laborde, M., Kassell, G., and Wiedensohler, A.: Design and performance of a three-wavelength  
27 LED-based total scatter and backscatter integrating nephelometer, *Atmos. Meas. Tech.*, 4, 1291-1303,  
28 <https://doi.org/10.5194/amt-4-1291-2011>, 2011.
- 29  
30 Nyeki, S., Baltensperger, U., Colbeck, I., Jost, D.T., Weingartner, E., Gäggeler, H.W.: The Jungfraujoch high-  
31 alpine research station (3454 m) as a background continental site for the measurement of aerosol  
32 parameters, *J. Geophys. Res.*, 103, 6097-6107, 1998.
- 33  
34 Nyeki, S., Halios, C.H., Baum, W., Eleftheriadis, K., Flentje, H., Gröbner, J., Vuilleumier, L., and Wehrli, C.:  
35 Ground-based aerosol optical depth trends at three high-altitude sites in Switzerland and southern Germany  
36 from 1995 to 2010, *J. Geophys. Res.*, 117, D18202, doi:10.1029/2012JD017493, 2012.
- 37  
38 Obiso, V., and Jorba, O.: Impact of aerosol physical properties on atmospheric radiative effects due to aerosol-radiation interaction, *Sci. Tot. Environ.*, 112, 68-82, 2017.
- 39  
40  
41 O'Connor, T.C., Jennings, S.G., O'Dowd, C.D.: Highlights of fifty years of atmospheric aerosol research at  
42 Mace Head, *Atmos. Res.*, 90, 338–355, 2008.
- 43  
44 Ogren, J. A., Andrews, E., McComiskey, A., Sheridan, P., Jefferson, A., and Fiebig, M.: New insights into  
45 aerosol asymmetry parameter, in: *Proceedings of the 16th ARM Science Team Meeting*, Albuquerque, NM,  
46 USA, 2006.
- 47  
48 Pandolfi, M., Cusack, M., Alastuey, A., and Querol, X.: Variability of aerosol optical properties in the Western  
49 Mediterranean Basin, *Atmos. Chem. Phys.*, 11, 8189–8203, doi:10.5194/acp-11-8189-2011, 2011.
- 50  
51 Pandolfi, M., Ripoll, A., Querol, X., and Alastuey, A.: Climatology of aerosol optical properties and black  
52 carbon mass absorption cross section at a remote high-altitude site in the western Mediterranean Basin,  
53 *Atmos. Chem. Phys.*, 14, 6443-6460, doi:10.5194/acp-14-6443-2014, 2014.
- 54  
55 Pandolfi, M., Querol, X., Alastuey, A., Jimenez, J. L., Jorba, O., Day, D., Ortega, A., Cubison, M. J.,  
56 Comerón, A., Sicard, M., Mohr, C., Prévôt, A. S. H., Minguillón, M. C., Pey, J., Baldasano, J. M., Burkhardt, J.  
57 F., Seco, R., Peñuelas, J., van Drooge, B. L., Artiñano, B., Di Marco, C., Nemitz, E., Schallhart, S., Metzger,  
58 A., Hansel, A., Lorente, J., Ng, S., Jayne, J., and Szidat, S.: Effects of sources and meteorology on  
59 particulate matter in the Western Mediterranean Basin: An overview of the DAURE campaign, *J. Geophys.  
60 Res.-Atmos.*, 119, 4978–5010, doi:10.1002/2013JD021079, 2014a.
- 61  
62 Pandolfi, M., Alastuey, A., Pérez, N., Reche, C., Castro, I., Shatalov, V., and Querol, X.: Trends analysis of  
63 PM source contributions and chemical tracers in NE Spain during 2004–2014: a multi-exponential approach,  
64 *Atmos. Chem. Phys.*, 16, 11787-11805, doi:10.5194/acp-16-11787-2016, 2016.



- 1  
2 Pey, J., Querol, X., Alastuey, A., Forastiere, F., and Stafoggia, M.: African dust outbreaks over the  
3 Mediterranean Basin during 2001–2011: PM10 concentrations, phenomenology and trends, and its relation  
4 with synoptic and mesoscale meteorology, *Atmos. Chem. Phys.*, 13, 1395–1410, doi:10.5194/acp-13-1395-  
5 2013, 2013.
- 6  
7 Putaud, J.P., Raes, F., Van Dingenen, R., Brüggemann, E., Facchini, M.C., Decesari, S., Fuzzi, S., Gehrig,  
8 R., Hüglin, C., Laj, P., Lorbeer, G., Maenhaut, W., Mihalopoulos, N., Müller, K., Querol, X., Rodriguez, S.,  
9 Schneider, J., Spindler, G., Ten Brink, H., Tørseth, K., Alfred Wiedensohler, A.: European aerosol  
10 phenomenology d2: chemical characteristics of particulate matter at kerbside, urban, rural and background  
11 sites in Europe, *Atmos. Environ.*, 38, 2579-2595, 2004.
- 12  
13 Putaud, J.P., Van Dingenen, R., Alastuey, A., Bauer, H., Birmili, W., Cyrus, J., Flentje, H., Fuzzi, S., Gehrig,  
14 R., Hansson, H.C., Harrison, R.M., Hermann, H., Hitzenberger, R., Hüglin, C., Jones, A.M., Kasper-Giebl, A.,  
15 Kiss, G., Kousa, A., Kuhlbusch, T.A.J., Lösschau, G., Maenhaut, W., Molnar, A., Moreno, T., Pekkanen, J.,  
16 Perrino, C., Pitz, M., Puxbaum, H., Querol, X., Rodriguez, S., Salma, I., Schwarz, J., Smolik, J., Schneider,  
17 J., Spindler, G., ten Brink, H., Tursic, J., Viana, M., Wiedensohler, A., Raes, F.: A European aerosol  
18 phenomenology d 3: physical and chemical characteristics of particulate matter from 60 rural, urban, and  
19 kerbside sites across Europe, *Atmos. Environ.*, 44, 1308-1320, 2010.
- 20  
21 Putaud, J. P., Cavalli, F., Martins dos Santos, S., and Dell'Acqua, A.: Long-term trends in aerosol optical  
22 characteristics in the Po Valley, Italy, *Atmos. Chem. Phys.*, 14, 9129-9136, doi:10.5194/acp-14-9129-2014,  
23 2014.
- 24  
25 Querol, X., Pey, J., Pandolfi, M., Alastuey, A., Cusack, M., Perez, N., Moreno, T., Viana, M., Mihalopoulos,  
26 N., Kallos, G., and Kleanthous, S.: African dust contributions to mean ambient PM10 mass-levels across the  
27 Mediterranean Basin, *Atmos. Environ.*, 43, 4266–4277, doi:10.1016/j.atmosenv.2009.06.013, 2009.
- 28  
29 Querol, X., Alastuey, A., Pandolfi, M., Reche, C., Pérez, N., Minguillón, M. C., Moreno, T., Viana, M.,  
30 Escudero, M., Orió, A., Pallarés, M., and Reina, F.: 2001–2012 trends on air quality in Spain, *Sci. Total*  
31 *Environ.*, 490, 957–969, doi:10.1016/j.scitotenv.2014.05.074, 2014.
- 32  
33 Revuelta, M.A., Artiñano, B., Gómez-Moreno, F.J., Viana, M., Reche, C., Querol, X., Fernández, A.J.,  
34 Mosquera, J.L., Núñez, L., Pujadas, M., Herranz, A., López, B., Molero, F., Bezares, J.C., Coz, E., Palacios,  
35 M., Sastre, M., Fernández, J.M., Salvador, P., Aceña, B.: Ammonia levels in different kinds of sampling sites  
36 in the central Iberian Peninsula, Proceedings of the 2nd Iberian meeting on aerosol science and technology,  
37 RICTA 2014.
- 38  
39 Ripoll, A., Pey, J., Minguillón, M. C., Pérez, N., Pandolfi, M., Querol, X., and Alastuey, A.: Three years of  
40 aerosol mass, black carbon and particle number concentrations at Montsec (southern Pyrenees, 1570 m  
41 a.s.l.), *Atmos. Chem. Phys.*, 14, 4279-4295, <https://doi.org/10.5194/acp-14-4279-2014>, 2014.
- 42  
43 Rodríguez, S., Alastuey, A., Alonso-Pérez, S., Querol, X., Cuevas, E., Abreu-Afonso, J., Viana, M., Pérez,  
44 N., Pandolfi, M., and de la Rosa, J.: Transport of desert dust mixed with North African industrial pollutants in  
45 the subtropical Saharan Air Layer, *Atmos. Chem. Phys.*, 11, 6663-6685, doi:10.5194/acp-11-6663-2011,  
46 2011.
- 47  
48 Rodríguez, S., Cuevas, E., Prospero, J. M., Alastuey, A., Querol, X., López-Solano, J., García, M. I., and  
49 Alonso-Pérez, S.: Modulation of Saharan dust export by the North African dipole, *Atmos. Chem. Phys.*, 15,  
50 7471-7486, <https://doi.org/10.5194/acp-15-7471-2015>, 2015.
- 51  
52 Rose C., K. Sellegri, Fernando Velarde, Isabel Moreno, Kay Weinhold, Ali Wiedensholer, and Laj, P.:  
53 Frequent nucleation events at the high altitude station of Chacaltaya (5240 m a.s.l.), Bolivia, *Atmos. Environ.*,  
54 102, 18-29, doi :10.1016/j.atmosenv.2014.11.015, 2015.
- 55  
56 Rotstayn, L. D., Collier, M. A., Chrastansky, A., Jeffrey, S. J., and Luo, J.-J.: Projected effects of declining  
57 aerosols in RCP4.5: unmasking global warming?, *Atmos. Chem. Phys.*, 13, 10883-10905, doi:10.5194/acp-  
58 13-10883-2013, 2013.
- 59  
60 Sherman, J. P., Sheridan, P. J., Ogren, J. A., Andrews, E., Hageman, D., Schmeisser, L., Jefferson, A., and  
61 Sharma, S.: A multi-year study of lower tropospheric aerosol variability and systematic relationships from  
62 four North American regions, *Atmos. Chem. Phys.*, 15, 12487-12517, [https://doi.org/10.5194/acp-15-12487-](https://doi.org/10.5194/acp-15-12487-2015)  
63 2015, 2015.
- 64

- 1 Schuster, G. L., Dubovik, O., and Holben, B. N.: Angstrom exponent and bimodal aerosol size distributions,  
2 J. Geophys. Res., 111, D07207, doi:10.1029/2005JD006328, 2006.
- 3
- 4 Seinfeld, J. H. and Pandis, S. N.: Atmospheric Chemistry and Physics, John Wiley and Sons, New York,  
5 1998.
- 6
- 7 Sen, P. K.: Estimates of regression coefficient based on Kendall's tau, J. Am. Stat. Assoc., 63, 1379–1389,  
8 1968.
- 9
- 10 Spindler, G., Brüggemann, E., Gnauk, T., Gruner, Müller, A. K., Herrmann, H.: A four-year size-segregated  
11 characterization study of particles PM<sub>10</sub>, PM<sub>2.5</sub> and PM<sub>1</sub> depending on air mass origin at Melpitz, Atmos.  
12 Environ., 44, 164-173, 2010.
- 13
- 14 Stohl, A., Aamaas, B., Amann, M., Baker, L. H., Bellouin, N., Berntsen, T. K., Boucher, O., Cherian, R.,  
15 Collins, W., Daskalakis, N., Dusinska, M., Eckhardt, S., Fuglestedt, J. S., Harju, M., Heyes, C., Hodnebrog,  
16 Ø., Hao, J., Im, U., Kanakidou, M., Klimont, Z., Kupiainen, K., Law, K. S., Lund, M. T., Maas, R., MacIntosh,  
17 C. R., Myhre, G., Myriokefalitakis, S., Olivie, D., Quaas, J., Quennehen, B., Raut, J.-C., Rumbold, S. T.,  
18 Samset, B. H., Schulz, M., Seland, Ø., Shine, K. P., Skeie, R. B., Wang, S., Yttri, K. E., and Zhu, T.:  
19 Evaluating the climate and air quality impacts of short-lived pollutants, Atmos. Chem. Phys., 15, 10529-  
20 10566, doi:10.5194/acp-15-10529-2015, 2015.
- 21
- 22 Ström, J., Umegård, J., Tørseth, K., Tunved, P., Hansson, H. C., Holmen, K., Wismann, V., Herber, A., and  
23 König-Langlo, G.: One year of particle size distribution and aerosol chemical composition measurements at  
24 the Zeppelin Station, Svalbard, March 2000-March 2001, Phys. Chem. Earth, 28, 1181–1190, 2003.
- 25
- 26
- 27 Theil, H.: A rank invariant method of linear and polynomial regression analysis, I, II, III, Proceedings of the  
28 Koninklijke Nederlandse Akademie Wetenschappen, Series A, Mathematical Sciences, 386–392, 521–525,  
29 1397–1412, 1950.
- 30
- 31 Titos, G., Foyo-Moreno, I., Lyamani, H., Querol, X., Alastuey, A., Alados-Arboledas, L.: Optical properties  
32 and chemical composition of aerosol particles at an urban location: An estimation of the aerosol mass  
33 scattering and absorption efficiencies, J. Geophys. Res. Atm., 117, 4, D04206, 2012.
- 34
- 35 Titos, G., Lyamani, H., Pandolfi, M., Alastuey, A., Alados-Arboledas, L.: Identification of fine (PM<sub>1</sub>) and  
36 coarse (PM<sub>10-1</sub>) sources of particulate matter in an urban environment, Atmos. Environ., 89, 593-602, 2014.
- 37
- 38 Titos, G., del Águila, A., Cazorla, A., Lyamani, H., Casquero-Vera, J.A., Colombi, C., Cuccia, E., Gianelle, V.,  
39 Močnik, G., Alastuey, A., Olmo, F.J., Alados-Arboledas, L.: Spatial and temporal variability of carbonaceous  
40 aerosols: Assessing the impact of biomass burning in the urban environment, Sci. of Tot. Environ., 578, 613-  
41 625, 2017.
- 42
- 43 Tørseth, K., Aas, W., Breivik, K., Fjærraa, A. M., Fiebig, M., Hjellbrekke, A. G., Lund Myhre, C., Solberg, S.,  
44 and Yttri, K. E.: Introduction to the European Monitoring and Evaluation Programme (EMEP) and observed  
45 atmospheric composition change during 1972–2009, Atmos. Chem. Phys., 12, 5447–5481, doi:10.5194/acp-  
46 12-5447-2012, 2012.
- 47
- 48 Tunved, P., Hansson, H.-C., Kerminen, V.-M., Ström, J., Dal Maso, M., Lihavainen, H., Viisanen, Y., Aalto, P.  
49 P., Komppula, M., Kulmala, M.: High Natural Aerosol Loading over Boreal Forests, Science, 312, 5771, 261-  
50 263, DOI: 10.1126/science.1123052, 2006.
- 51
- 52 Valenzuela, A., Olmo, F.J., Lyamani, H., Antón, M., Titos, G., Cazorla, A., Alados-Arboledas, L.: Aerosol  
53 scattering and absorption Angström exponents as indicators of dust and dust-free days over Granada  
54 (Spain), Atmos. Res., 154, 1-13, 2015.
- 55
- 56 Van Dingenen, R., Putaud, J.P., Raes, F., Baltensperger, U., Charron, A., Facchini, M.C., Decesari, S.,  
57 Fuzzi, S., Gehrig, R., Hansson, H.C., Harrison, R.M., Hüglin, C., Jones, A.M., Laj, P., Lorbeer, G., Maenhaut,  
58 W., Palgren, F., Querol, X., Rodriguez, S., Schneider, J., Ten Brink, H., Tunved, P., Tørseth, K., Wehner, B.,  
59 Weingartner, E., Wiedensohler, A., Wählin, P.: A European aerosol phenomenology\_1: physical  
60 characteristics of particulate matter at kerbside, urban, rural and background sites in Europe, Atmos.  
61 Environ., 38, 2561-2577, 2004.
- 62

- 1 van Donkelaar, A., Randall, M., Brauer, M., Kahn, R., Levy, R., Verduzco, C., and Villeneuve, P. J. Global  
2 estimates of exposure to fine particulate matter concentrations from satellite-based aerosol optical depth,  
3 *Environ. Health Persp.*, 118, 847–855, doi:10.1289/ehp.0901623, 2010.
- 4
- 5 Venzac, H., Sellegri, K., Villani, P., Picard, D., and Laj, P.: Seasonal variation of aerosol size distributions in  
6 the free troposphere and residual layer at the puy de Dome station, France, *Atmos. Chem. Phys.*, 9, 1465–  
7 1478, doi:10.5194/acp-9-1465-2009, 2009.
- 8
- 9 Virkkula, A., Backman, J., Aalto, P. P., Hulkkonen, M., Riuttanen, L., Nieminen, T., dal Maso, M., Sogacheva,  
10 L., de Leeuw, G., and Kulmala, M.: Seasonal cycle, size dependencies, and source analyses of aerosol  
11 optical properties at the SMEAR II measurement station in Hyytiälä, Finland, *Atmos. Chem. Phys.*, 11, 4445–  
12 4468, doi:10.5194/acp-11-4445-2011, 2011.
- 13
- 14 Vrekoussis, M., Liakakou, E., Koc-ak, M., Kubilay, N., Oikonomou, K., Sciare, J., Mihalopoulos, N.:  
15 Seasonal variability of optical properties of aerosols in the Eastern Mediterranean, *Atmosp. Environ.*, 39,  
16 7083–7094, 2005.
- 17
- 18 WMO/GAW report 227: Aerosol Measurement Procedures, Guidelines and Recommendations, 2nd Edition,  
19 2016, 103 pp. August 2016 (WMO-No. 1177).
- 20
- 21 Zanatta, M., Gysel, M., Bukowiecki, N., Müller, T., Weingartner, E., Areskoug, H., Fiebig, M., Yttri, K.E.,  
22 Mihalopoulos, N., Kouvarakis, G., Beddows, D., Harrison, R.M., Cavalli, F., Putaud, J.P., Spindler, G.,  
23 Wiedensohler, A., Alastuey, A., Pandolfi, M., Sellegri, K., Swietlicki, E., Jaffrezo, J.L., Baltensperger, U., Laj,  
24 P.: A European aerosol phenomenology-5: Climatology of black carbon optical properties at 9 regional  
25 background sites across Europe, *Atm. Env.*, 145, 346-364, 2016.
- 26
- 27 Zieger, P., Fierz-Schmidhauser, R., Gysel, M., Ström, J., Henne, S., Yttri, K. E., Baltensperger, U., and  
28 Weingartner, E.: Effects of relative humidity on aerosol light scattering in the Arctic, *Atmos. Chem. Phys.*, 10,  
29 3875–3890, doi:10.5194/acp-10-3875-2010, 2010.
- 30
- 31 Zieger, P., Kienast-Sjögren, E., Starace, M., von Bismarck, J., Bukowiecki, N., Baltensperger, U., Wienhold,  
32 F. G., Peter, T., Ruhtz, T., Collaud Coen, M., Vuilleumier, L., Maier, O., Emili, E., Popp, C., and Weingartner,  
33 E.: Spatial variation of aerosol optical properties around the high-alpine site Jungfraujoch (3580 m a.s.l.),  
34 *Atmos. Chem. Phys.*, 12, 7231-7249, doi:10.5194/acp-12-7231-2012, 2012.
- 35
- 36 Zieger, P., Fierz-Schmidhauser, R., Poulain, L., Müller, T., Birmili, W., Spindler, G., Wiedensohler, A.,  
37 Baltensperger, U. and Weingartner, E.: Influence of water uptake on the aerosol particle light scattering  
38 coefficients of the Central European aerosol, *Tellus B: Chemical and Physical Meteorology*, 66:1, 22716,  
39 DOI: 10.3402/ tellusb.v66.22716, 2014.
- 40
- 41 Zieger, P., Väisänen, O., Corbin, J.C., Partridge, D.G., Bastelberger, S., Mousavi-Fard, M., Rosati, B., Gysel,  
42 M., Krieger, U.K., Leck, C., Nenes, A., Riipinen, I., Virtanen, A., and Salter, M.E.: Revising the hygroscopicity  
43 of inorganic sea salt particles, *Nature Communication*, DOI: 10.1038/ncomms15883, 2017.
- 44  
45  
46  
47  
48  
49  
50  
51  
52  
53  
54  
55  
56  
57  
58  
59  
60  
61  
62  
63  
64

## 1 Tables

2

## 3 Table 1: List of ACTRIS observatories providing aerosol particle scattering measurements

Observatory name/setting (1)	Country	Observatory code	Lat, Long	Altitude [m a.s.l.]	Geographical location	Inlet	Nephelometer model	Period (a)
<b>Arctic observatories</b>								
Zepelin (ZEP)	Svalbard (Norway)	NO0042G	78.9067 N, 11.8883 E	474	Nordic and Baltic	PM <sub>10</sub>	TSI3563	07/2010 –12/2014
Pallas (PAL)	Finland	FI0096G	67.97 N, 24.12 E	565	Nordic and Baltic	PM <sub>5</sub> ; PM <sub>2.5</sub> ; PM <sub>10</sub> (b)	TSI3563	02/2000 –12/2015
<b>Antarctic observatories</b>								
Troll (TRL)	Antarctica	NO0058G	-72.0167 N, 2.5333 E	1309	Antarctica	whole air; PM <sub>10</sub> (c)	TSI3563	02/2007 –12/2015
<b>Mountain observatories</b>								
Puy de Dome (PUY)	France	FR0030R	45.7667 N, 2.95 E	1465	West	whole air	TSI3563	01/2007 –12/2014
Izaña (IZO)	Spain	ES0018G	28.309 N, -16.4994 E	2373	Southwest	PM <sub>10</sub>	TSI3563	03/2008 – 12/2015
Montsec (MSA)	Spain	ES0022R	42.0513 N, 0.44 E	1570	Southwest	PM <sub>2.5</sub> ; PM <sub>10</sub> (d)	ECOTECH Aurora3000	01/2013 – 12/2015
Jungfraujoch (JFJ)	Switzerland	CH0001G	46.5475 N, 7.985 E	3578	Central	whole air	TSI3563	07/1995 –12/2015
Mt. Cimone (CMN)	Italy	IT0009R	44.1833 N, 10.7 E	2165	Central	whole air	ECOTECH  Aurora M9003;  TSI 3563 (e)	05/2007 –12/2015
Hohenpeissenberg (HPB)	Germany	DE0043G	47.8 N, 11.0167 E	985	Central	PM <sub>10</sub>	TSI3563	01/2006 –12/2015
Beo Moussala (BEO)	Bulgaria	BG0001R	42.1667 N, 23.5833 E	2971	East	whole air	TSI3563	03/2007 –12/2015
Mt. Chacaltaya (CHC)	Bolivia	BO0001R	-16.2000 N, -68.09999 E	5240	South America	whole air	ECOTECH Aurora3000	01/2012 – 12/2015 (f)
<b>Coastal observatories</b>								
Preila (PLA)	Lithuania	LT0015R	55.35 N, 21.0667 E	5	Nordic and Baltic	PM <sub>10</sub>	TSI3563	12/2012 –04/2014
Mace Head (MHD)	Ireland	IE0031R	53.3258 N, -9.8994 E	5	West	whole air	TSI3563	07/2001 –12/2013
Finokalia (FKL) (2)	Greece	GR0002R	35.3167 N, 25.6667 E	250	Southeast	whole air; PM <sub>1</sub> ; PM <sub>10</sub> (g)	RR M903; Ecotech Aurora1000 (h)	04/2004 –12/2015
<b>Regional/rural observatories</b>								
Birkenes II (BIR)	Norway	NO0002R	58.3885 N, 8.252 E	219	Nordic and Baltic	PM <sub>10</sub>	TSI3563	07/2009 –12/2015
Hyytiälä (SMR)	Finland	FI0050R	61.85N, 24.2833 E	181	Nordic and Baltic	PM <sub>10</sub>	TSI3563	05/2006 –12/2015
Vavihill (VHL) (3)	Sweden	SE0011R	56.0167 N, 13.15 E	175	Nordic and Baltic	PM <sub>10</sub>	ECOTECH Aurora3000	03/2008 –04/2014
Observatory Perenne (OPE)	France	FR0022R	48.5622 N, 5.505555 E	392	West	whole air; PM <sub>10</sub> (j)	ECOTECH Aurora3000	09/2012 –12/2015
Cabauw (CBW) (4)	The Netherlands	NL0011R	51.9703 N, 4.9264 E	1	West	PM <sub>10</sub>	TSI3563	01/2008 –12/2012
Montseny (MSY)	Spain	ES1778R	41.7667 N, 2.35 E	700	Southwest	PM <sub>10</sub>	ECOTECH Aurora3000	01/2010 –12/2015
Košice (KOS)	Czech Republic	CZ0007R	49.58333N, 15.0833 E	534	Central	PM <sub>10</sub>	TSI3563	03/2013 – 12/2015
Melpitz (MPZ) (5)	Germany	DE0044R	51.53 N, 12.93 E	86	Central	PM <sub>10</sub>	TSI3563	01/2007 –12/2015
Ispra (IPR)	Italy	IT0004R	45.8 N, 8.6333 E	209	Central	PM <sub>10</sub>	TSI3563	01/2004 –12/2014
K-Pusztta (KPS)	Hungary	HU0002R	46.9667 N, 19.5833 E	125	East	PM <sub>1</sub> ; PM <sub>10</sub> (j)	TSI3563	05/2006 –12/2014

<b>Urban/sub-urban observatories</b>								
SIRTA <b>(SIR)</b>	France	FR0020R	48.7086 N, 2.1589 E	162	West	PM <sub>1</sub>	ECOTECH M9003	07/2012 –12/2013
Madrid <b>(MAD)</b>	Spain	ES1778R	40.4627 N, -3.717 E	669	Southwest	PM <sub>2.5</sub> ; PM <sub>10</sub> (k)	ECOTECH Aurora3000	01/2014 – 12/2014
Granada <b>(UGR)</b>	Spain	ES0020U	37.164 N, -3.605 E	680	Southwest	whole air	TSI3563	01/2006 –12/2015
Athens <b>(DEM)</b>	Greece	GR0100B	37.9905 N, 23.8095 E	270	Southeast	PM <sub>10</sub>	ECOTECH Aurora3000	01/2012 –12/2015

1 (1) Observatory codes from EBAS; (2) GAW code: FIK; (3) GAW code: VAV; (4) GAW code: CES; (5) GAW code: MEL; (a) start-end of  
2 measurements; total aerosol particle scattering was used as reference for measurement period; (b) PM<sub>5</sub> (2000-08/2005), PM<sub>2.5</sub> (08/2005-  
3 2007) and PM<sub>10</sub> (2008-2015); (c) whole air (2007-2009) and PM<sub>10</sub> (2010-2015); (d) PM<sub>2.5</sub> (2013-03/2014) and PM<sub>10</sub> (04/2014-2015); (e)  
4 ECOTECH Aurora M9003 during 2007-2013 and TSI 3563 (2014-2015); (f) only measurements performed during the year 2012 were  
5 used in this investigation; (g) whole air (2004-2008), PM<sub>10</sub> (2009-2011), PM<sub>1</sub> (2011-2012), PM<sub>10</sub> (2013-2015); (h) RR M903 during 2004-  
6 2011, Ecotech AURORA1000 during 2012-2015; (i) whole air (2012-08/2013) and PM<sub>10</sub> (09/2014-2015); (j) PM<sub>1</sub> (2006-04/2008) and PM<sub>10</sub>  
7 (05/2008-2014); (k) PM<sub>10</sub> from 03/2014.

8  
9  
10  
11  
12  
13  
14  
15  
16  
17  
18  
19  
20  
21  
22  
23  
24  
25  
26  
27  
28  
29  
30  
31  
32  
33  
34  
35  
36  
37  
38  
39  
40  
41  
42  
43  
44  
45  
46  
47  
48  
49  
50  
51  
52  
53  
54  
55  
56  
57  
58  
59  
60  
61

1 **Table 2:** Trends of aerosol particle scattering coefficient ( $\sigma_{sp}$ ), scattering Ångström exponent (SAE) and backscatter fraction (BF). Three trends for SAE are reported: SAE calculated as a linear fit  
2 using; three wavelengths (b-g-r), using the blue and green wavelengths (b-g) and using the green  
3 and red wavelengths (g-r). Trend results are reported for the whole period available at each station  
4 until 2015 (bold) and for the periods reported in Collaud Coen et al. (2013) and Asmi et al. (2013).  
5 Trends are considered as statistically significant for a p-value of <0.05. Statistically significant  
6 increasing or decreasing trends are highlighted with up (↑) and down (↓) red and green arrows,  
7 respectively. Non-statistically significant increasing or decreasing trends are highlighted with up (↑)  
8 and down (↓) grey arrows, respectively. Grey coloured table cells highlight stations included in this  
9 work but not included in the works of Collaud Coen et al. (2013) or Asmi et al. (2013). \$: parameters  
10 removed in this work and in the work of Collaud Coen et al. (2013) because of measurement gaps,  
11 low data coverage or break points for one or more wavelengths. #: Only available for 2014-2015; ±  
12 not available.

Station	period	Trend (This work)					MK Trend (Collaud Coen et al., 2013)					MK Trend (Asmi et al., 2013)		
		$\sigma_{sp}$	SAE			BF	$\sigma_{sp}$	SAE			BF	Particle number		
			b-g-r	b-g	g-r			b-r	b-g	g-r		N	N20 (20-500 nm)	N100 (100-500 nm)
<b><i>Nordic and Baltic</i></b>														
PAL	<b>2000 - 2015</b>	↑	↓	↓	↓	↑								
	2000 - 2010	↓	↓	\$	\$	↑	↓	↑	\$	\$	↑			
	2001 - 2010	↓	↓	\$	\$	↑	↓	↑	\$	\$	↑	↓ (10-500 nm)	↔	↑
	1996 - 2010											↓ (10-500 nm)		
SMR	<b>2006 - 2015</b>	↓	↑	↑	↑	↑								
	1996 - 2011												↓	↓
	2001 - 2010												↓	↓
<b><i>Western</i></b>														
MHD	<b>2001 - 2013</b>	↓	\$	\$	\$	\$								
	2000 - 2010											↓ (3-500 nm)		
	2001 - 2010	↑	\$	\$	\$	\$	↑	\$	\$	\$	\$	↑ (3-500 nm)		
PUY	<b>2007 - 2014</b>	↓	↓	↓	↓	↑								
<b><i>Central</i></b>														
HPB	<b>2006 - 2015</b>	↓	↑	↑	↑	↑								
	2001 - 2010						↑	\$	\$	\$	\$			
	2002 - 2010						↓	\$	\$	\$	\$			
	1995 - 2011												↑ (15-500 nm)	
IPR <sup>(1)</sup>	<b>2004 - 2014</b>	↓	↑	↑	↑	↑								
MPZ	<b>2007 - 2015</b>	↓	↓	↓	↓	↑								
	1997 - 1998 and 2004 - 2010												↑	↑
JFJ	<b>1995 - 2015</b>	↓	\$	\$	\$	\$								
	1995 - 2010	↑	\$	\$	\$	\$	↑	\$	\$	\$	\$			
	1996 - 2010	↑	\$	\$	\$	\$	↑	\$	\$	\$	\$			
	2001 - 2010	↓	\$	\$	\$	\$	↓	\$	\$	\$	\$	↓ (10-500 nm)		
	1997 - 2010	↑	\$	\$	\$	\$							↑ (10-500 nm)	
CMN	<b>2007 - 2015</b>	↓	#	#	#	#								
<b><i>Eastern</i></b>														
BEO	<b>2007 - 2015</b>	↓	↓	↓	↓	↓								

KPS	2006 - 2014	↑	↓	↓	↑	↑								
<b>Southwestern</b>														
IZO	2008 - 2015	↓	↑	↑	↑	\$								
UGR	2006 - 2015	↓	↑	↑	↑	↑								

1 (1) A statistically significant decreasing trend of  $\sigma_{sp}$  at IPR was also reported by Putaud et al. (2014) for the period 2002 – 2010.

2

3

4

5 **Table 3:** Daytime (08:00 to 16:00 GMT) and night time (21:00 to 05:00 GMT)  $\sigma_{sp}$  trends by season calculated  
6 for the periods considered in this work. Sp: Spring; Su: Summer; Au: Autumn; Wi: Winter. Trends are  
7 considered as statistically significant at a p-value of <0.05. Statistically significant increasing or decreasing  
8 trends are highlighted with up (↑) and down (↓) red and green arrows, respectively. Non-statistically significant  
9 increasing or decreasing trends are highlighted with up (↑) and down (↓) grey arrows, respectively.

Station	period	SCATTERING					
		daytime		nighttime		24h	
		Sp	Su	Sp	Su	Sp	Su
		Au	Wi	Au	Wi	Au	Wi
JFJ	1995 - 2015	↓	↓	↓	↓	↓	↓
		↑	↓	↑	↓	↑	↓
HPB	2006 - 2015	↓	↓	↓	↓	↓	↓
		↓	↓	↓	↓	↓	↓
PUY	2006 - 2014	↓	↓	↓	↓	↓	↓
		↓	↓	↓	↓	↓	↓
CMN	2007 - 2015	↓	↑	↓	↓	↓	↓
		↓	↓	↓	↓	↓	↓
BEO	2007 - 2015	↓	↓	↓	↑	↓	↓
		↓	↓	↓	↑	↓	↑
IZO	2008 - 2015	↓	↓	↓	↓	↓	↓
		↑	↓	↑	↓	↑	↓

10

11

12

13

14

15

16

17

18

19

20

21

22

23

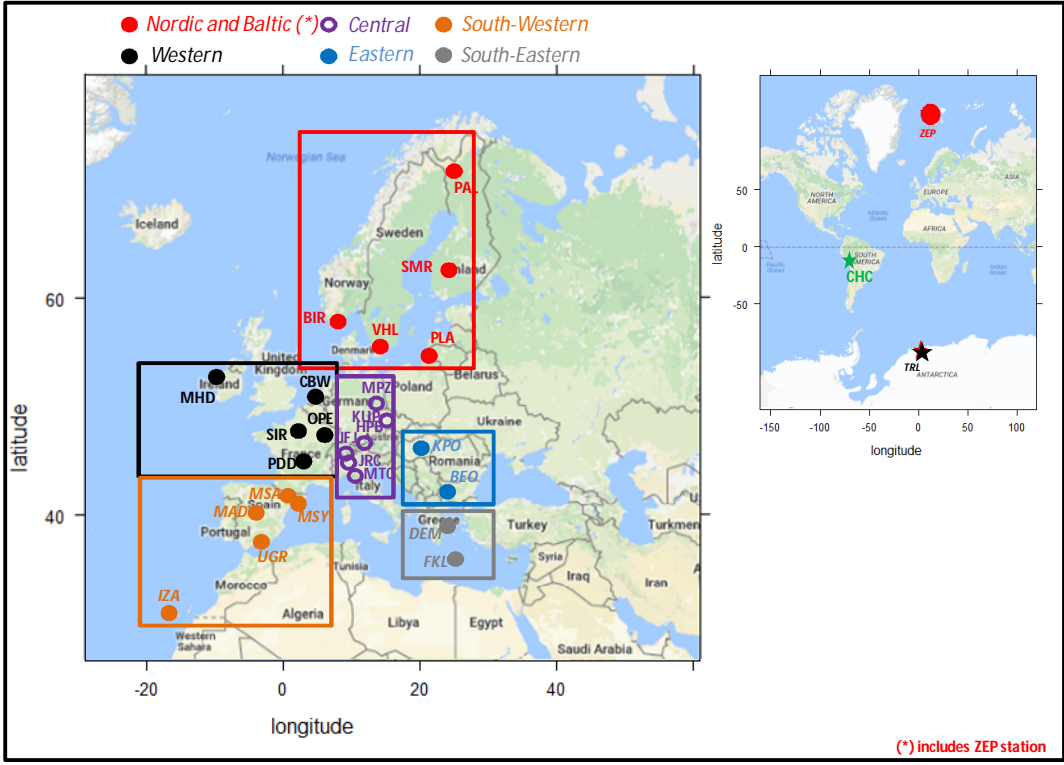
24

1 **Figures**

2

3

4



5

6 **Figure 1:** Locations of the 28 ACTRIS stations included in this work.

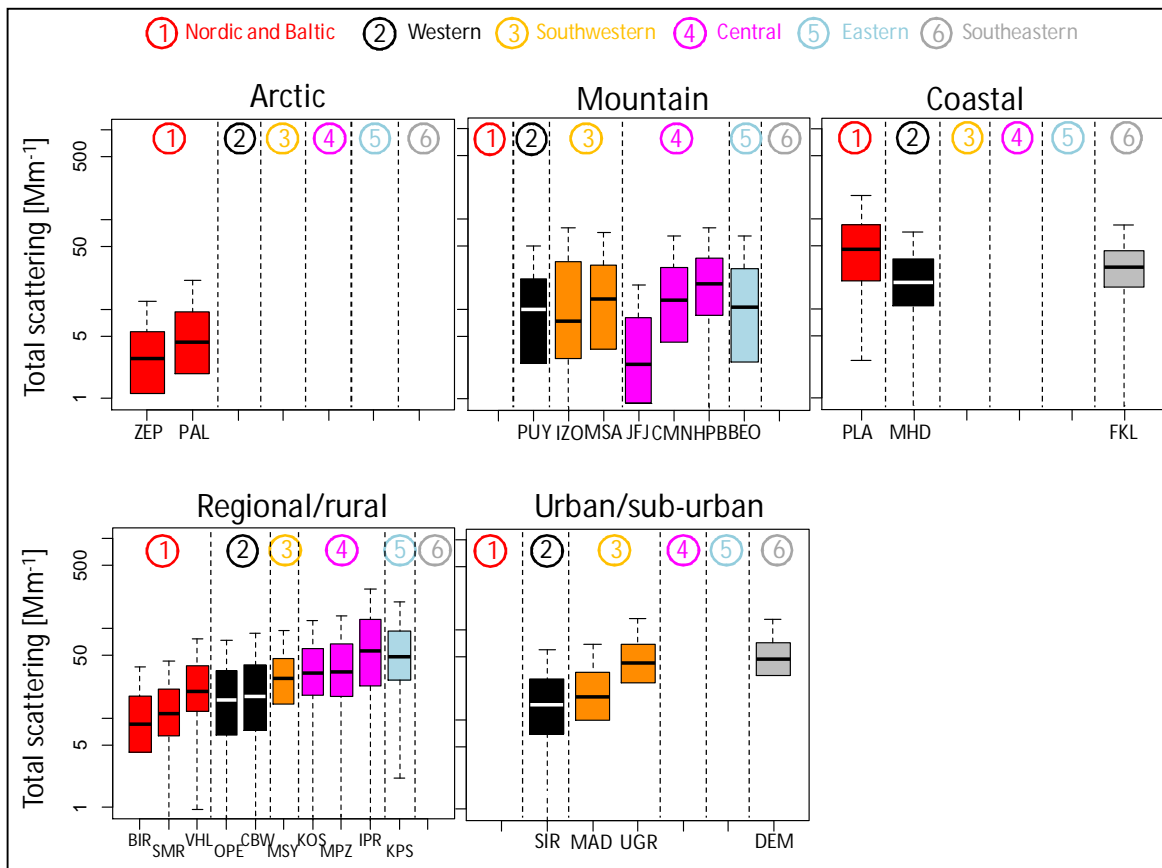
7

8

9

10





1

2

3

4

5

6

7

8

9

10

11

12

13

14

15

16

17

18

19

20

21

22

23

24

25

**Figure 2:** Total aerosol scattering coefficients in the green divided by station setting. Different colours highlight different geographical locations. At SIR, aerosol scattering was available only at 450 nm. Medians (horizontal lines in the boxes), percentiles 25 and 75 (lower and upper limits of the boxes, respectively) and percentiles 5 and 95 (lower and upper limits of the vertical dashed lines) are reported. Hourly data were used for the statistics.

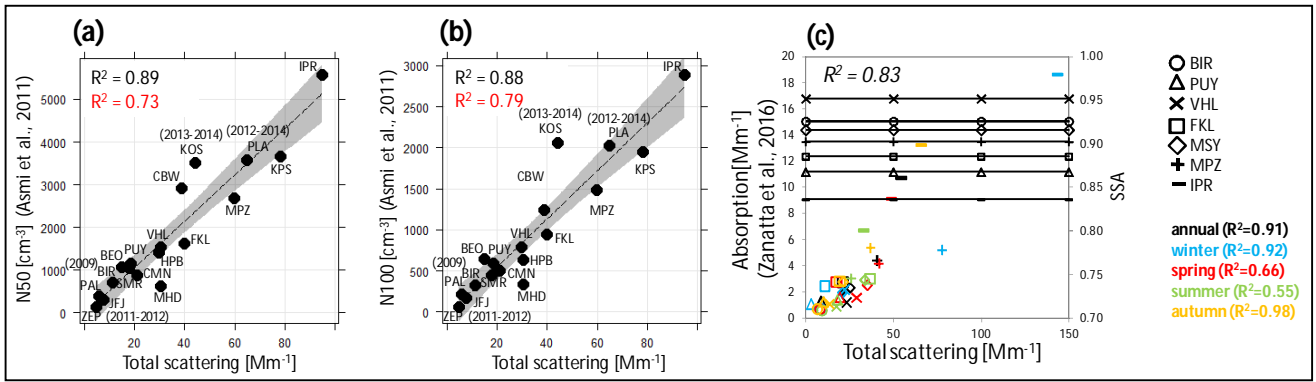


**Figure 3:** Relationship between: (a) N50 (mean particle number concentration between 50 nm and 500 nm), (b) N100 (mean particle number concentration between 100 nm and 500 nm), (c) absorption coefficient and mean aerosol particle total scattering coefficient. (a) and (b): data averaged over the period 2008 to 2009. For ZEP, BIR, KOS and PLA aerosol particle scattering measurements were not available during 2008 to 2009 and different periods were used. R<sup>2</sup> values, highlighted in red, were obtained using the median values. (c) Data averaged as in Zanatta et al. (2016). Figure 3c also reports the geometric mean of SSA.

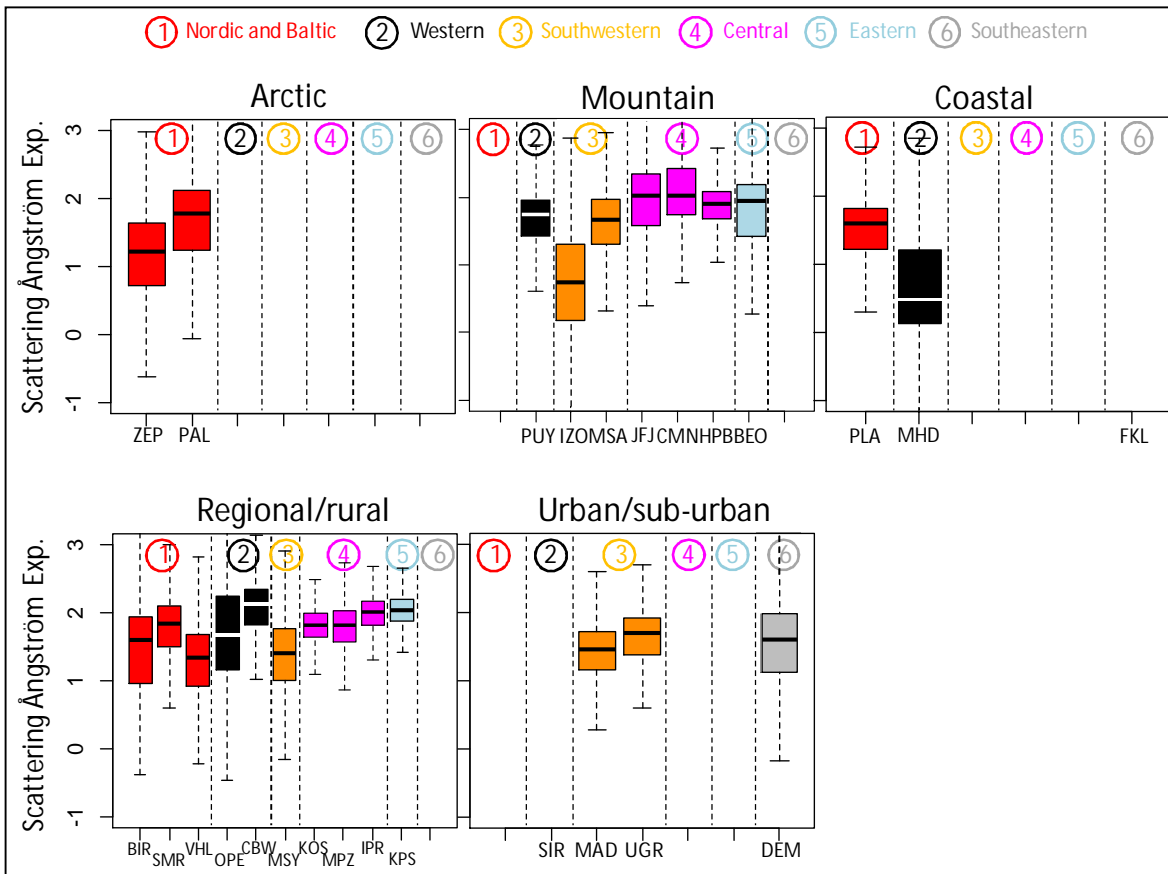
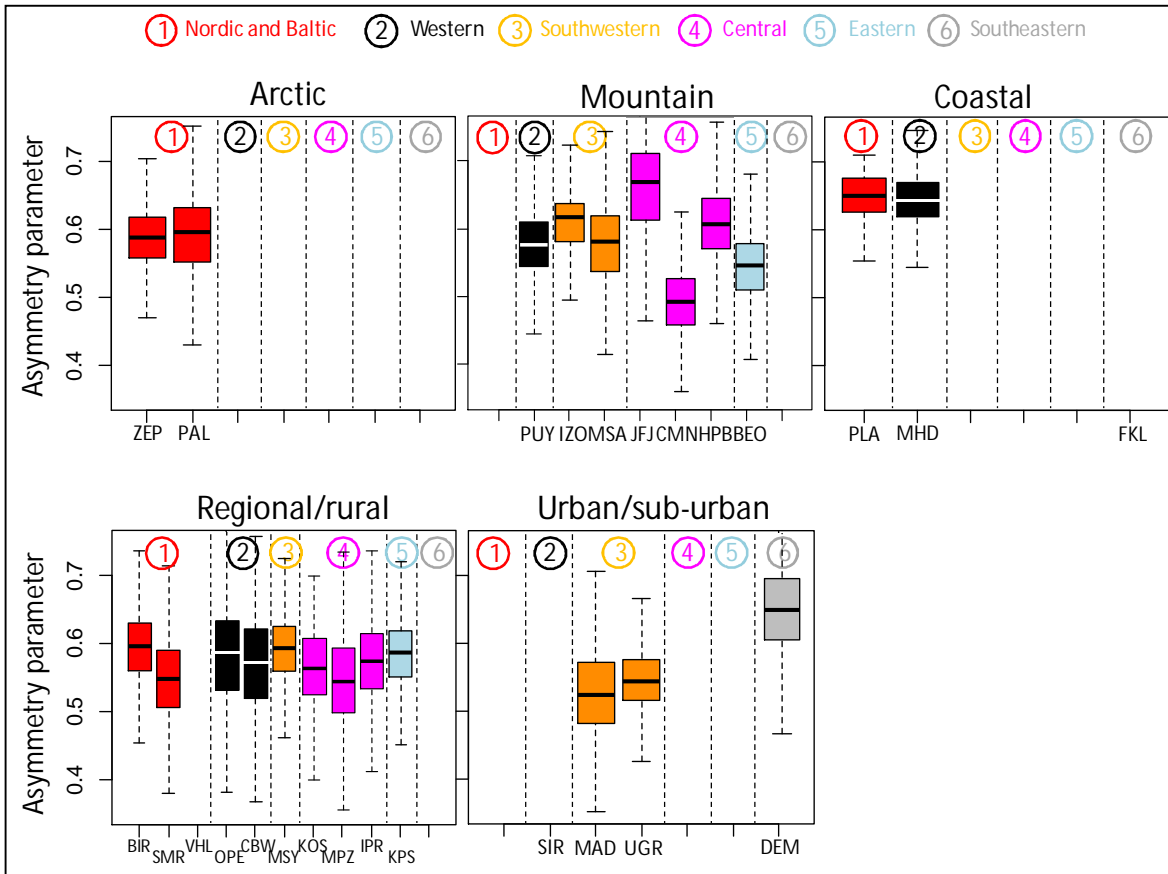


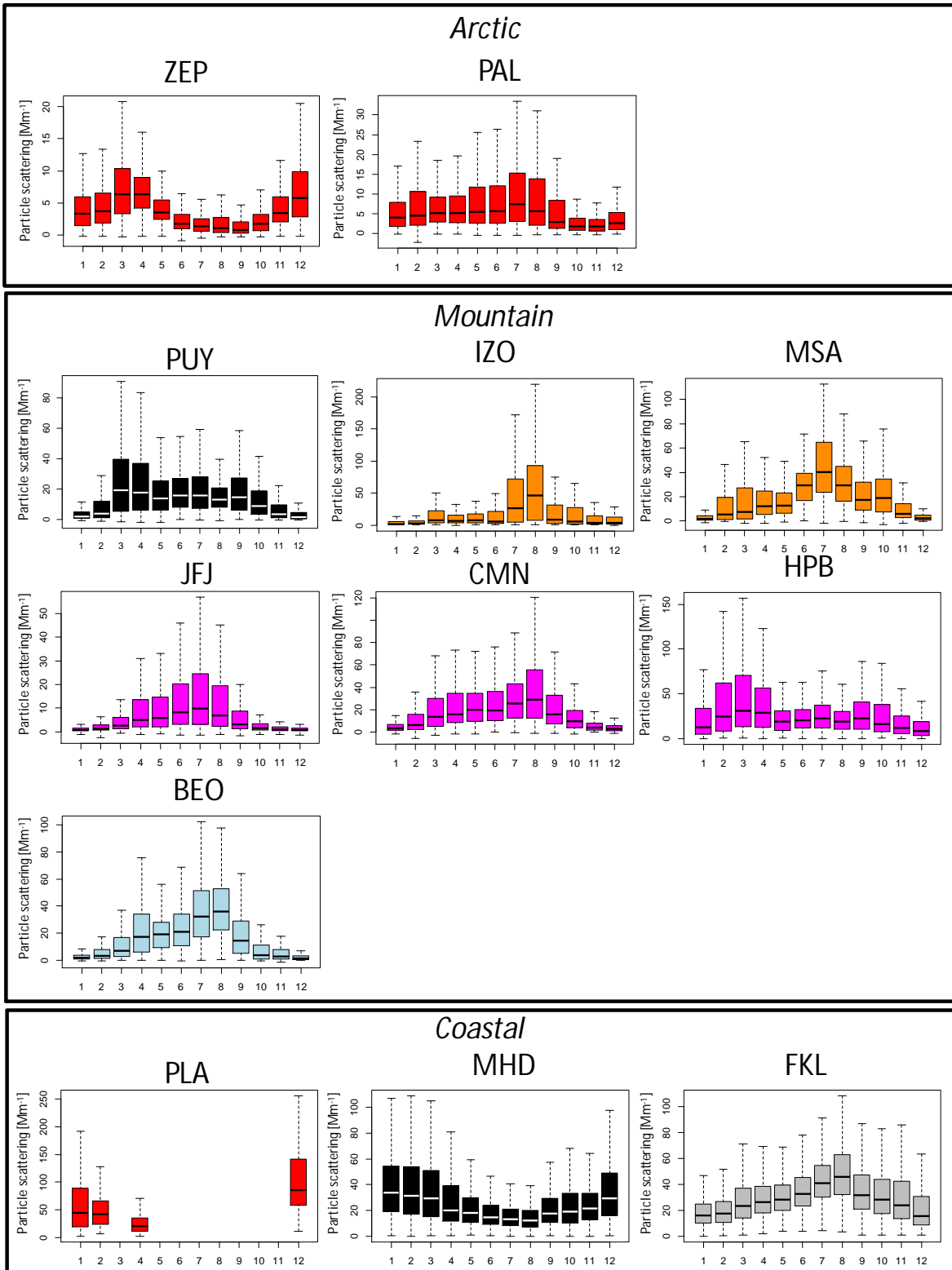
**Figure 4:** Scattering Ångström exponent divided by station setting. Different colours highlight different geographical locations. Medians (horizontal lines in the boxes), percentiles 25 and 75 (lower and upper limits of the boxes, respectively) and percentiles 5 and 95 (lower and upper limits of the vertical dashed lines) are reported. Hourly data were used for the statistics.



1  
2  
3  
4  
5  
6  
7  
8  
9  
10

**Figure 5:** Asymmetry parameter in the green divided by station setting. Different colours highlight different geographical locations. Medians (horizontal lines in the boxes), percentiles 25 and 75 (lower and upper limits of the boxes, respectively) and percentiles 5 and 95 (lower and upper limits of the vertical dashed lines) are reported. Hourly data were used for the statistics.

■ Nordic and Baltic 
 ■ Western 
 ■ Southwestern 
 ■ Central 
 ■ Eastern 
 ■ Southeastern



1  
2  
3  
4  
**Figure 6:** Seasonal cycles of  $\sigma_{sp}$  [Mm<sup>-1</sup>] measured in the green nephelometer wavelength.

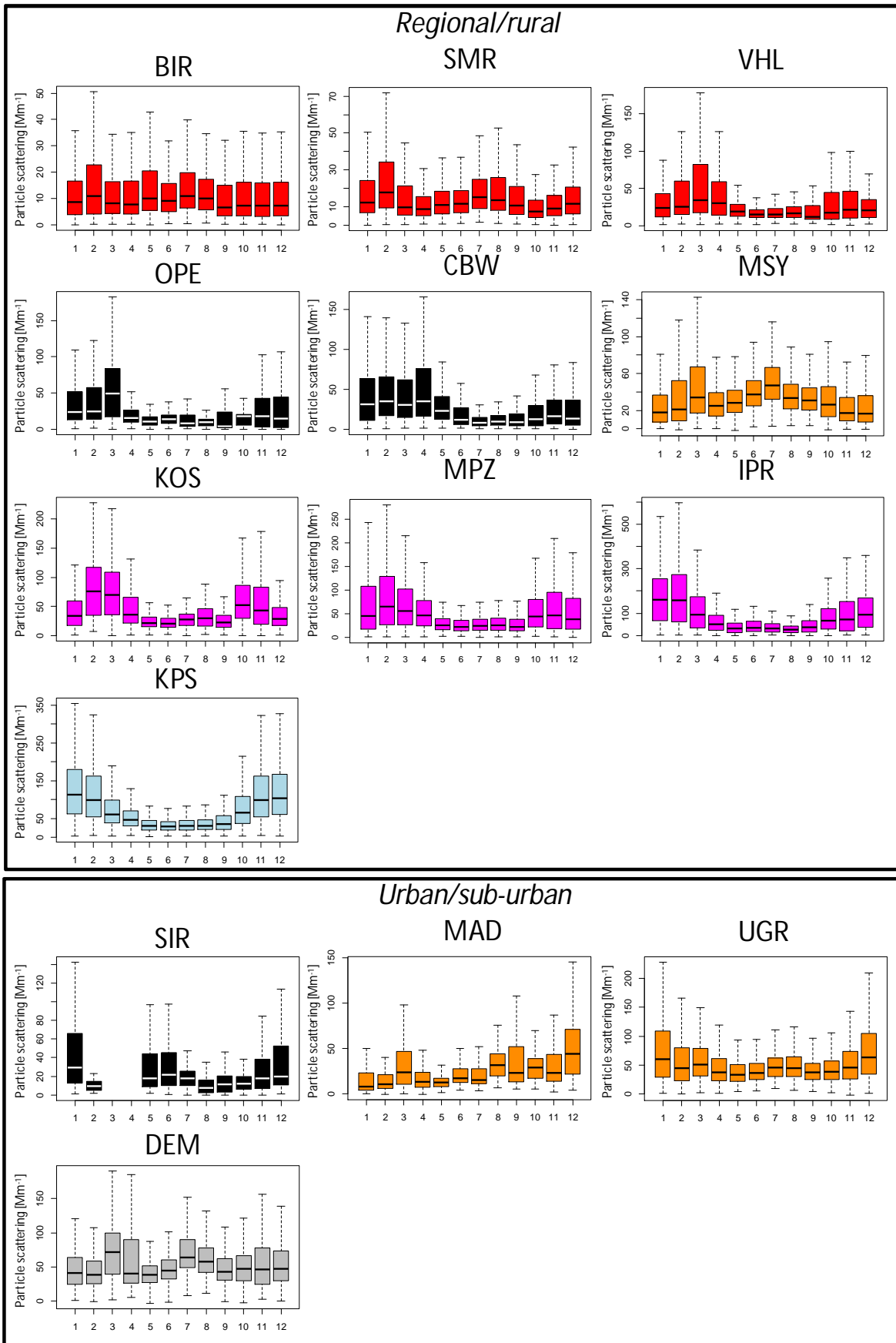
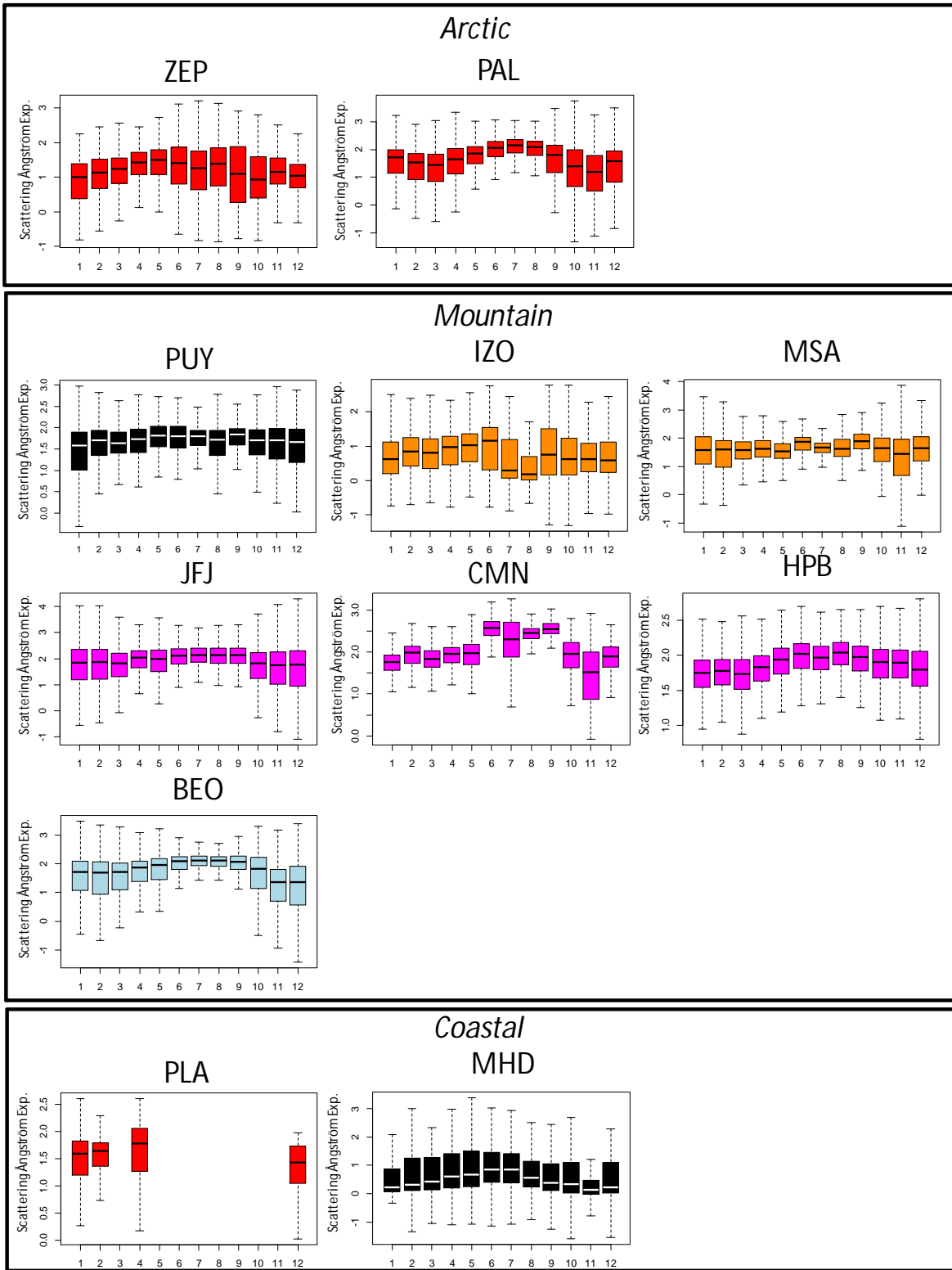


**Figure 6:** (Continued) Seasonal cycles of  $\sigma_{sp}$  [ $Mm^{-1}$ ] measured in the green nephelometer wavelength.

1  
2  
3  
4  
5  
6

■ Nordic and Baltic 
 ■ Western 
 ■ Southwestern 
 ■ Central 
 ■ Eastern 
 ■ Southeastern



1  
2  
3 **Figure 7: Seasonal cycles of SAE (calculated using the three nephelometer wavelengths).**

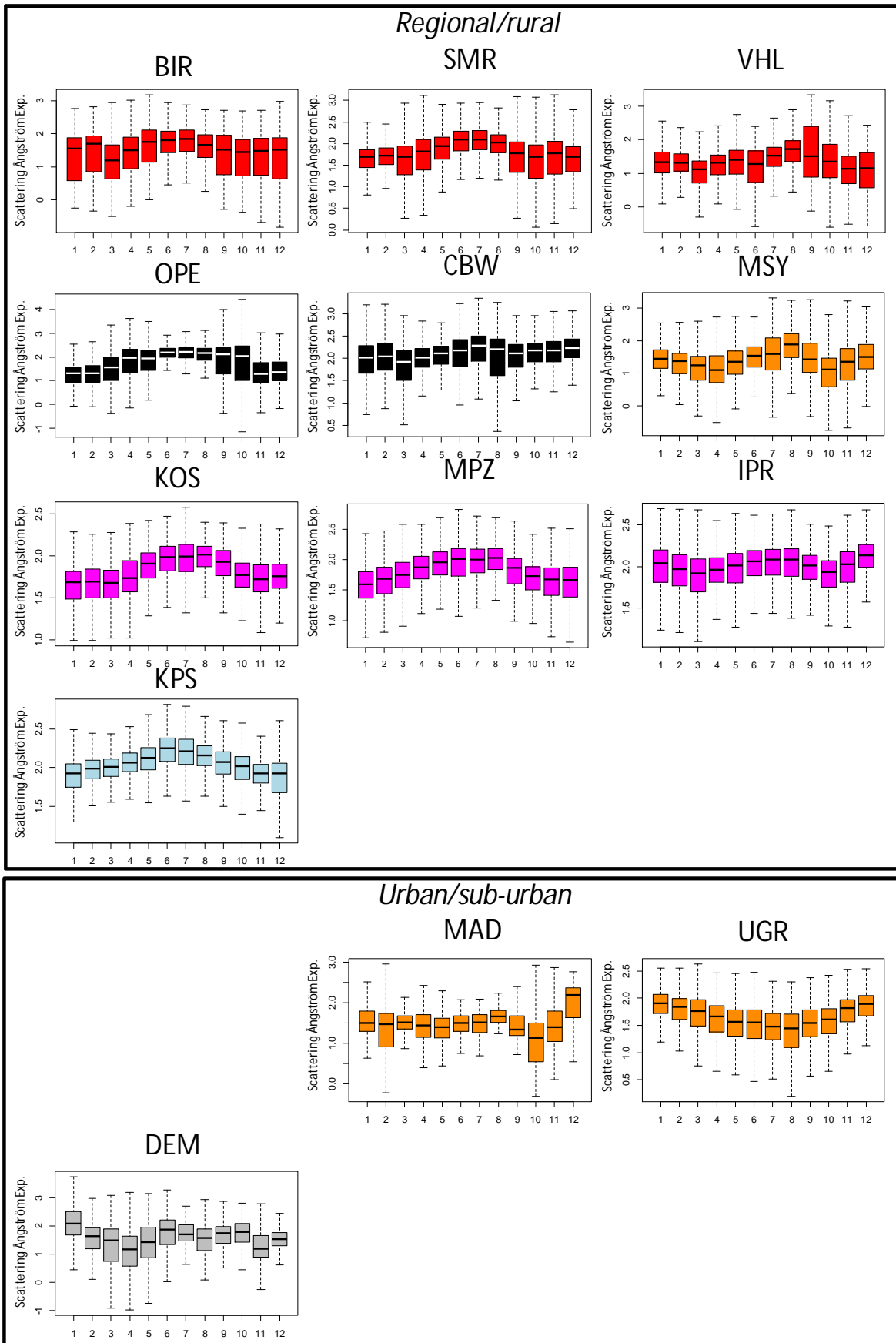
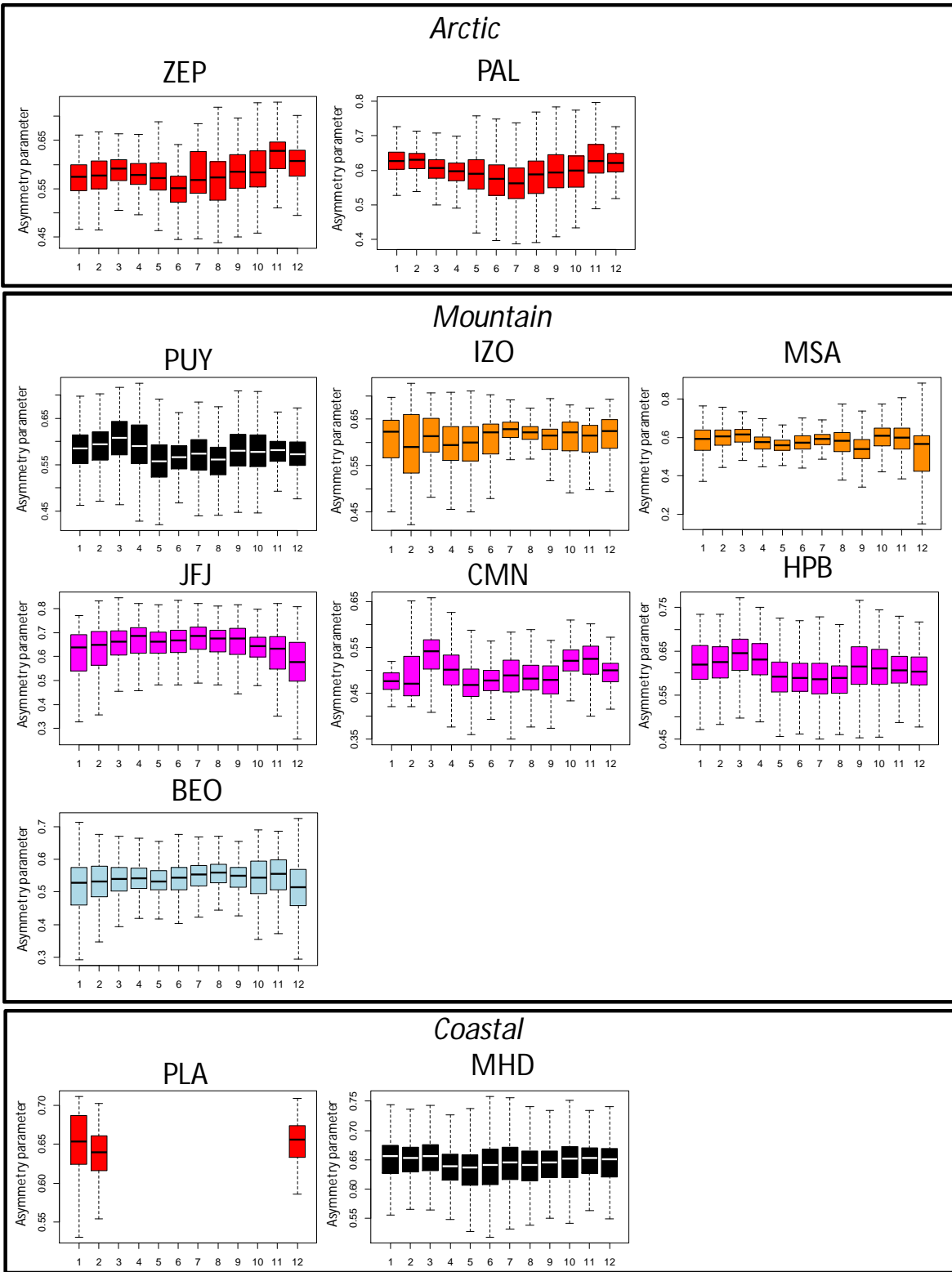


**Figure 7:** (Continued) Seasonal cycles of SAE (calculated using the three nephelometer wavelengths).

1  
2  
3  
4  
5  
6

■ Nordic and Baltic 
 ■ Western 
 ■ Southwestern 
 ■ Central 
 ■ Eastern 
 ■ Southeastern



1  
2  
3  
**Figure 8:** Seasonal cycles of  $g$  (calculated for the green wavelength).



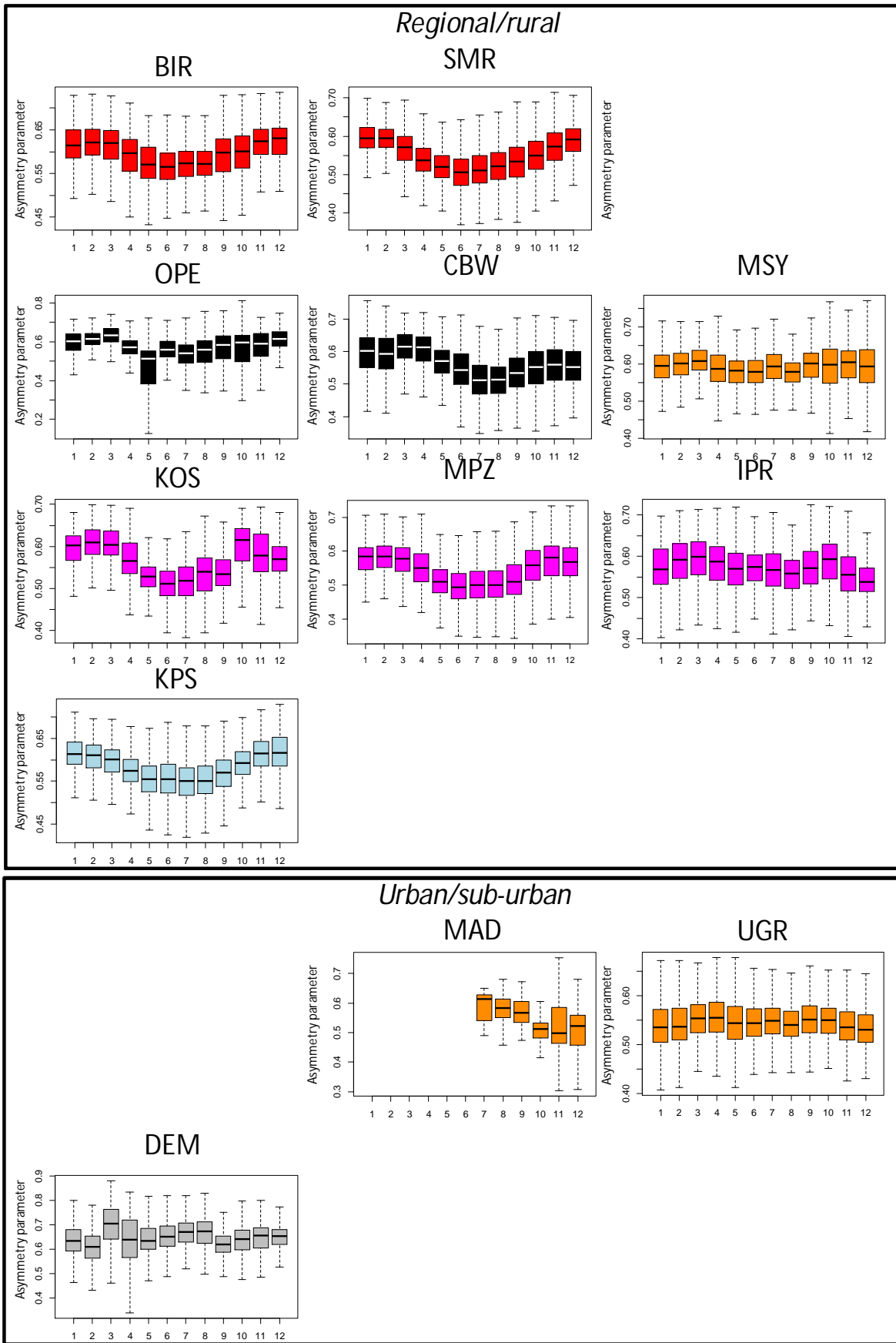
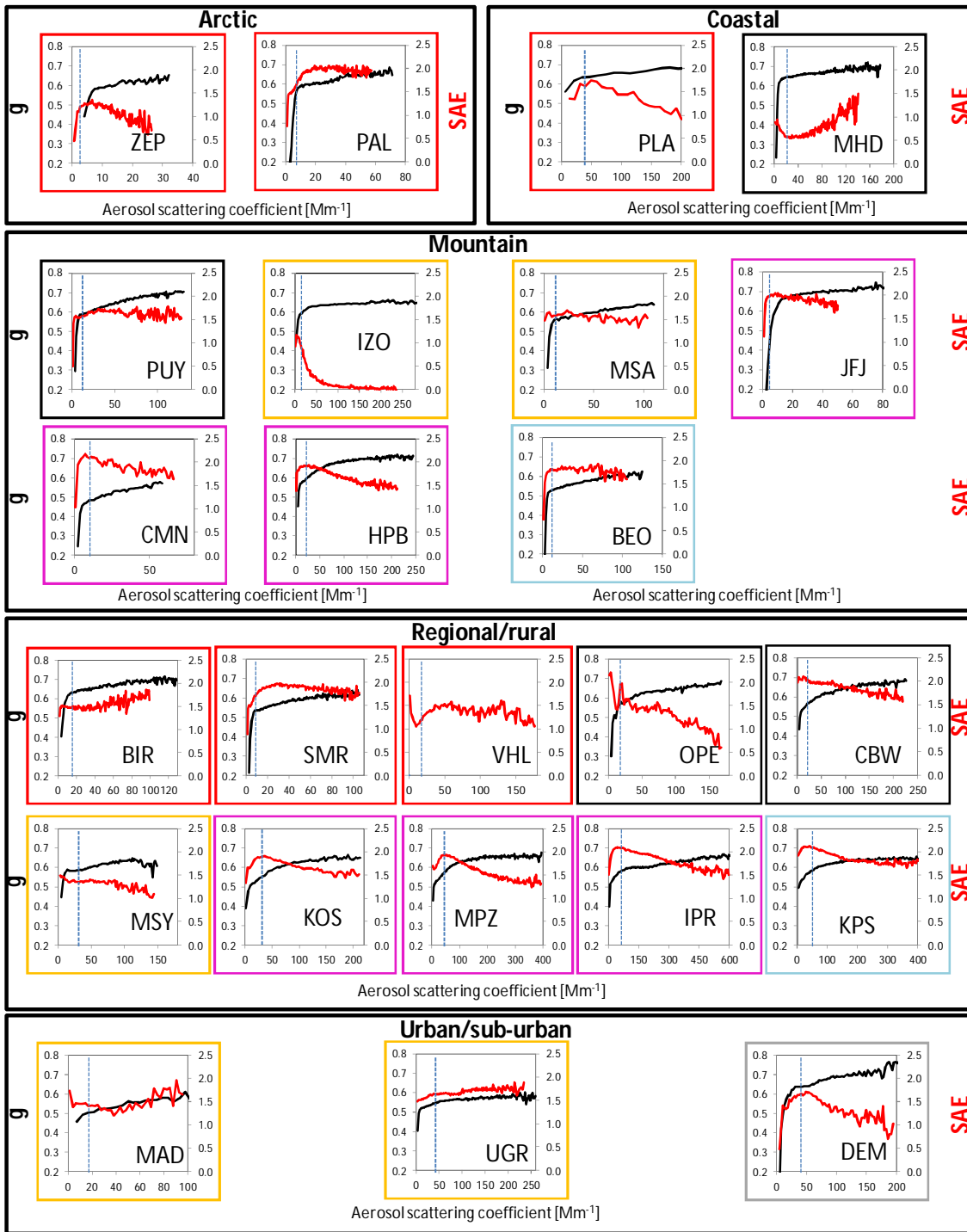


**Figure 8:** (Continued) Seasonal cycles of  $g$  (calculated for the green wavelength).

1  
2  
3  
4  
5



1  
2  
3  
4  
5  
6

**Figure 9:** Scatterplots between  $\sigma_{sp}$  (x-axes) and SAE (right y-axes; red lines) and  $g$  (left y-axes; black lines). Dashed lines represent median  $\sigma_{sp}$  values at each station. Different colours highlight different geographical locations as in Figures 2, 4 and 5.